RAILWAY FORMATION CONDITION ASSESSMENT USING SEISMIC SURFACE WAVES

by

Afonso José Ronda

Submitted in partial fulfilment of the requirements for the degree

Master of Science (Transportation)

in the

Department of Civil Engineering

Faculty of Engineering, Built Environment and Information Technology

UNIVERSITY OF PRETORIA

December 2016

ABSTRACT

RAILWAY FORMATION CONDITION ASSESSMENT USING SEISMIC SURFACE WAVES

by

Afonso José Ronda

Supervisor: Prof. PJ Gräbe

Co-Supervisor: Prof. G Heymann

Department: Civil Engineering

University: University of Pretoria

Degree: Master of Science (Transportation)

The demands of railway transport have been changing over the 150 years of existence of this type of transport in South Africa, specifically the performance requirements of the formation to cater for new traffic requirements. As such, it is important to assess the condition of this vital part of a railway track.

This dissertation covers a research project conducted on two railway lines in which measurements of ground vibration were conducted in order to perform geophysical analysis and characterise the formation based on the results obtained. Measurements were taken on a 26 ton axle load track (Coal line, at Bloubank) and on a 20 ton axle load track (at Amandelbult) in South Africa.

Planning and implementation of several test procedures to characterise track formation require considerable effort to minimize the impact on railway operations. Coupled with track occupation and the destructive nature of some of the test procedures, it is relevant to investigate alternative testing techniques to address the issues stated above.

The use of surface waves for geotechnical characterization of sites is increasing worldwide. Applications to railway engineering have so far been limited to light load, high speed lines to minimize the use of poor geomaterials with reduced Rayleigh wave velocity.

Four sites were identified where trains are operated at heavy loads, with the formation condition varying from poor to good. Seismic testing (geophysical) and conventional testing (deflection measurements) were performed at the identified sites. Seismic measurements were recorded using geophones as receivers, coupled to an amplifier and a computer. The source of the seismic events was the trains operating on the track and a hammer for impact testing. For the deflection measurements, the Remote Video Monitoring (RVM) technique was adopted.

Dispersion analysis of the ground vibration experimental data was conducted using the multiple receiver method. The main conclusions reached with the analysis indicated that:

- Dispersion analysis had a good correlation with the formation deflection analysis;
- Phase velocity can be used as an indicator of the quality of a certain site;
- There are limitations when using trains as the energy source in terms of the generation of excitation frequency, which greatly reduces the phase velocity information in individual layers in the formation (i.e. wavelengths are not short enough).

ACKNOWLEDGEMENTS

The completion of this thesis would not have been made possible without the support and help of the following institutions:

- Department of Civil Engineering at the University of Pretoria, for allowing me to pursue my post graduate studies;

- The Chair of Railway Engineering at the University of Pretoria for providing the funding and equipment required to perform my testing.

I am grateful to both of my supervisors for the guidance provided during my Master's degree studies. Prof Heymann for all the discussions we had related to my topic, which sometimes posed seemingly hard challenges. For Prof Gräbe, a special thanks for the relentless support and motivation during my period at the Department. My gratitude is endless.

I would also like to say thank you to my colleagues at the Chair for all the support they provided during my testing, for all the hard work they put in. Special thanks to Rudi for the camaraderie during the good and tough times I had.

The completion of this dissertation would not be possible without the support of my family. My wife's support and love throughout the time I spent away from home is something I will always appreciate. Without my kids understanding of my long absences I would struggle to focus on my work. Thank you to both of them.

TABLE OF CONTENTS

LIST OF FIGURES

LIST OF TABLES

LIST OF SYMBOLS

ω - Circular frequency

f - Cyclic frequency

λ - Wavelength

k - Cyclic wavenumber

γ - Coherence function

ε - Strain

σ - Normal stress

ν - Poisson's ratio

J - Creep tensor

S - Cross power spectrum

V - Velocity

G - Shear Modulus

θ - Phase

u - Track modulus

K - Track stiffness

E - Elastic Modulus

LIST OF ABBREVIATIONS

BOEF	- Beam on Elastic Foundation
CMSW	- Continuous Monitoring System (software package developed by TLC)
CPT	- Cone Penetration Test
CSW	- Continuous Surface Wave
FFT	- Fast Fourier Transform
Izolof AR	- Izolof after rehabilitation (testing in Izolof performed after May 2015 track reconstruction between MP73/5 and MP73/6)
Izolof BR	- Izolof before rehabilitation (testing in Izolof performed before May 2015 track reconstruction between MP73/5 and MP73/6)
LHS	- Left Hand Side
LVDT	- Linear Variable Differential Transformer
MOPA	- Multi-Offset Phase Angle
SPAC	- Spatial Autocorrelation
RVM	- Remote Video Monitoring
RHS	- Right Hand Side
SASW	- Spectral Analysis of Surface Waves
SPT	- Standard Penetration Test

1. INTRODUCTION

One of the major roles of railway track foundation layers is to reduce vehicle induced stresses applied to the underlying subgrade to a level that limits the progressive build-up of permanent deformation. The ability of track foundation layers to satisfy this requirement is dependent upon the materials used for construction and their thickness (Nelder et al., 2008).

Ballasted rail tracks serve as one of the major infrastructure components for freight transport in South Africa. During the last 10 – 15 years, an increasing demand for such transport has led to the use of considerably heavier and faster trains. Large cyclic stresses due to heavier and faster trains can induce large deformations and cause degradation of the track, especially the formation. This, in turn, adversely affects track stability and has serious implications for track maintenance.

Construction of railways in South Africa started some 150 years ago. At this time the design and requirements for track, substructure and subsoil were very much different from those for modern railway operations. Axle loads, speeds and demands on quality of railway transport have increased severely during this period. Existing railways will be used in the future for new traffic conditions, which makes the performance of the formation even more important.

1.1 DESCRIPTION OF THE PROBLEM

On sites with poorly performing track formations, significant formation deformation has been observed visually propagating in front of the train in the direction of travel. These visual deformations, although not documented or discussed in relevant technical documents pertaining to railway engineering, might be related to the condition and performance of the track, especially the track formation.

Figure 1-1 below illustrates a section of the Coal line with mud pumping problems. Evidence of this phenomenon on the railway track is indicative of failure of one or more components of the subgrade (formation layers or the natural ground).

Figure 1-1: Railway track with poorly performing formation (Coal line, Empangeni)

Current in situ testing methods for railway track formations require considerable track occupation, disrupting railway operations and causing long lead times to be taken before the testing itself is carried out.

A variety of conventional in-situ testing methods are available to determine parameters for predicting formation performance. Amongst those testing methods reference can be made to the Standard Penetration Test (SPT), Cone Penetration Test (CPT), vane shear, piezometer installations, plate load and in-situ density tests.

Geophysical technique tests for formations include surface wave tests (Continuous Surface Wave (CSW), Spectral Analysis of Surface Waves (SASW) and multi channel tests) and body wave tests (seismic cone, down-hole, cross-hole and seismic refraction tests).

Apart from the surface wave testing, all other testing methods require significant track occupation, coupled with some of them being destructive, as they require the area to be instrumented and be dug up to place the instrumentation at the required depth. This requires

considerable mobilization and planning effort to have ancillary equipment available to perform drilling/excavation. Some of the conventional test methods and the body wave test methods (geophysical testing) have limitations in terms of type of geomaterials that are suitable for testing and the properties being measured.

All the above in-situ testing methods can assess track response and performance within the applicable parameters that they can measure. However, each method has its advantages and limitations, both in terms of measured parameters, sampling size, applicability and mobilization requirements. As such, there is a growing need to assess conditions of existing railway tracks, especially the formation, when subjected to loading from moving trains, without the disruption to operations arising from destructive testing.

Due to increased interest in employing seismic testing, particularly surface wave methods to perform near-surface site characterization, a research project to assess site conditions employing geophysical techniques was initiated.

The methods associated with surface wave testing were developed with equipment to generate ground motion (or disturbance) – controlled sources such as mechanical shakers or impact devices – and from the literature review discussed in Chapter 2, it is anticipated that the dispersive characteristics of the sites being tested will be mainly influenced by the geomaterials' characteristics and less influenced by the source generating such disturbances. As such, the dynamic track response that will be investigated will be based on the disturbance mentioned in the first paragraph of this section, caused by the passage of a train. Geophones were therefore used to measure the track formation ground response and performance.

A typical cross section of a railway track formation is shown in Figure 1-2. Formation layers consist of the granular layer underneath the ballast and the subgrade (placed soil and natural ground).

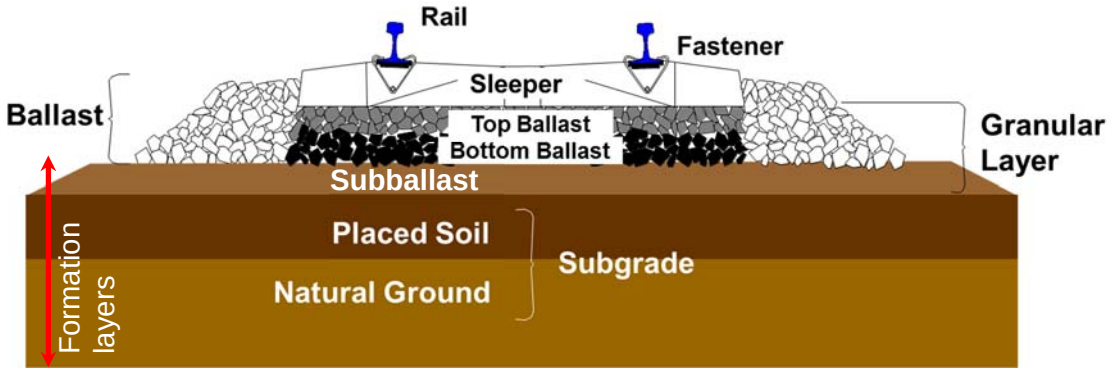

Figure 1-2: Typical cross section of a heavy haul line.

1.2 OBJECTIVES OF THE STUDY

The overall objective of the study was to develop and validate non-destructive, minimal disruptive testing procedures, on or adjacent an operating railway line, in order to assess its formation condition. The following main objectives were determined for this research:

- Validate methods to measure dynamic track formation vibrations (or vertical motions), using geophones (and accelerometers if required);
- Collect a series of dynamic track displacements under loading and analyse the collected data;
- Compare track response under different loading conditions (train speed and loading conditions);
- Compare track response before and after rehabilitation (i.e. poor and good formation conditions);

1.3 THESIS STRUCTURE

The following structure was used to prepare the research report:

An Introduction chapter, (Chapter 1), where the problem is stated, along with the research outline.

Chapter 2 is the literature review, including a brief overview of the research done on ballasted tracks using geophysical techniques. A brief overview of the propagation theory is given, as well as a detailed overview of the propagation mechanisms of Rayleigh waves (surface waves). This establishes the foundation for the dispersion analysis methods and inversion procedures that are required for the determination of the shear velocity profiling.

Chapter 3 discusses the instrumentation set-up and data acquisition procedures adopted to measure track response. A brief discussion of the equipment used and local site conditions are also included.

Chapter 4 presents the data analysis and discussion of the deflection measurements and the seismic recordings.

Chapter 5 draws conclusions and makes recommendations on the results obtained.

2. LITERATURE REVIEW

This chapter reviews the current understanding of surface waves methods to characterize sites, and specifically the track formation geomaterials. Additionally, alternative methods used to evaluate the results obtained by the experimental work are also discussed.

Disturbance resulting from load application propagates as a wave through a physical medium. Discussion of wave propagation is conducted broadly. Surface waves are discussed in more detail.

Section 2.1 discusses elasticity theory. Focus is given to the regime in which the dynamically loaded geomaterials behave in common surface wave testing. Due to the (very) small strains, linear elasticity is discussed in detail. To account for the dispersive nature of the geomaterials, where the energy of the propagating waves is attenuated through material and geometric damping, linear viscoelastic models are also discussed.

Section 2.2 discusses wave theory and propagation. Body and surface wave generation and propagation mechanisms are introduced. Particular emphasis is given to Rayleigh waves, which form part of surface waves.

Section 2.3 covers aspects related to dispersion analysis of surface waves. Several methods are discussed. Spectral analysis, regression based methods and transform based methods are introduced.

An overview of research carried out and published regarding geotechnical characterization using geophysical methods and related wave propagation issues in the railway operations domain is given in Section 2.5 to establish the scope of research already done and the areas which might be possible to make a contribution due to limited research done up to date.

2.1 ELASTICITY THEORY

The displacement of the formation referred to in the introduction of this chapter will cause a strain magnitude in the medium where the deformation occurred.

As such, soil behaviour will be greatly influenced by the strain magnitude caused by the disturbance of the medium. Soil behaviour can be modelled in the following way:

- Increasing strain magnitude for static loads (linear elastic, non-linear elastic, non-linear elasto-plastic or perfectly plastic medium).
- Accounting for dissipative phenomena for dynamic behaviour (visco-elastic models).

2.1.1 Linear elasticity

Elastic media can be characterized by a relationship between stress (σ) and strain (ε) and can be written as (Lai and Rix, 1998):

$$\sigma_{ij} = a_{ijkl} \cdot \varepsilon_{kl} \tag{2.1}$$

where a is a 4th order tensor. This tensor can have 21 independent constants and is generally valid for an anisotropic medium. If a hypothesis of complete isotropy is assumed, Equation 2.1 can be re-written as:

$$\sigma_{ij} = \lambda \cdot \varepsilon_{kk} \cdot \delta_{ij} + 2\mu \cdot \varepsilon_{ij} \tag{2.2}$$

where: δ_{ij} is the Kronecker delta function and the two elastic constants are λ and μ (known as Lamé's parameters).

Table 2.1 below shows a summary of the most widely used pairs of parameters with the relative cross relationships which can be useful to express the stress-strain relationship.

Table 2-1: Relationship between elastic constants, adapted from Foti (2000)

	λ , μ	G , ν	E , ν	K , G
λ	λ	$\frac{2G\nu}{1-2\nu}$	$\frac{\nu E}{(1+\nu)(1-2\nu)}$	$K-\frac{2}{3}G$
$\mu \equiv G$	μ	G	$\frac{E}{2(1+\nu)}$	G
K	$\frac{(3\lambda+2\mu)}{3}$	$\frac{2G(1+\nu)}{3(1-2\nu)}$	$\frac{E}{3(1-2\nu)}$	K
E	$\frac{\mu(3\lambda+2\mu)}{\lambda+\mu}$	$2(1+\nu)G$	E	$\frac{9KG}{3K+G}$
ν	$\frac{\lambda}{2\cdot(\lambda+\mu)}$	ν	ν	$\frac{3K-2G}{2(3K+G)}$

2.1.2 Linear visco-elasticity

Experimental evidence shows that in this region of the strain spectrum, soils subjected to dynamic excitations have both the ability to store strain energy (elastic behaviour), and to dissipate strain energy over a finite period of time (viscous behaviour) (Lai and Rix, 1998).

The stress tensor $\sigma_{ij}(t)$ is related to the past strain history by the linear function (Lai and Rix, 1998):

$$\sigma_{ij}(t) = \int_{-\infty}^{t} G_{ijkl}(t-\tau)\frac{d\varepsilon_{kl}(\tau)}{d\tau}d\tau \tag{2.3}$$

where ε_{kl} is the infinitesimal strain tensor and G_{ijkl} is a fourth order tensor-valued function called the relaxation tensor function of the material. Equation (2.3) above was derived assuming that the strain history is continuous.

Another important assumption required for the derivation of Equation (2.3) is the time translation invariance hypothesis, which states that the material response is independent of any shift along the time axis. Equation (2.3) can be inverted to yield:

$$\varepsilon_{ij}(t) = \int_{-\infty}^{t} J_{ijkl}(t-\tau)\frac{d\sigma_{kl}(\tau)}{d\tau}d\tau \tag{2.4}$$

where J_{ijkl} is a fourth order tensor-valued function called the creep tensor function of the material. For an isotropic, linear, viscoelastic material, the creep and relaxation tensor functions have only two independent components and they are sufficient to completely describe the mechanical response of the material.

The creep and relaxation functions are material response functions. They are analogous to the elastic constants in linear elasticity. The important difference is that the creep and relaxation functions are no longer constants but time-dependent functions (see Figure 2-1).

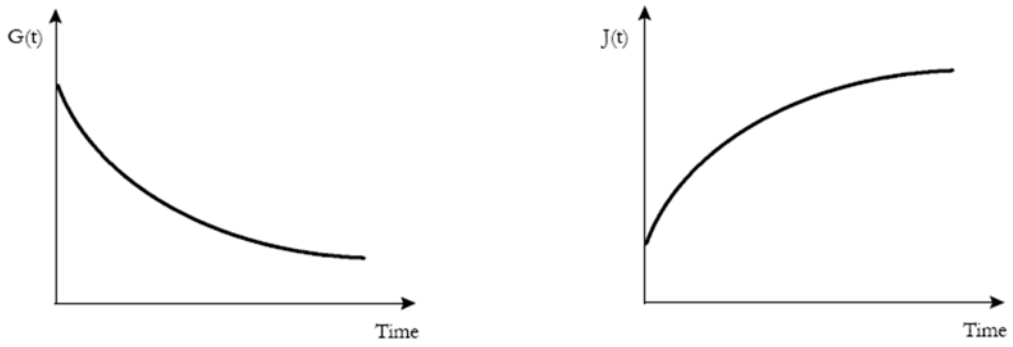

Figure 2-1: Typical Relaxation and Creep Functions for a Viscoelastic Solid, adapted from Lai and Rix (1998)

The constitutive relationships of viscoelastic materials are often given a physical interpretation in terms of mechanical models. These are formed by various combinations of elementary units including linear elastic springs and linear viscous dashpots. Details of such models are not within the scope of this work.

A more reasonable approach to the problem of modelling the dynamic behaviour of soils at very small strains would be to assume a material response function (say the relaxation or the creep function) that is able to capture the essential aspects of the experimental results. This assumed material response function would in general depend on parameters which will be the equivalent of the elastic constants of linear elasticity. These parameters will be determined by

a model fitting procedure applied to some experimental data in a manner identical to that used when soils are assumed to behave as elastic materials.

This procedure is currently used successfully in modelling other types of viscoelastic materials such as polymers (Ferry, 1980). It has the great advantage of generality, which makes it suitable to accommodate a large variety of experimental results while remaining consistent with the fundamental postulates of the theory of linear viscoelasticity.

Examples of application of this approach to geologic materials include the work of Liu et al. (1976) who assumed a hyperbolic distribution of the relaxation spectrum, and that of Kjartansson (1979) who adopted a power law time dependence for the creep response function. Both models are able to accurately predict several features of the behaviour of geologic materials including the frequency independence of energy losses in the seismic band and material dispersion effects (Lai and Rix, 1998).

2.2 WAVE PROPAGATION THEORY

To discuss train-induced dynamic motion, it is necessary to provide a background on wave (vibration) theory as it pertains to moving loads. This is because all dynamic loading generates waves, and the strain, deflection and stress at any point on or within the track formation is due to the waves generated by this dynamic loading.

A wave may be defined as any recognizable disturbance that is transferred from one part of a medium to another with a recognizable velocity of propagation. The disturbance may distort, attenuate, and change its velocity provided it is still recognizable (Whitham, 2011).

2.2.1 Mechanisms of generating ground vibration

There are many modes of train-induced ground vibrations that vary in both amplitude and frequency. All vibrations are induced in the same way; a change in loading is applied to a material in the form of an increase or decrease in load, an impulse or a moving load. This change in load induces strain and shear strain gradients within the material which are propagated as a wave outward from the source (Hall, 2003; Krylov et al., 2000).

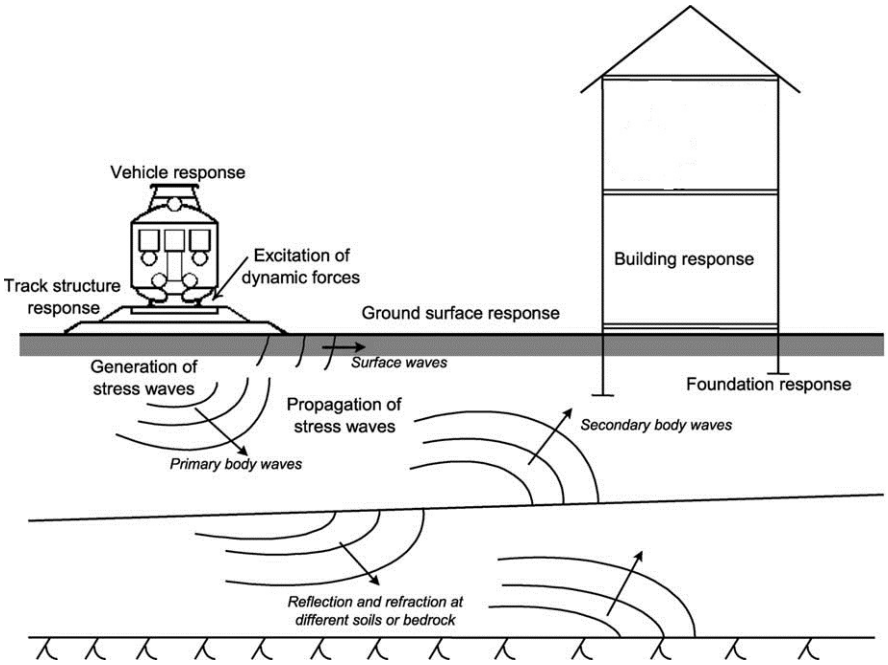

Figure 2-2: Mechanism of train induced ground vibration, adapted from Hall (2003)

The mechanisms include (i) the wheel pressure on the track; (ii) the effects of joints in the rails; (iii) the unevenness of rails or wheels; and (iv) the dynamically induced forces by the rolling stock and wheel vibrations excited mainly by unevenness of wheels and rails.

Additionally, surface wave generation results from the presence of interfaces separating layers of different velocities. A detailed discussion of the factors influencing the level and characteristics of train induced vibration is presented by Hall (2003).

2.2.2 Wave propagation

2.2.2.1 Waves in linear media

The main types of waves that can be propagated in a homogeneous elastic halfspace are shown in Figure 2-3 below.

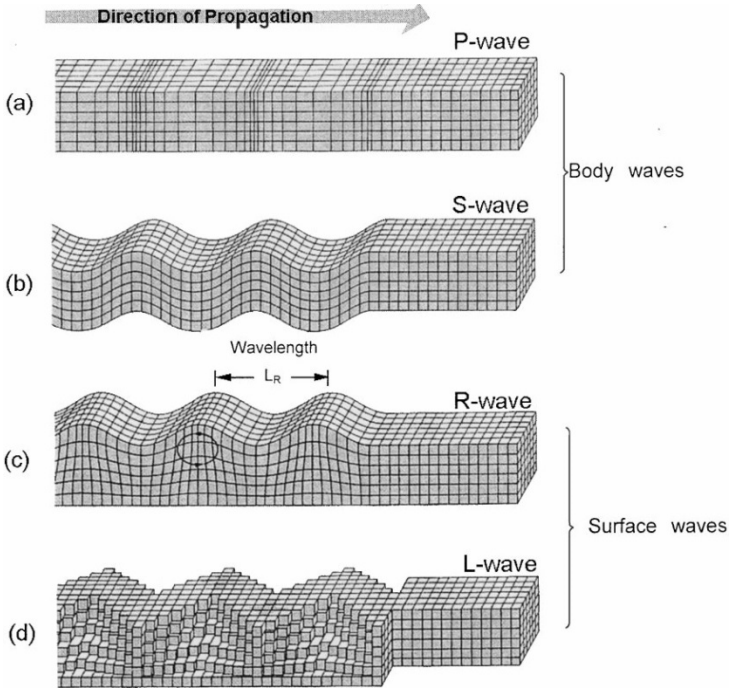

Figure 2-3: Seismic waves: (a) compressional – dilational waves; (b) shear waves; (c) Rayleigh waves; and (d) Love waves, adapted from Athanasopoulos et al. (2000)

Body waves can travel within the interior or along the surface of the ground and may be compressional waves (P-waves),—travelling with velocity, V_P—Fig. 2.2a, or distortional, i.e. shear waves (S-waves), Fig. 2.2b.

The velocities of P-waves and S-waves can be calculated using the equations shown below (Strobbia, 2003):

$$V_P = \sqrt{\frac{\lambda + 2\mu}{\rho}} \tag{2.5}$$

$$V_S = \sqrt{\frac{\mu}{\rho}} \tag{2.6}$$

The surface waves can travel only in the vicinity of the ground surface and may be either out-of-plane Love waves (L-waves) or in-plane Rayleigh waves (R-waves). The L-waves are horizontally polarized shear waves and they exist only when there is a surface low-velocity layer on top of a higher velocity layer. Their velocity of propagation does not differ appreciably from that of S-waves.

The propagation velocity of R-waves, V_R, is slightly lower than V_S, and their particle motion has both vertical and horizontal components. The diagram in Figure 2-4 below depicts the accelerated attenuation of vibration amplitude of R-waves with depth from the surface. It can be concluded that the R-waves propagate along a superficial layer equivalent to one wavelength of thickness. R-waves are non-dispersive in an homogeneous halfspace (Athanasopoulos et al., 2000).

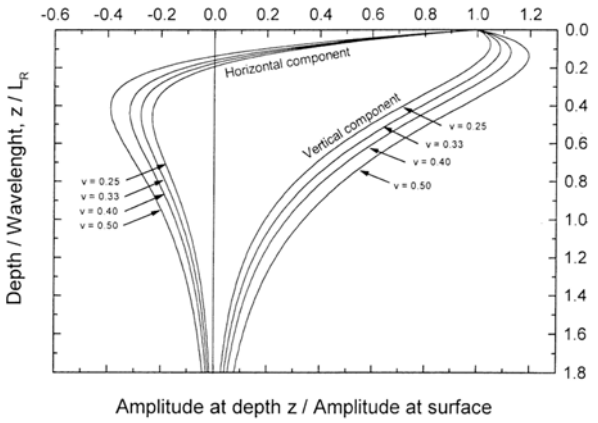

Figure 2-4: Displacement versus depth for Raleigh waves, adapted from Esveld (2001)

At increasing distances from the source of vibration, the R-waves become the dominant type of wave due to their much lower rate of attenuation and the high percentage of vibration energy (about 70% of the total energy) conveyed by them (Richart et al., 1970). It must be emphasized that (surface) waves do not transport mass, but energy.

Propagation of R-waves are complex for layered elastic halfspace systems. Particle motion is governed by higher modes of vibration and the R-wave velocity becomes frequency dependent. For each mode of vibration, a dispersion curve will describe the relationship between the R-wave velocity and the wavelength. More details are provided in Section 2.2.4 below.

Stoneley waves are the most important interference waves. They travel across a mechanical impedance discontinuity and rapidly attenuate going away from the interface. It can be shown that such waves can exist only for given values of the ratio between stiffness properties of the two adjacent layers (Graff, 1975).

2.2.2.2 Waves in linear viscoelastic media

A linear elastic constitutive model is not enough to characterize soil behaviour, if dissipative behaviour must be accounted for, even at very low strain levels.

According to the correspondence principle of linear viscoelasticity, the wave equations for linear viscoelastic media can be obtained from the elastic ones substituting the complex-valued viscoelastic moduli with the real-valued elastic ones (Foti et al., 2014).

2.2.3 Site characterization using seismic waves

Calculation of mechanical properties of geomaterials using characteristics of wave propagation is of common use in engineering, mainly assuming elastic behaviour and using Equations (2.5) or (2.6) to calculate stiffness once the velocity of propagation of the type of wave under analysis has been derived.

In the field of geotechnical engineering the methods based on the measurements of wave propagation are generally addressed as seismic methods. The methods are:

- Cross-Hole and Down-Hole;
- Seismic cone and P-S well logging;
- Seismic reflection and refraction (mainly for geophysical testing).

2.2.4 Discussion of Rayleigh waves

Surface waves are generated only in the presence of a free boundary and they can essentially be of two types: Love waves and Rayleigh waves. As mentioned, Love waves can exist only in the presence of a soft superficial layer over a stiffer halfspace and they are produced by energy trapping in the softer layer for multiple reflections. Rayleigh waves are always generated when a free surface exists in a continuous body.

Body wave theory could not explain some seismic observations. These observations recorded first arrivals as being minor tremors corresponding to P and S waves as part of a major tremor

(Strutt and Rayleigh, 1885). The late tremor had a greater amount of energy compared to a body wave and indications were that this late tremor attenuated less when propagating through the same medium. The assumption was then made that this wave phenomenon was confined to the surface (Graff, 1975).

In 1904 Lamb solved the problem of a point harmonic force acting on the ground surface. He used the Fourier synthesis concept to propose a solution for a general pulse. Because surface waves could be detected at the surface, it became evident that they could be used for medium characterization, including development of non-invasive techniques (Viktorov, 1970).

Due to the nature of this research work, Rayleigh waves will be discussed for vertically heterogeneous media. References that are included can be consulted for homogeneous halfspace medium.

2.2.4.1 Linear elastic media

Mathematical formulation of R-waves for anisotropic and heterogeneous media is complex (in some anisotropic media a solution does not exist). For transverse isotropic media having a free surface parallel to the plane of isotropy, R-waves do exist (Foti, 2000).

Solving this problem involves determining the eigenvalue associated with the propagation of free surfaces. Secondly, the geometric dispersion is determined (calculation of excitation frequency dependent phase velocity).

2.2.4.2 Linear viscoelastic media

The approach used to define the Rayleigh eigenvalue problem in elastic media was based on the application of Lagrange's equations for a vertically heterogeneous elastic medium. A solution of the resulting Navier's equations of motion was then sought in the form of a harmonic displacement field satisfying the boundary conditions of surface waves. The generalization of this procedure to viscoelastic media requires the use of certain variational theorems of linear viscoelasticity. The equations of motion and the associated boundary conditions are then established from the stationary condition of an energy function (Lai and Rix, 1998).

2.3 OVERVIEW OF SURFACE WAVE METHODS – DISPERSION ANALYSIS

Surface wave testing encompasses acquiring information of the geometric dispersion of surface waves from readings of the particle motion at two or more receiver locations. The information is then presented in the form of dispersion curves that show the variation of surface wave phase or group velocity versus frequency or wavelength.

Surface wave methods offer a non-intrusive and economical approach for determining V_s. According to the energy sources used, surface wave methods can be categorized into active-source and passive-source methods. Active-source methods measure surface waves generated by dynamic sources such as sledge hammers, drop weights, bulldozers and hydraulic Vibrosis equipment, while passive-source methods utilize ambient vibrations caused by natural (ocean wave activity, wind) and man-made (traffic, construction, factories) activities.

The methods may be classified according to the procedure adopted (Foti et al., 2014):

- Direct assessments of the propagation parameters (e.g., wavelength in the steady-state Rayleigh method or phase delay in the two-station spectral analysis of surface waves [SASW]);

- Regression methods, in which the propagation parameters are obtained by fitting the experimental data with the expected theoretical functions (multi-offset phase analysis [MOPA], spatial autocorrelation [SPAC], transfer function);

- Transform-based methods, in which the experimental data are transformed from the original space–time domain into a different domain in which the propagation parameters are easily identified as spectral maxima (e.g., frequency – wavenumber, frequency – slowness, frequency – velocity analysis);

Dispersive waves (surface waves in heterogeneous media) are characterized by two distinct velocities: the phase and group velocities. The phase velocity is the speed of propagation of a single phase of the waveform (e.g., a peak or trough), whereas the group velocity is the velocity of a packet of waves (Foti et al., 2014).

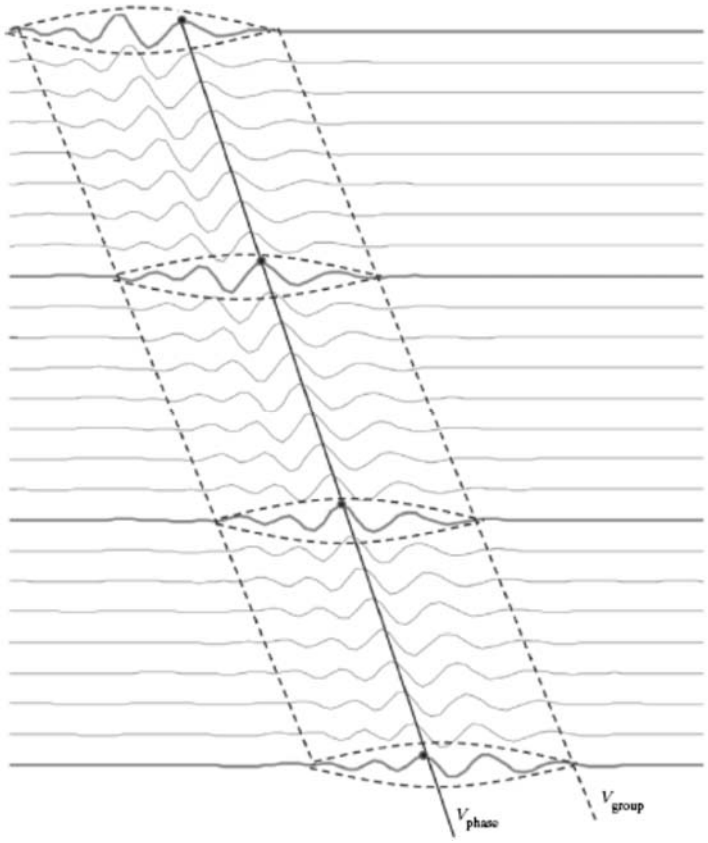

Figure 2-5: Phase velocity and group velocity, adapted from Foti et al. (2014)

The phase and group velocity can be expressed mathematically as:

$$V_{phase} = \frac{f}{k} = f\lambda$$
$$V_{group} = \frac{\partial f}{\partial k} \tag{2.7}$$

$$V_{group} = V_{phase} + k\frac{dV_{phase}}{dk} = V_{phase}\left(1 - k\frac{dV_{phase}}{d\omega}\right)^{-1} \tag{2.8}$$

Equation (2.8) shows the relationship between phase and group velocity. One implication of that equation is that when the derivatives of phase velocity are equal to zero (i.e., the material is nondispersive), the phase and group velocities are identical.

2.3.1 Spectral analysis of surface waves (SASW)

This method uses two receivers aligned with an active source. The spacing requires that the source is placed at the same distance as the spacing between the receivers (see Figure 2-6). Velocity is estimated as the ratio of the distance divided by time delay. For a single harmonic wave, the time delay is evaluated on a given phase of the signal. The method can be implemented using either harmonic sources or impulsive sources. Harmonic sources have the energy concentrated at a given frequency (high reliability in the determination as frequency is known). The advantage of using an impulsive source is that information over a wide range of frequencies is obtained with a single acquisition, allowing fast operations in the field (Foti et al., 2014).

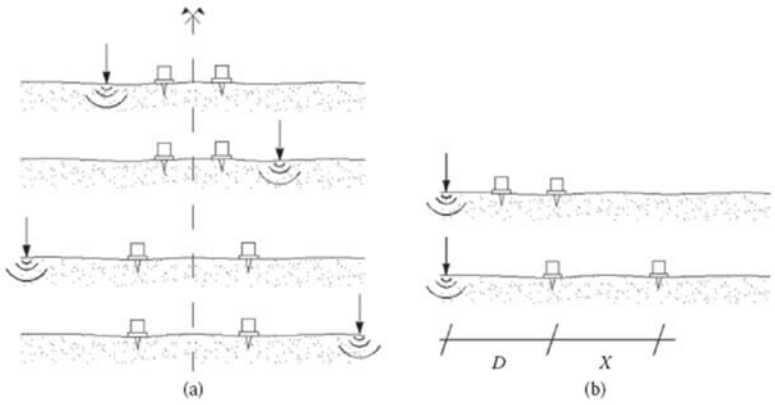

Figure 2-6: Test setup schemes for SASW testing: (a) common receivers midpoint; (b) common source

The time domain measurement data is transformed to the frequency domain:

$$s\left(x_m,t\right)\xrightarrow{F}S\left(x_m,\omega\right)=\left|S\left(x_m,\omega\right)\right|e^{i\left[\phi(\omega)+k(\omega)x_m\right]} \tag{2.9}$$

where $\phi\left(w\right)$ is the arbitrary source phase and $m=1,2$. The cross-power spectrum between the two signals is:

$$S_{12}=\overline{S}_1\left(\omega\right)S_2\left(\omega\right)=\left|S\left(x_1,\omega\right)\right|\left|S\left(x_2,\omega\right)\right|e^{ik(\omega)(x_2-x_1)} \tag{2.10}$$

where $\overline{S}$ denotes the complex conjugate of S. In practice, ensemble averaging is used to reduce the variance of the measured cross-power spectra (Bendat and Piersol, 2011).

$$\hat{S}_{12}(\omega) = \frac{1}{N}\sum_{k=1}^{N} \overline{S}_k(x_1,\omega) S_k(x_2,\omega) \tag{2.11}$$

where N is the number of spectra that are averaged. To extract the phase from the cross-power spectrum:

$$\theta_{12}(\omega) = \arg\left(\hat{S}_{12}(\omega)\right) = k(\omega)(x_2 - x_1) \tag{2.12}$$

To calculate the phase velocity dispersion curve we use Equation (2.13):

$$V_R(f) = \frac{\omega(x_2, x_1)}{\theta_{12}(\omega)} \tag{2.13}$$

To use Equation 2.13, it is required to unwrap the phase angle $\theta_{12}(\omega)$ for the frequency range of interest by adding integer multiples of 2π in the following manner:

$$\theta_{unwrap}(\omega) = \theta_{wrap}(\omega) \pm 2n\pi, \quad n = 0,1,2... \tag{2.14}$$

To evaluate signal quality it is necessary to assess the *coherence function*. The coherence function is a spectral function obtained by comparing different registrations, that is a measure of the degree by which input and output signals are linearly correlated as a function of the frequency. A value close to unity is an indication of good correlation. The coherence function between two receivers, γ_{12}, is defined as:

$$\gamma_{12}^2(w) = \frac{\hat{S}_{12}(\omega) \cdot \overline{\hat{S}_{12}(\omega)}}{S_{11}(\omega) \cdot S_{22}(\omega)} \tag{2.15}$$

where the upper bar denotes the complex conjugate.

2.3.2 Multi-offset phase analysis (MOPA)

MOPA is a surface wave analysis technique in which the phase versus offset of particle motion is processed to estimate the phase velocity (Strobbia and Foti, 2006). The algorithm is based on the fact that the surface wave displacement in the frequency domain, in a laterally

homogeneous medium and at a far offset from the source, can be written as a modal summation, separating the frequency-dependent and offset-dependent terms.

$$s(\omega,x) = \sum_{m} I(\omega) R_{m}(\omega) \frac{e^{-\alpha_{m}(\omega)x}}{\sqrt{x}} e^{i\left(\omega t - k_{m}(\omega)x + \varphi_{0}(\omega)\right)} \tag{2.16}$$

where $I(\omega)$, $R_{m}(\omega)$, $\alpha_{m}(\omega)$, and $\varphi_{0}(\omega)$ are the amplitude spectrum of the source, the site response for mode m, the intrinsic attenuation for mode m and the phase spectrum of the source, respectively.

When a single mode is present or dominant, the amplitude and the phase can be represented as:

$$A(\omega,x) = I(\omega) R(\omega) \frac{e^{-\alpha(\omega)x}}{\sqrt{x}} \tag{2.17}$$

$$\varphi(\omega,x) = -k(\omega) \cdot x + \varphi_{0}(\omega) \tag{2.18}$$

Within this procedure, the extraction of the phase information in the experimental data allows the estimation of the phase velocity as well as the identification of lateral variations and of near-field effects.

Wavenumber at each frequency and the associated standard deviation can be calculated using statistical data. Phase is described by a linear model as represented by Equation (2.19), which can be written for each receiver as:

$$\varphi_{i} = k \cdot x_{i} + \varphi_{0} \tag{2.19}$$

where the phase φ_{i} at the offset x_{i} depends on the unknown wavenumber k. Considering an array with N receivers, we obtain:

$$\begin{cases} \varphi_1 = k \cdot x_1 + \varphi_0 \\ \varphi_2 = k \cdot x_2 + \varphi_0 \\ \quad \vdots \\ \varphi_N = k \cdot x_N + \varphi_0 \end{cases} \tag{2.20}$$

that in matrix form can be expressed as:

$$\Phi = \mathbf{G} \cdot \mathbf{M} \tag{2.21}$$

where $\Phi = \begin{bmatrix} \varphi_1 & \varphi_2 & \dots & \varphi_N \end{bmatrix}^T$ is the vector of the experimental phases, $\mathbf{M} = \begin{bmatrix} k & \varphi_0 \end{bmatrix}^T$ is the vector of the unknown model parameters, and $\mathbf{G} = \begin{bmatrix} x_1 & 1 \\ x_2 & 1 \\ \vdots & \vdots \\ x_N & 1 \end{bmatrix}$ is the data kernel matrix, depending on the geometry (Menke, 2012).

The model parameters can be estimated in the least-squares sense by the pseudoinverse $\mathbf{G}^{-g}$

$$\mathbf{M} = \mathbf{G}^{-g} \cdot \Phi \tag{2.22}$$

with $\mathbf{G}^{-g} = \left(\mathbf{G}^T \cdot \mathbf{G}\right)^{-1} \cdot \mathbf{G}^T$.

Once the model parameters (wavenumber) have been determined, the phase velocity can be computed as:

$$V = \frac{2\pi \cdot f}{k} \tag{2.23}$$

Tarantola (2005) introduced a variation method to estimate the model parameter by using a weighted least-squares and replacing the pseudoinverse $\mathbf{G}^{-g}$ with the corresponding weighted version $\mathbf{G}_W^{-g}$. With the assumption of normally distributed and independent data, the linear relationship between the experimental phases and the model parameters is:

$$\mathbf{M} = \mathbf{G}_W^{-g} \cdot \Phi \tag{2.24}$$

and implies that:

$$\sigma_M^2 = \mathbf{G2}_W^{-g} \cdot \sigma_\Phi^2 \tag{2.25}$$

where σ_M^2 and σ_Φ^2 are the covariance matrices of the model parameters and of the data respectively, and $\mathbf{G2}_W^{-g}$ is the matrix containing the squares of the elements of $\mathbf{G}_W^{-g}$ (Santamarina and Fratta, 2005).

At each frequency of interest the mean value of the wavenumber and standard deviation can be calculated and then using Equation (2.23) phase velocity can be calculated. The standard deviation of the phase velocity is then estimated with a first-order approximation:

$$\sigma_V = \frac{2\pi \cdot f}{k^2}\sigma_K \tag{2.26}$$

For a laterally homogeneous medium and in the far-field of the source the phase is a linear function of the offset. However, this assumption is not valid for sites with lateral variations and some receivers may fall in the near-field for some frequencies (depending on source and array configuration) (Foti et al., 2014).

2.4 CHARACTERIZATION OF RAILWAY TRACK DEFLECTION

One of the methods for railway track and/or formation characterization that is generally accepted is through the calculation of track stiffness or track modulus using measured deflections imposed by known loads, generally moving rolling stock in the section under analysis. Several methods used for such characterization are briefly summarized below.

2.4.1 Beam on elastic foundation (BOEF) method

This method measures the vertical deflection y, at the point of an applied load P (load value is known). The ratio between the applied load and the deflection is known as track stiffness K and is given by Equation (2.27):

$$K = \frac{P}{y} \tag{2.27}$$

Track stiffness can be related to track modulus u, assuming a linear and elastic relationship between rail supporting load and deflection. These assumptions are known as the Winkler model and the resulting track modulus can be given by:

$$u = \sqrt[3]{\frac{K^4}{64EI}} \tag{2.28}$$

E is the modulus of elasticity of the rail and I is the moment of inertia of the rail. One limitation with this method is that it does not capture the changes in load – deflection curve present in real track (load – deflection curve is not linear).

2.4.2 Deflection basin method

The deflection based method uses the vertical equilibrium of the loaded rail and several deflection measurements (see Figure 2-7). Rail deflection caused by point loads is measured in several locations along the rail and the deflected area is calculated (Selig and Li, 1982):

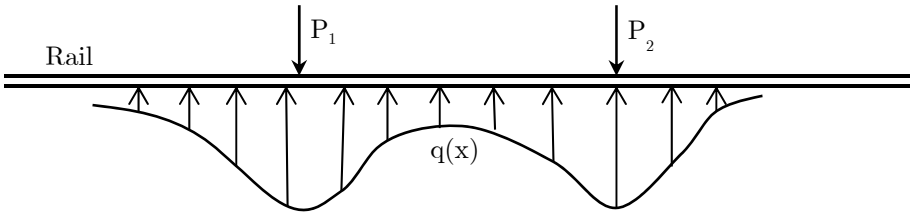

Figure 2-7: Deflection basin, adapted from Selig and Li (1982)

$$\sum P = \int_{-\infty}^{\infty} q(x)dx = \int_{-\infty}^{\infty} uy(x)dx = uA_y \tag{2.29}$$

A major limitation with this method is that it does not take into account the non-linearity of the load – deflection curve, due mainly to the seating of the sleeper on the ballast.

2.4.3 Heavy-Light load method

This method makes use of two stages of loading that are called seating load (load that enables the sleeper to make contact with the ballast) and full load (at maximum deflection, with high

load). A linear relationship is assumed for the load – deflection curve between these two points for calculating the track stiffness.

$$K = \frac{P_2 - P_1}{y_2 - y_1} \tag{2.30}$$

Index 2 represents the full load and index 1 represents the seating load.

2.5 OVERVIEW OF RESEARCH WORK ON RAILWAY TRACK FORMATIONS USING VIBRATION AND GEOPHYSICAL TECHNIQUES

Most of the vibration research work that has been carried out is due to the complaints the rail transport operators have received by people living alongside or above underground lines. The disturbance is caused by the direct emission of noise or vibration from the railway or vibration of walls in buildings causing indoor noise.

Typically, these vibration problems are associated with passenger rail systems, which have an increased demand for capacity over the years, resulting in higher train operating speeds and operations.

Several authors studied this phenomenon. In particular, research work performed by Krylov and Ferguson (1993) and Krylov (1995), presented a theoretical model for the excitation mechanism of ground vibrations generated by trains, using Green's function formalism. Expressions for the ground vibration spectra have been obtained as functions of track, train and soil parameters. Vibration spectra depend strongly on the axle loads of the carriages: if the axle load exceeds a critical value beyond which peripheral bulges appear in the track, the vibration level increases significantly, especially at higher frequencies. By proper selection of the distance between wheel axles in a bogie, and between bogies in a carriage (or between sleepers in a track) it is possible to effectively suppress vibration levels at the train passage frequencies.

The increased speeds of modern trains are normally accompanied with increased transient movements of the rail and ground, which are especially high when train speeds approach some critical wave velocities in the track – ground systems (Krylov et al., 2000).

Suiker et al. (1999) discussed propagation of surface waves in a stratified half space (elastic granular layer resting on a half-infinite elastic substratum), considering the influence of ballast particle size, ballast layer thickness and formation on the critical behaviour of the track system. Making analogy to the South African track systems, the elastic granular layer represents the ballast, whilst the half-infinite elastic substratum represents the formation system (see Figure 2-8). Several considerations for the ballast thickness and particle sizes were made and a soft (sand material) & stiff (rock material – for ballasted tracks in tunnels) were made for the half-infinite elastic substratum.

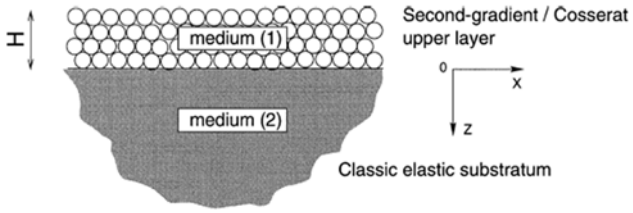

Figure 2-8: Upper layer resting on a classic elastic half-infinite substratum, adapted from Suiker et al. (1999).

The main conclusions that Suiker et al. (1999) established are listed below.

- Multiple surface wave modes are generated in the case of a soft layer on top of a stiff halfspace. The number of modes decreases with increase in particle size. Phase velocity of higher modes can be higher than the maximum shear wave velocity;

- One wave mode is generated when a stiff layer rests on a soft substratum as a result of high frequency waves being dissipated into the substratum;

For the critical behaviour of the stratified half space under a moving vibrating load the following was concluded (Suiker et al., 1999):

i. The case of a ballast layer on a stiff rock formation was also examined. In the high-frequency range this case is also representative of ballast layers on concrete slabs (railway tunnels, railway bridges), because short wave lengths will not be affected by the half-infinite character of the substratum. They demonstrated that both the layer thickness and the grain size influence the critical behaviour, where the lowest critical load velocity appears to be within the velocity domain of a high-speed train. When the rail is supported by sleepers, an increasing ballast layer thickness leads to a decreasing critical velocity. If, instead of using a discrete sleeper support, the track is continuously supported, the lowest critical velocity considerably increases and will be equal to the Rayleigh wave velocity of the ballast layer. This critical velocity is independent of the ballast layer thickness.

ii. For the case of a ballast layer on a soft substratum, the lowest critical velocity equals the Rayleigh wave velocity of the substratum. As discussed, excitation sources such as the sleeper distance effect will not influence the magnitude of this critical velocity.

Hall (2003) conducted experimental studies (see Figure 2-9) and then developed mathematical and numerical methods in time and frequency domains. 2D and 3D models were studied. He found that 3D models gave better simulation of the problem, although 2D models could be used to study certain effects of train-induced ground vibrations. Additionally, he concluded that at train speeds lower than the propagation velocity of the ground, the induced wave fronts were perpendicular to the loads. For train speed faster than the shear and Rayleigh propagation velocity of the ground, the induced wave fronts showed a plough-shaped behaviour following the loads. Moreover, the motion orbits calculated from the three-dimensional analyses indicated that the Rayleigh wave was the dominating wave type outside the embankment.

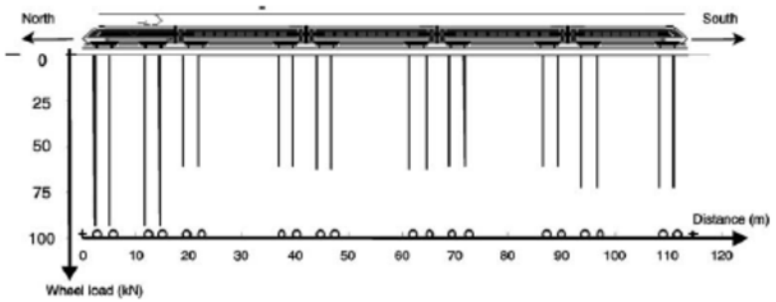

Fig. 5. Wheel load of the X2000 train used in the Ledsgaard tests.

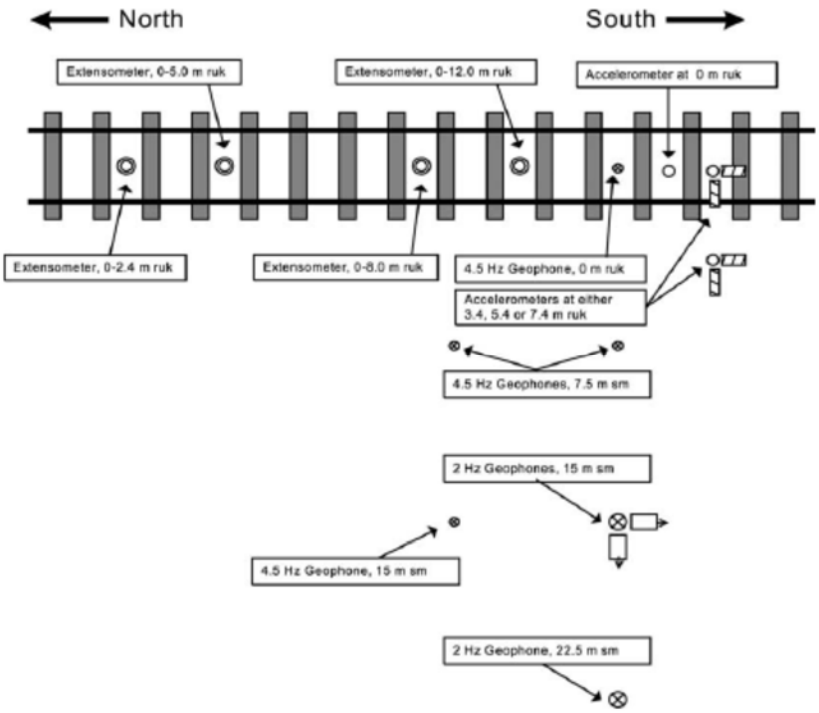

Figure 2-9: Test setup for ground motion measurements of train-induced ground vibrations, adapted from Hall (2003)

Other researchers also developed models to predict ground vibrations induced by high speed trains, such as the work from Paolucci et al. (2003). Yang et al. (2003), Connolly and Forde (2015) performed parametric studies to determine amongst other parameters, the critical train speeds. The latter work established that conventional site investigations do not yield data appropriate for input parameters in non-linear FE models. However, using empirical analysis developed by Jamiolkowski et al. (1979), results from conventional site investigations could be used.

Jongmans and Demanet (1993) discussed the importance of surface waves in vibration studies and the use of Rayleigh waves for estimating the dynamic characteristics of soils. Vibrations generated during civil engineering work are often dominated by surface waves, the propagation of which is strongly influenced by site conditions. They investigated the effects of soil properties on the characteristics of Rayleigh waves and concluded that the wave characteristics were very sensitive to soil conditions and that their dispersion properties could be used for determining the dynamic shear characteristics of the superficial soil deposits in horizontally layered media.

Kaewunruen and Remennikov (2007) performed in-situ dynamic testing to assess the condition of railway track structure and components, using an impact excitation technique called *"modal testing"*. They determined the dynamic stiffness and damping constants of track components which could then be used to determine maximum speed and axle load for future track upgrades. They combined the experimental modal analysis and finite element modelling to evaluate the dynamic parameters of the track components. Track components investigated were fastening systems and concrete sleepers. The testing equipment comprised a hammer and an accelerometer to measure track response. The test section was a ballasted coal export line. Typical results obtained were stiffness and damping ratio values for rail pads and ballast. They concluded that this type of testing can provide maintenance crew information regarding the current state of the track (and its components) and a benchmark for health monitoring. In addition, the experimentally determined resonance frequencies along with the dynamic properties of the track components can provide an important input to the dynamic analysis of railway track for determining the maximum speed and axle load for future track upgrades or functional change.

Dynamic displacements of railway tracks under loading from moving rolling stock, measured with vertically orientated geophones were investigated by Bowness et al. (2007), using two relatively new techniques (remote video monitoring and geophones). From this work they established suitable operations range in which the geophones could be employed to accurately measure track displacement history from a train passage.

Following on the work performed by Bowness et al. (2007), research work was carried out by Priest et al. (2010) to measure the dynamic response of the ground below a ballasted track during passage of a heavy haul train. The aim of the study was to improve understanding of ground behaviour during dynamic loading and to calibrate a numerical model.

2.6 DISCUSSION

From Sections 2.1 to 2.4, the relevant research work and literature currently available in the fields of geotechnical engineering and wave propagation theory, applicable to the problem being addressed in this research project, were outlaid.

From the published work it is possible to establish that the majority of research work in the field of railway operations induced vibration or disturbances has been to mitigate the adverse effects that are raised when surrounding infra-structure adjacent to the railway tracks are subjected to such vibrations. Numerical models have been established for freight trains and high speed trains to predict behaviour of track – ground systems.

The increased use of high speed trains to accommodate new traffic or demand scenarios have also contributed towards research work being devoted to better understanding and prediction of the train critical velocity from Rayleigh waves and ground borne vibrations.

Research work using geophones and accelerometers, to measure track formation response at surface and depth during train passage has also been carried out on South African lines (Coal line) and abroad. However, this approach considered the displacements that can be obtained by integrating the recorded velocity or acceleration of the geophysical receiver when loaded by the train wheels. This approach does not take into account the ground motion or disturbance caused by the propagation of waves, along the formation layerworks, as observed on extremely poor formations along the heavy haul lines in South Africa.

Theory of elasticity and wave propagation was briefly discussed. The magnitude of strain imposed on the medium being loaded has an influence on the models that can be used to simulate the behaviour of the medium as well as energy dissipation. Taking into account the propagation characteristics and energy distribution of the two main types of waves, namely

body and surface waves, it is possible to establish that surface wave components can be adopted for characterizing near-surface sites.

In the literature it was found that methods for dispersion analysis of surface waves are based on two types of tests: active and passive. Active tests are performed with the source of the waves being a (mechanical) shaker for continuous wave generation or a hammer/dropped weight for impulse wave generation. Linear arrays are associated with these type of tests. Passive tests are associated with civil engineering or environmental action in the vicinity of the site being tested. Non-linear arrays are normally used.

Considering that the testing protocol being adopted for this research work considers the rolling stock on the railway track as the source of generating the waves and the linearity of the train movement, a linear array was adopted. However, because the energy levels being transmitted to the media from the train are unknown, both active and passive methods will be adopted for the dispersion analysis, in order to check the reliability of the testing protocol and suitability of the methods to the railway environment.

3. INSTRUMENTATION SETUP AND DATA ACQUISITION

3.1 Introduction

This chapter provides the methodology employed during the collection of site data and the measurement of the dynamic vibration and displacement of the track formation. A brief summary of the geological conditions in which the sites are located will be given.

A description of the testing and array setup will be given and the equipment used for the geophysical testing will be discussed in detail. Major findings from literature review contributed to defining the experimental setup. These points are briefly discussed below.

3.2 Definition of experimental setup

As discussed in Chapter 2, the vertical component of the Rayleigh wave's dissipative characteristics makes them ideal for shallow geotechnical characterisation of sites. Having considered this, the testing protocol established for this research programme comprised placing the receivers on top of the formation[1] where the vertical component of ground motion would be measured.

Figure 3-1 below illustrates the location of the receivers on top of the subballast layer. The dotted (red) line indicates the position of receivers. Geophones, capable of measuring vertical component of ground movement were adopted as receivers.

It was also highlighted during literature review that available dispersion analysis methods for passive or active testing considered several array configurations based on the knowledge (or not) of the source of disturbance. In this particular case, the sources of ground disturbance are the moving trains and a hammer impacting the railhead. As such, a linear array was adopted.

[1] For the purpose of this report, formation is to be understood as the part of the railway track comprises the following layers: subballast, fill (placed soil) and in-situ material (natural subgrade)

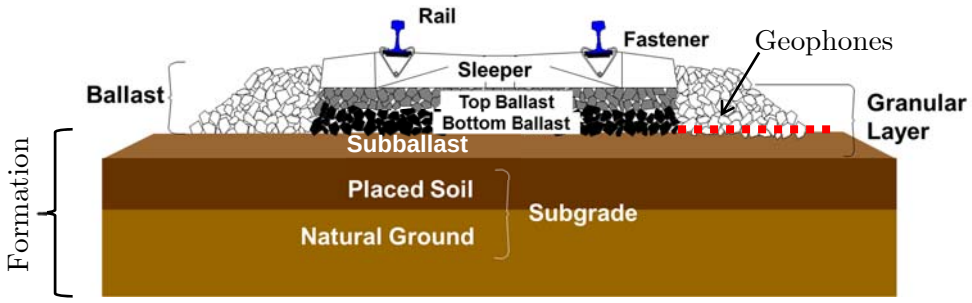

Figure 3-1: Typical cross section of a freight railway line track and the location of the receivers.

It was also highlighted that reviewed dispersion analysis methods were derived for very small strain regimes. Therefore, it was reasoned that all data to be accepted for processing would have to fall under this criteria. This is discussed in the following paragraphs.

Rolling stock related events were recorded from the moment the train was sighted (typically in excess of 20 seconds before reaching the instrumented site) until the last wagon had passed the measurement area. Data that was accepted for processing from this type of events was the portion of the recording before the train had reached the measurement site.

Hammer generated vibrations were recorded from a few seconds before impact until the end of a multiple blow (typically 4 blows, spaced at 10 seconds interval). All data generated from these measurements were accepted for processing.

In conjunction with the geophysical exploration to investigate the waves propagating in the formation, deflection data was also obtained using Remote Video Monitoring technology. Test setup and measurement procedures will be explained.

3.3 BACKGROUND OF TEST SITES

Sites for testing were selected in the Limpopo and KwaZulu-Natal (KZN) provinces on existing railway lines. The following sites were chosen:

- Test section 1 – Amandelbult, on the Rustenburg – Thabazimbi Line (20 t axle load);
- Test section 2 – Bloubank, on the Coal Line (26 t axle load);

- Test section 3 – Izolof, on the Coal Line (26 t axle load). This test is further subdivided in two sessions split between rehabilitation work carried out in May 2015.

3.3.1 Test section 1 – Amandelbult

The test section on the Rustenburg – Thabazimbi line was located between MP 213/5 (213+301 m) and MP 213/6 (213+371 m). Tests at Amandelbult were performed between 02 and 06 March 2015. See Figure 3-2 for a geological map of the Amandelbult area.

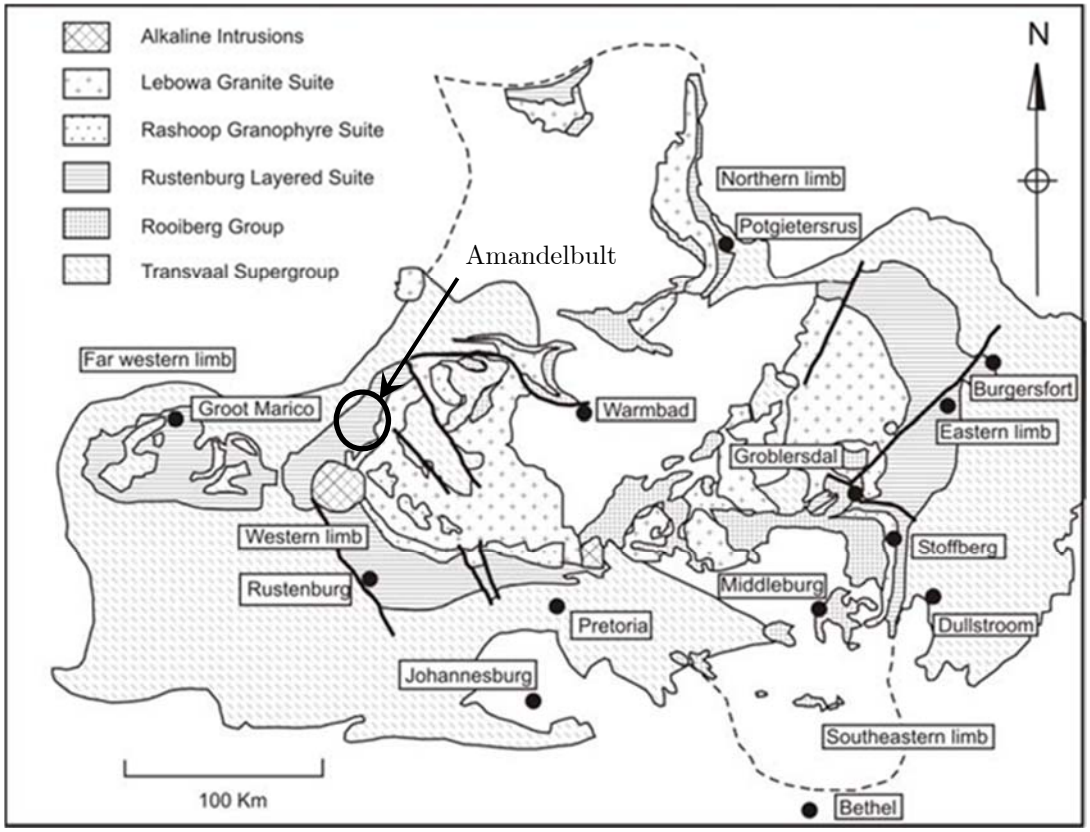

Figure 3-2: Geological map of the Amandelbult area, adapted from Kinnaird (2005)

The site is located in the Transvaal system & Bushveld complex. It has basic crystalline rocks (Gabbro and Norite) which weathers to highly reactive montmorillonite clay (840 m^2/g). The area is dominated by the occurrence of intrusive igneous rock (gabbro and norite).

The presence of potentially expansive soil profiles resulted in extensive rehabilitation work on the line during the 2000 – 2005 period. Approximately 63% of the 191.6 km of the line was prioritized for rehabilitation.

The railway track at this site is in relative good condition, accommodating traffic with an axle load of up to 20 tonnes. Although a considerable portion of the railway track at the site was rehabilitated, and several subgrade improvement techniques have been experimented with, the formation on the specific test site instrumented with the geophysical receivers was not upgraded and was used as a control section for some of the improvement techniques. As such, the original formation is still in place, which consists of:

- natural gravel material (imported material) to form a subballast layer;
- a clayey (lithomorfic vertisols also known as "black turf") existing / insitu subgrade material with thickness of up to 1 m;
- weathered norite rock, underneath the "black turf".

Figure 3-3 and Figure 3-4 below depict the track structural layers and general conditions of the track.

Figure 3-3: Overview of existing layerworks at the Amandelbult test section

The site is at a crossing loop between the towns of Northam and Thabazimbi. All tests were performed on the main line that carries the loaded trains. Figure 3-4 gives an overview of the Test Section at Amandelbult.

Figure 3-4: Overview of track at Amandelbult with instrumentation ready for data collection

The section which was instrumented for the purposes of this research project is adjacent to a Tubular Modular Track (TMT) section and several improved subgrade sections. Additionally, the railway line runs parallel to a road which carries a considerable portion of heavy vehicles. The impact of the traffic on the measurements and on the results will be assessed in the subsequent chapters.

3.3.2 Test section 2 – Bloubank

Tests at Bloubank were performed between 16 and 20 March 2015. The test section was located between MP 60/17 and MP 60/18 of the Coal Line between Vryheid and Ulundi, KwaZulu-Natal. The railway track at this site was in good condition, accommodating traffic with an axle load of up to 26 t, and is located on a horizontal curve, with a relatively large radius.

The geology of the area comprises weathered tillites forming part of the Vryheid geological formation, Dwyka Group Formation (see Figure 3-5).

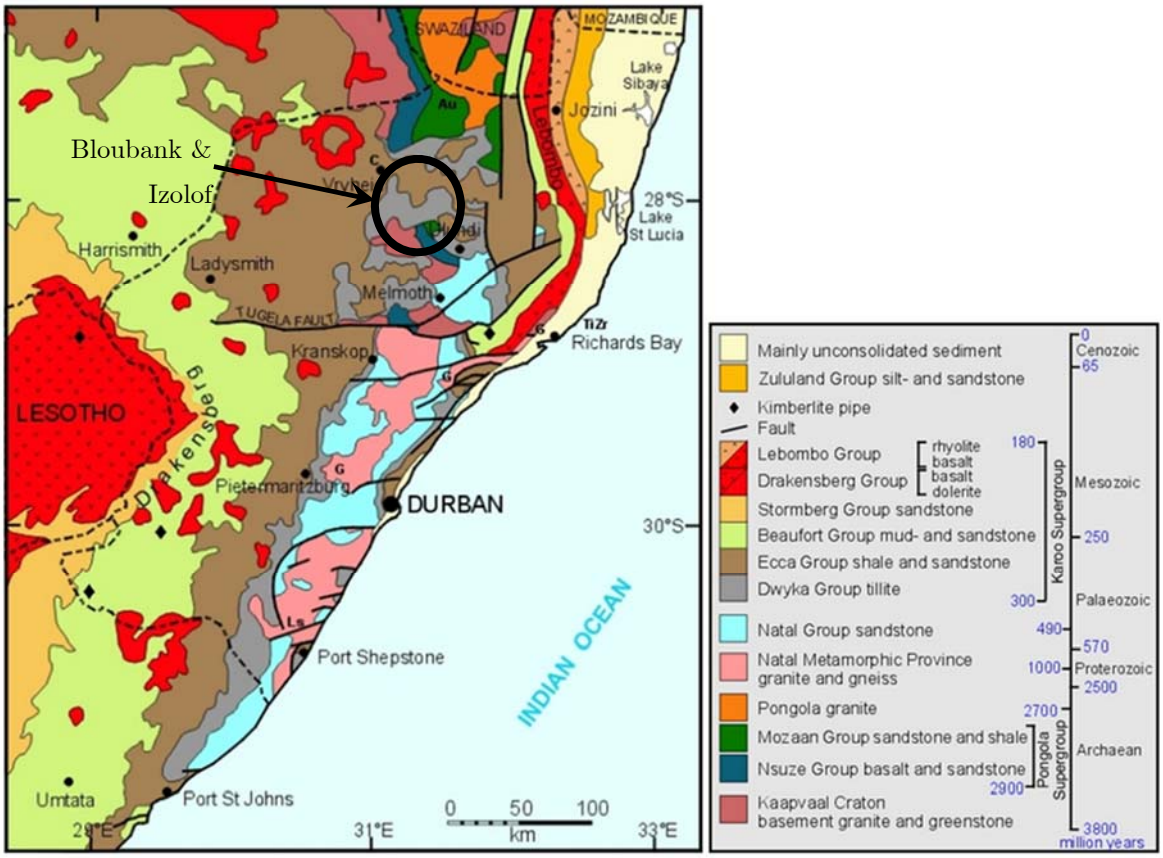

Figure 3-5: Simplified geological map of KwaZulu Natal.

Formation layers on this specific section of the track that was tested is depicted in Figure 3-6 below.

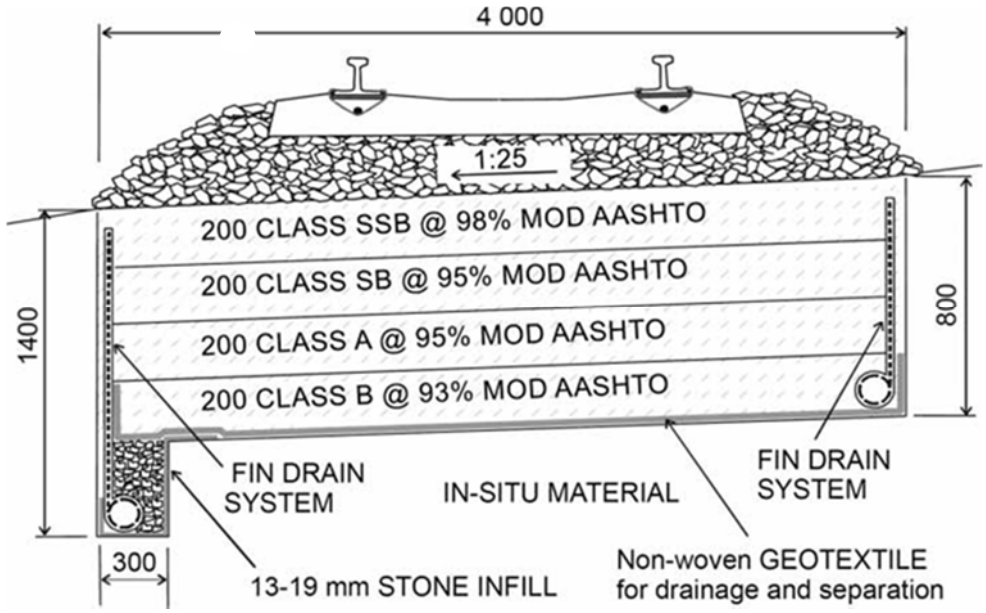

Figure 3-6: Formation layerworks for the Coal Line, adapted from Vorster and Grabe (2010).

All tests were performed on the Number 1 line that carries the loaded trains (see Figure 3-7). The layerworks comprised of the following:

- A special subballast layer (SSB layer), 200mm thick, of crushed stone material, compacted to a minimum of 98% modified AASHTO density;
- A subballast layer (SB layer), 200mm thick, of crushed stone material, compacted to a minimum of 95% modified AASHTO density;
- A selected layer (layer A), 200mm thick, of natural gravel material, compacted to a minimum of 95% modified AASHTO density;
- A selected layer (layer B), 200mm thick, of natural gravel material, compacted to a minimum of 93% modified AASHTO density;

Figure 3-7: Overview of testing section at Bloubank

3.3.3 Test section 3 – Izolof

Izolof is located 14 km from Bloubank on the Coal line. All details regarding the geology and track formation layers are similar to the Bloubank test site, except for the fact that the test site is located in a cut section, between MP 73/5 and MP 73/6.

Two sets of tests were conducted at this site. Test 1 was performed whilst track quality was poor, during the day of March 18th, 2015. It is however worthwhile to mention that ballast tamping was performed earlier in the morning, before the test measurements began. Figure 3-8 shows site conditions at the beginning of test session. Mud pumping increased the moisture content of the formation on the line under testing to high levels of saturation (see Figure 3-9).

Figure 3-8: Izolof site at the start of testing (March 2015)

Figure 3-9: Increased moisture during the testing (Izolof - March 2015)

A second session of tests were performed during August 2015, after the track formation of Line 1 was reconstructed between MP 73/5 and MP 73/6. At the time when this 2nd session of tests was conducted, track quality was good.

Figure 3-10: Test session at Izolof (August 2015)

3.4 TESTING EQUIPMENT

Surface wave tests are performed using a source, one or more receivers and instrumentation to record and process the data (see Figure 3-11). Sources may be either active or passive and may produce either transient or continuous surface wave energy. Equipment used for data collection as part of this research project included the following testing devices:

- Geophones were used as receivers;
- Data acquisition unit: HBM QuantumX MX410;
- Strain gauges to measure vertical wheel loads from moving rolling stock;
- Remote Video Monitoring (RVM) equipment;
- Source of ground disturbance: rolling stock operating on the line and a hammer;
- Data processing software: CatMan AP (data acquisition and FFT), CMSW (FFT) and Matlab v2013 (FFT and dispersion analysis).

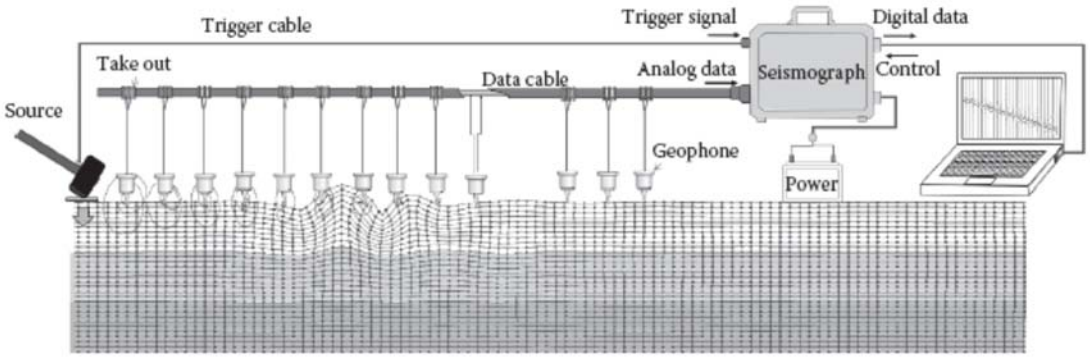

Figure 3-11: Typical surface wave testing configuration, adapted from Foti et. al (2014)

3.4.1 Sources for geophysical testing

All testing was conducted with the source of formation deformation being a moving train on the line under investigation. Track response to loaded and unloaded trains at different travelling speeds were recorded. A typical train travelling on the line under study is shown in Figure 3-12.

Additionally, for the purpose of validating and comparing the dispersion curves obtained for each of the sites tested, impulsive testing was also conducted by impacting the railhead with a hammer to produce vibrations.

Figure 3-12: Loaded train running on Line 1 of the Coal Line at Izolof

On the Thabazimbi – Northam railway line only type 7E locomotives were running and were therefore used in the measurements. On the Coal Line, 7E, 11E and 19E locomotive types are used and were therefore included in the test measurements.

3.4.2 Receivers

A total of 5 geophones were used as receivers to measure ground vibrations. Additionally, in some testing setups, one accelerometer was also used.

Geophones are velocimeters (i.e. electrodynamic velocity transducers). The vibration of the soil causes a displacement of the geophone casing. Due to its inertia, the relative movement of the coil produces a small voltage proportional to the relative velocity. The axis of movement can be horizontal or vertical. For this research, vertical geophones were used.

GS-11D geophones manufactured by Geospace were used as receivers. The GS-11D is a high output, rotating coil geophone designed and built to withstand the shocks of rough handling.

Gold plated contacts assure positive electrical connections. Natural frequency for this geophone is 4.5 Hz with standard coil resistance of 380 ohms. The PC-21 Land Case is used with the GS-11D geophone.

Figure 3-13: GS-11D placed on top of the subballast layer to measure vertical ground vibration

3.4.3 Data acquisition and processing systems

The main functions of data acquisition systems are conditioning, sampling and digitizing the signal generated by the transducers. These functions were performed by a central unit receiving the analog signals from the receivers array. For this research a 2 module system of HBM's QuantumX MX410 amplifiers were used (see Figure 3-14).

Figure 3-14: Data acquisition system used for testing

3.5 OVERVIEW OF TEST SETUPS

3.5.1 Setup for geophysical testing

In surface wave testing, several array configurations can be used for the measurement of ground vibrations, taking into account the type of testing being undertaken (active or passive testing). Taking into consideration the linearity of the rolling stock movement, linear array configurations were adopted for the purposes of this research. All receivers were therefore placed parallel to the railway track.

Table 3-1 below shows a summary of the test setup configurations at the different testing locations. Each testing setup adopted during field measurements are indicated and are briefly detailed below:

- Each reference row describes a particular test setup. Test setup identification is done in column 2 (Setup);

- Number of receivers used, average spacing and receiver array length are indicated in the subsequent columns 3 to 5;

- The figures given for column 6 (hammer offset) indicate the distance from Geophone 1 to the point of impact in the railhead. Exception to that rule is the figure indicated in

parentheses, which represents the distance in regard to Geophone 5 at one of the test setups in Amandelbult;

- The figures in parentheses shown in the column displaying the number of tests performed for each array configuration represent the number of measurements of the total that were done on the instrumented site (on Line 1) whilst the train was moving on Line 2 (applicable to Bloubank and Izolof). The number of hammer tests is indicated after the slash (/).

Table 3-1: Summary of testing records

Reference	Setup	Number receivers	Average spacing (mm)	Array length (mm)	Hammer offset (mm)	Number of tests (train/hammer)
Amandelbult 1	A1	5	2116	8465	10500 / (7000)	5 / 3
Amandelbult 2	A2	4	1363	4090	-	4
Bloubank 1	B1	5	1997	7990	-	12 (3)
Bloubank 2	B2	4	1983	5950	-	13 (5)
Bloubank 3	B3	2	2100	2100	-	7 (4)
Izolof Before 1	I1	5	1980	7920	-	10 (7)
Izolof Before 2	I2	4	1957	5870	-	1
Izolof Before 3	I3	4	1915	3830	10500	7 (4) / 2
Izolof After 1	I4	5	1995	7980	-	13 (6)

Illustrations of the array configurations summarized in Table 3-1 above, are shown in the figures below. It is important to state that in conjunction with this research, a second field measurement was also carried out, using at least one of the receivers available, and hence some of the setups did not make use of all 5 receivers available.

Details for each test performed are included in Appendix A. Details include train loads, speed, sampling frequency, direction of rolling stock movement and rolling stock characteristics.

3.5.1.1 Amandelbult Test setup 1 (A1)

Receivers were placed parallel to the railway line, with an offset of 240 mm from the edge of the sleeper. Hammer tests were conducted impacting the railhead in two locations: 0ne test at 10.5 m from Geophone 1 (closer to 213/MP 6) and two tests at 7 m from Geophone 5 (closer to 213/MP 5). This test setup is illustrated below (see Figure 3-15).

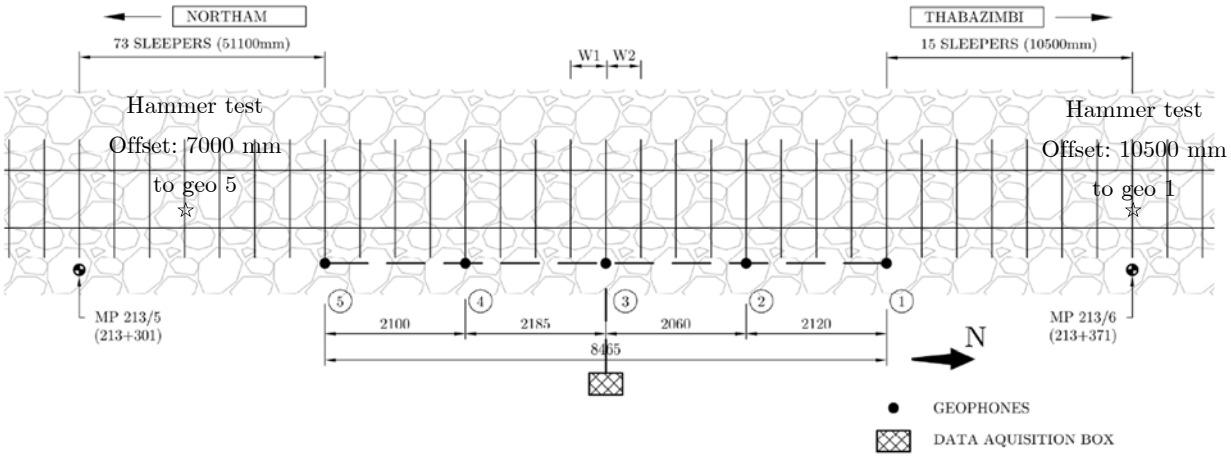

Figure 3-15: Amandelbult Test setup 1 (A1)

3.5.1.2 Amandelbult Test setup 2 (A2)

This setup makes use of 4 receivers at a smaller interval between receivers. The overall length of the receiver array is reduced to close to half of the length used on Setup A1. The offset of the receiver array to the edge/side of the sleeper is 170 mm.

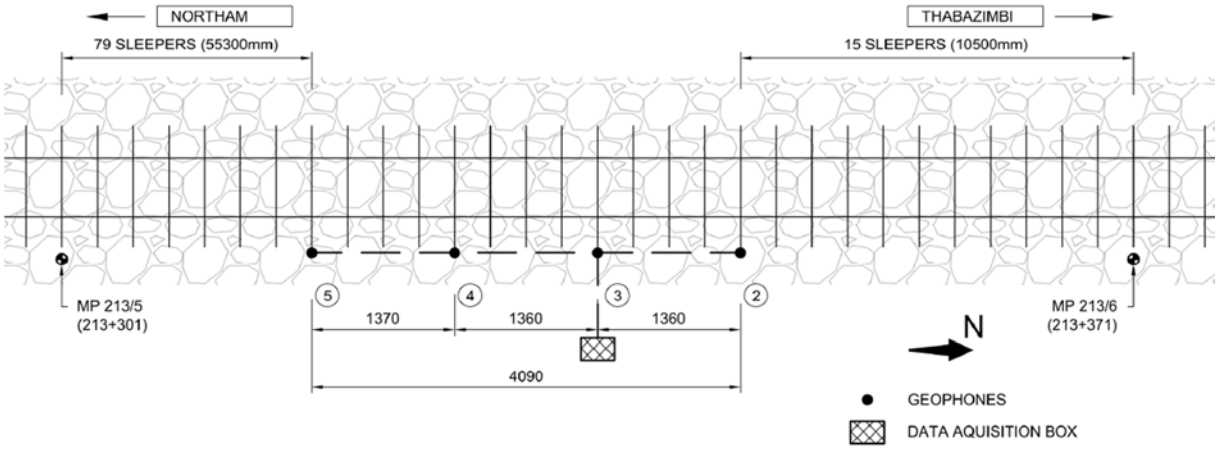

Figure 3-16: Amandelbult Test setup 2 (A2)

3.5.1.3 Bloubank test setup 1 (B1)

Five geophones were placed parallel to the railway line, with an offset of 490 mm from the edge of the sleeper. The total length of the test setup was 7990 mm. This test setup is illustrated in Figure 3-17.

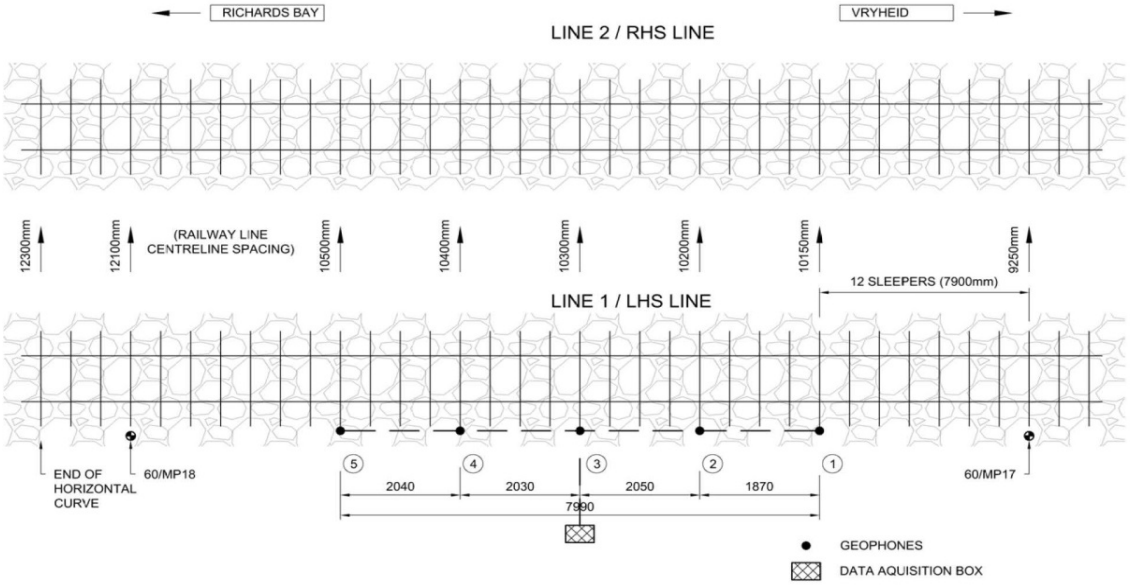

Figure 3-17: Bloubank Test setup 1 (B1)

3.5.1.4 Bloubank Test setup 2 (B2)

Test setup B2 used 4 geophones. Geophone 5 shown in Figure 3-17 above was placed on the sleeper aligned with Geophone 4, and it is not shown below. The total length of the array was 5950 mm.

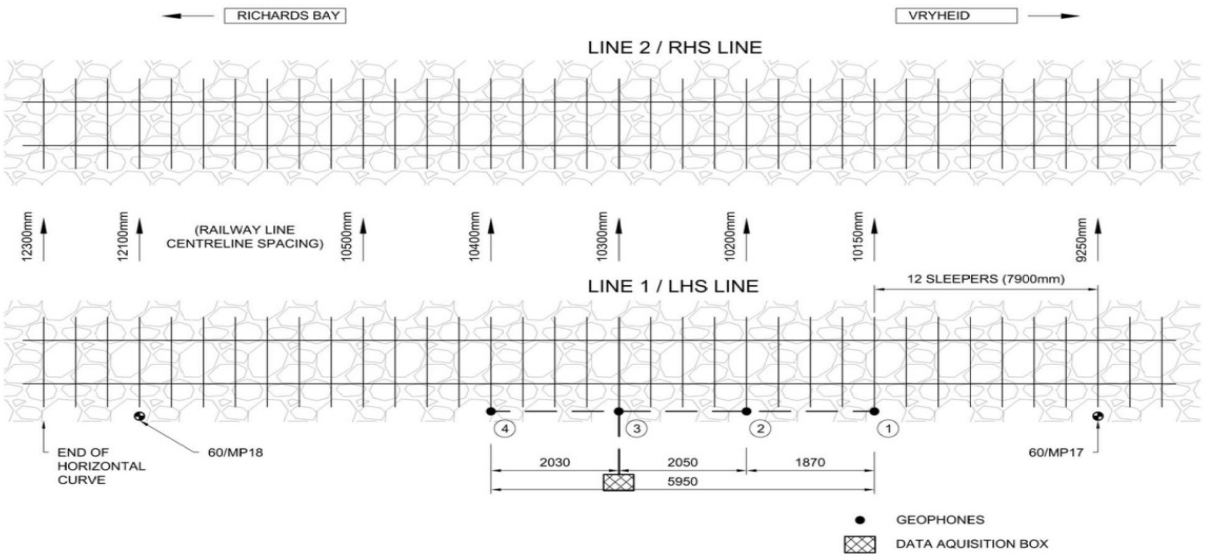

Figure 3-18: Bloubank Test setup 2 (B2)

3.5.1.5 Bloubank Test setup 3 (B3)

Test setup B3 was mainly used for attenuation analysis. As such, it did not have a linear array configuration similar to the configuration of the other test setups.

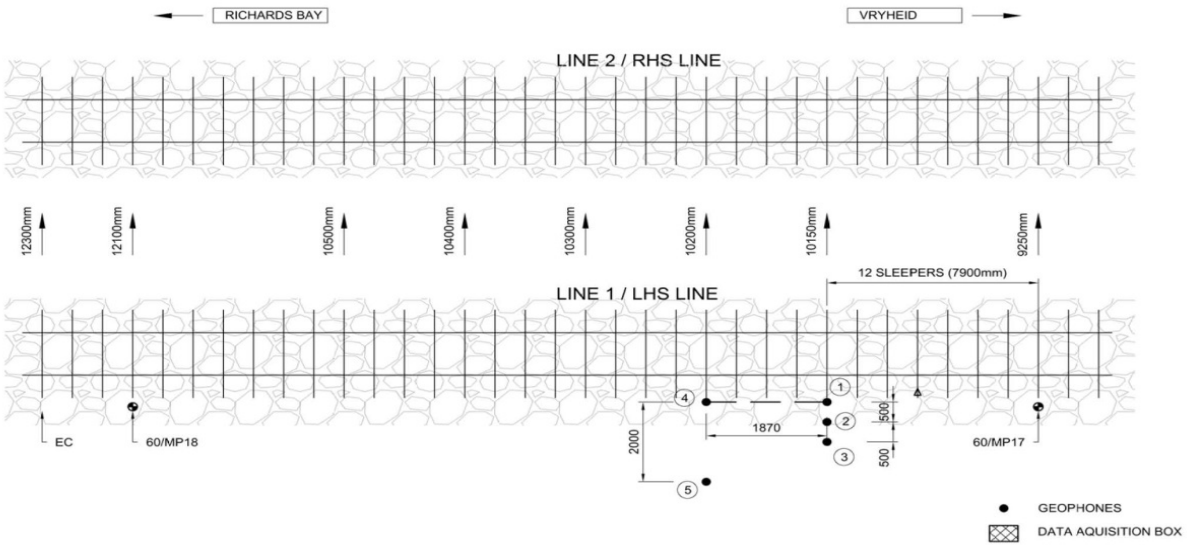

Figure 3-19: Bloubank Test setup 3 (B3)

3.5.1.6 Izolof Test setup 1 (I1)

Test setup I1 consisted of a linear array of 5 geophones with a total length of 7920 mm. The offset from sleeper edge was 490 mm on average. Because of tamping operations on Line 1, most of the measurements or tests done using this test setup were whilst ground motion was being caused by rolling stock moving on Line 2.

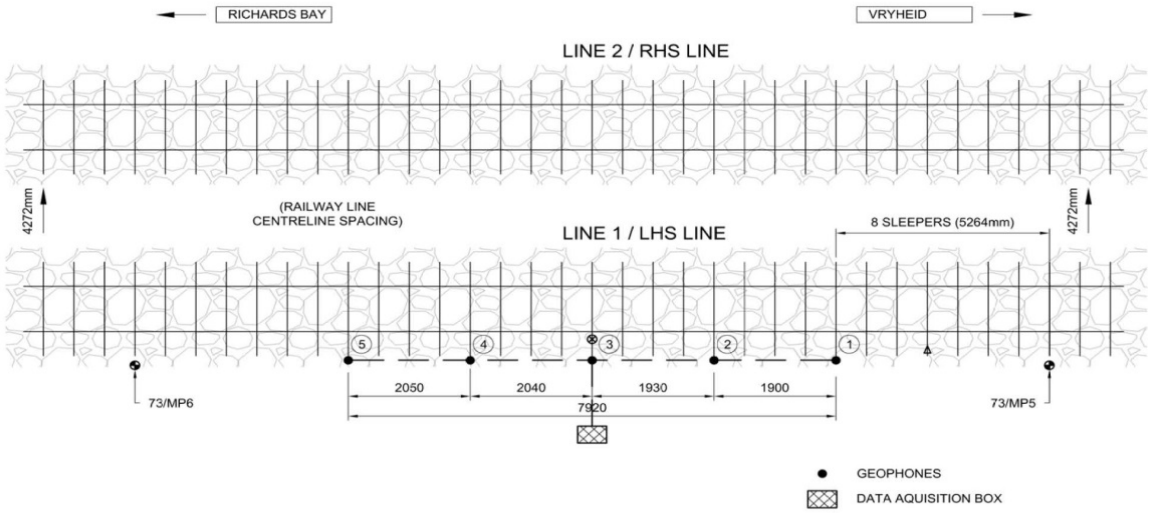

Figure 3-20: Izolof Test setup 1 (I1)

3.5.1.7 Izolof Test setup 2 (I2)

This test setup is similar to Test setup I1, the only difference being that Geophone 5 was not used.

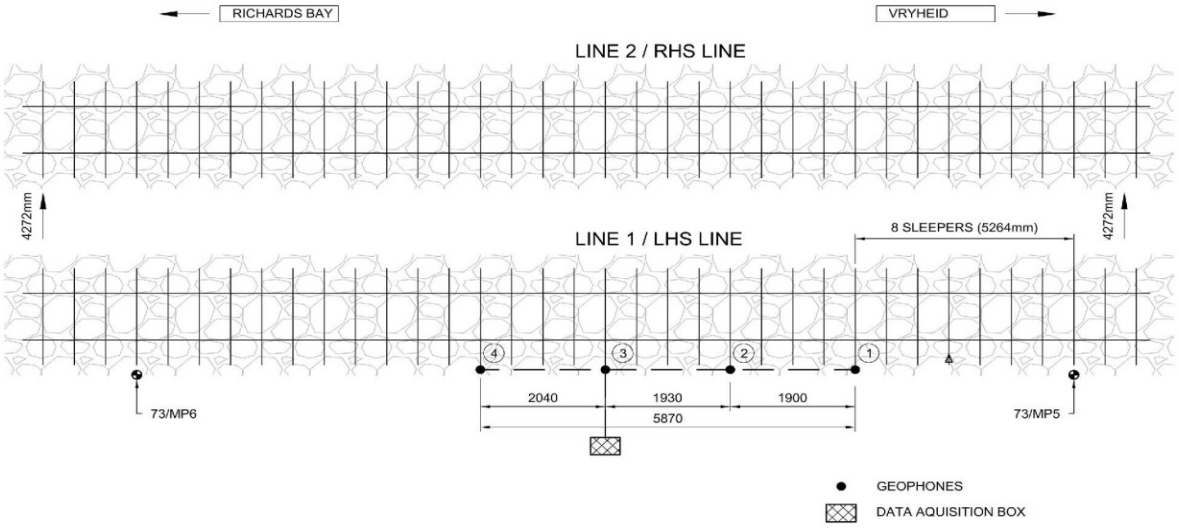

Figure 3-21: Izolof Test setup 2 (I2)

3.5.1.8 Izolof Test setup 3 (I3)

Test setup I3 was mainly used for attenuation analysis. As such, it did not have a linear array configuration similar to the configuration of other test setups. Hammer tests were conducted impacting the railhead at 5.264 m from Geophone 1 (located at 73/MP 6)

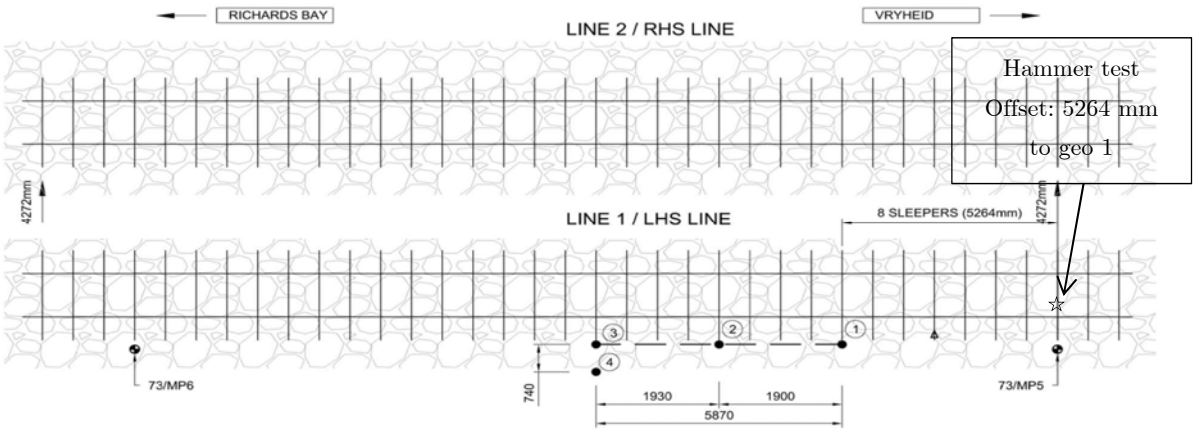

Figure 3-22: Izolof test setup 3 (I3)

3.5.1.9 Izolof test setup 4 (I4)

This test setup was adopted for the field experiment after this section of the coal line was rehabilitated. It consisted of a linear array of 5 geophones with a total length of 7980 mm. The offset from sleeper edge was 620 mm on average. Ground vibration derived from movement of rolling stock on lines 1 and 2 were recorded.

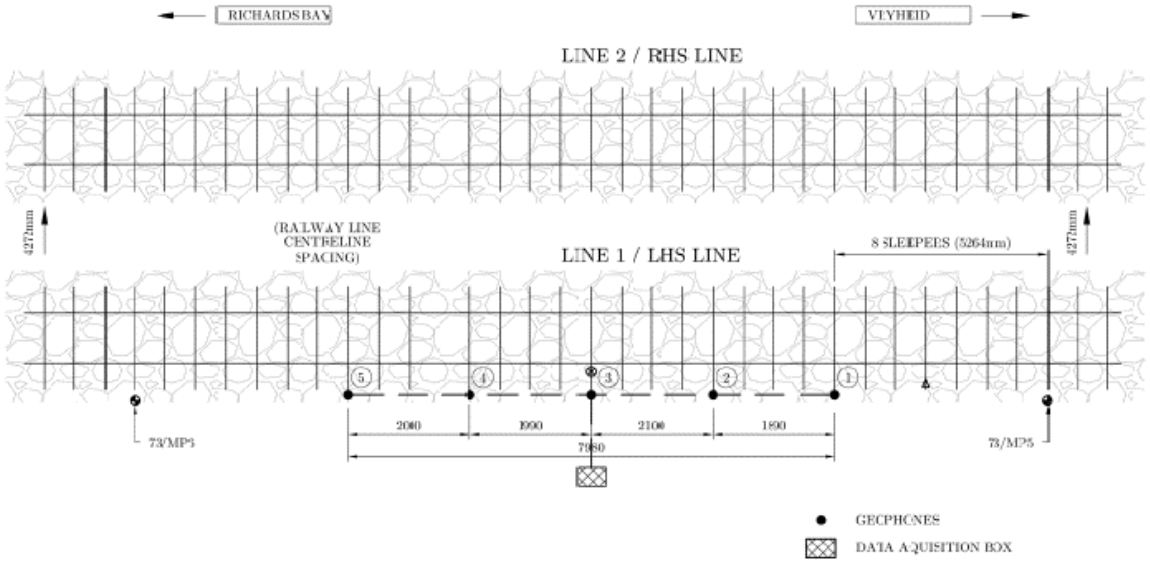

Figure 3-23: Izolof Test Setup 4 (I4)

3.5.2 Remote Video Monitoring Setup

For measuring track displacement at all instrumented sites, targets were installed on sleepers and additional targets were attached to rods driven into the subballast layer for measurements

of deflection on top of the formation. Cameras pointing to the targets were installed on tripods away from the track to record the displacements incurred by the targets during the passage of a train (see Figure 3-24).

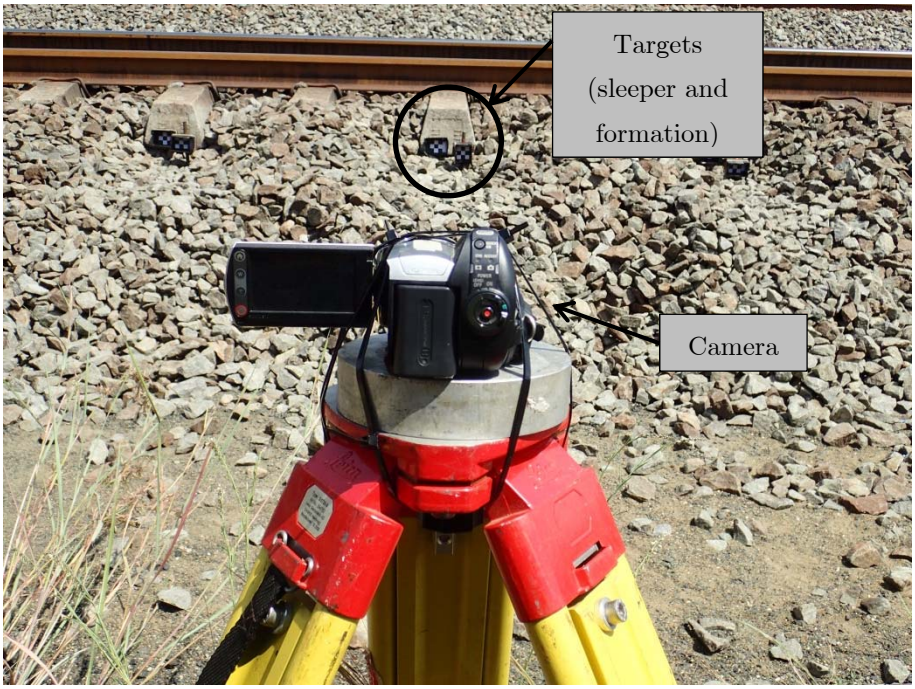

Figure 3-24: RVM Setup at Bloubank

3.5.3 Measurement of wheel loads

Vertical wheel loads were measured with full bridge strain gauges installed on the rail web (left and right rail), calibrated with a load frame and load cell (see Figure 3-25). The strain gauges were connected to the acquisition system and data was also captured by the acquisition software.

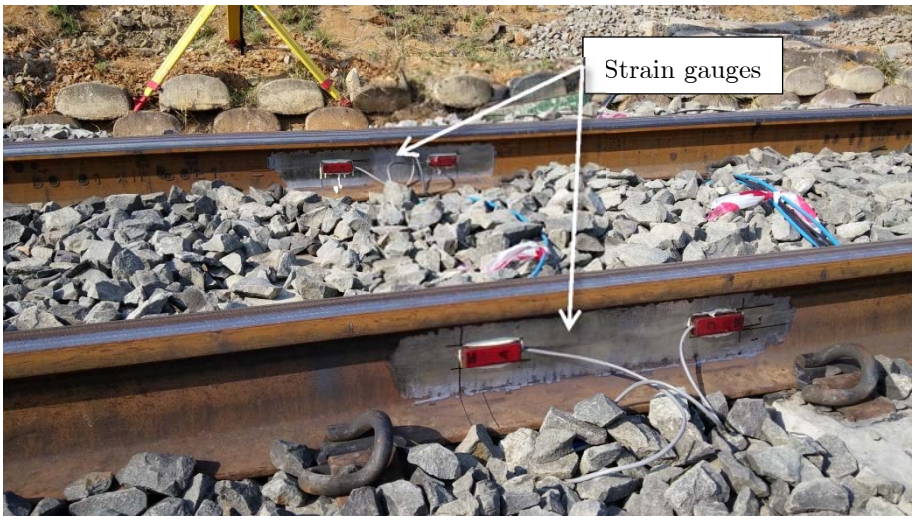

Figure 3-25: Strain gauges fixed to the rail at Izolof

3.5.4 Sampling frequencies

All tests were performed at sampling frequencies of 2400 Hz and 4807 Hz. Initially, the higher frequency was adopted, before a lower sampling frequency was also used for the Izolof test (after rehabilitation of Line 1). Initial data analysis suggested that all relevant information for the dispersion curve calculations would be found in a band from 5 Hz to 150 Hz.

Additionally, because all the analyses would be performed for the ground motion depicted before the rolling stock arrived at the receivers array, it was judged that a high enough sampling frequency would be required to accurately measure such disturbances.

Measurement of the locomotive and wagon wheel loads was done at frequencies of 600 Hz and 1200 Hz. The videos for the RVM deflection measurement were taken at a frame rate between 25 Hz and 60 Hz.

3.6 TYPICAL DATA OBTAINED FROM MEASUREMENTS

3.6.1 Geophysical testing

As highlighted in the previous section, several test setups were adopted for recording ground disturbances at each test section. Testing using two sources were performed, namely using a hammer and a moving train.

Measurements for trains started when the train was close to the geophones array. Allowance was made for data recording to start some time before the train reached the geophones, to depict track formation response when the train was far or closer to the receivers. Typical test data obtained from train measurements is shown in Figure 3-26.

From the measurements it was possible to establish when the first wheel of the train reached each receiver. It was also possible to establish the type of rolling stock (locomotive or wagon) in the time history. Locomotives generally induce more geophone output (i.e more displacement to the ground, inducing more geophone electrical output).

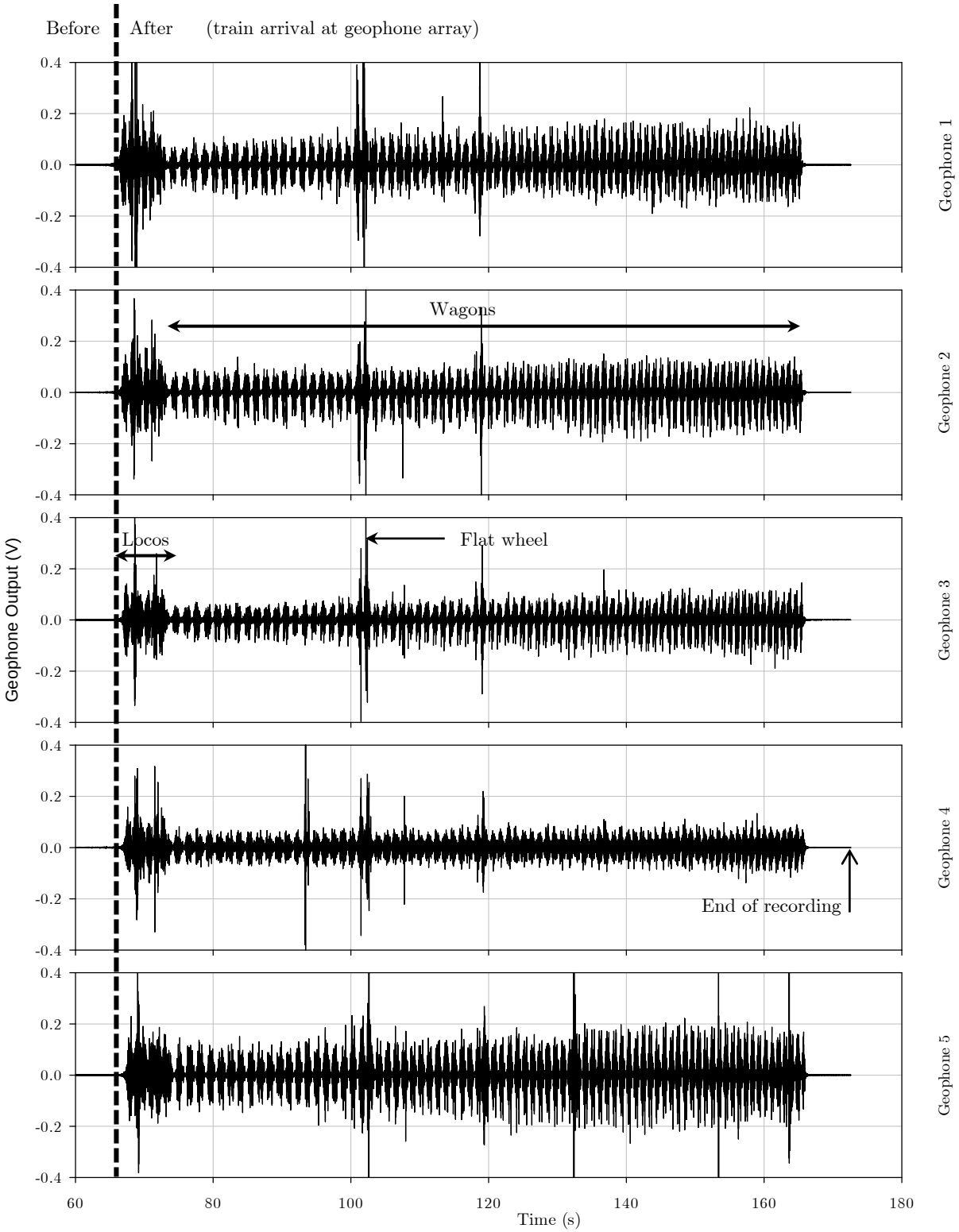

Figure 3-26: Typical data obtained recording a passage of a train

Measurements for hammer impact tests were done by impacting the railhead several times after the recording was started. Each hammer blow would typically be spaced by approximately 10 seconds. Typical data for a hammer impact test is shown in Figure 3-27.

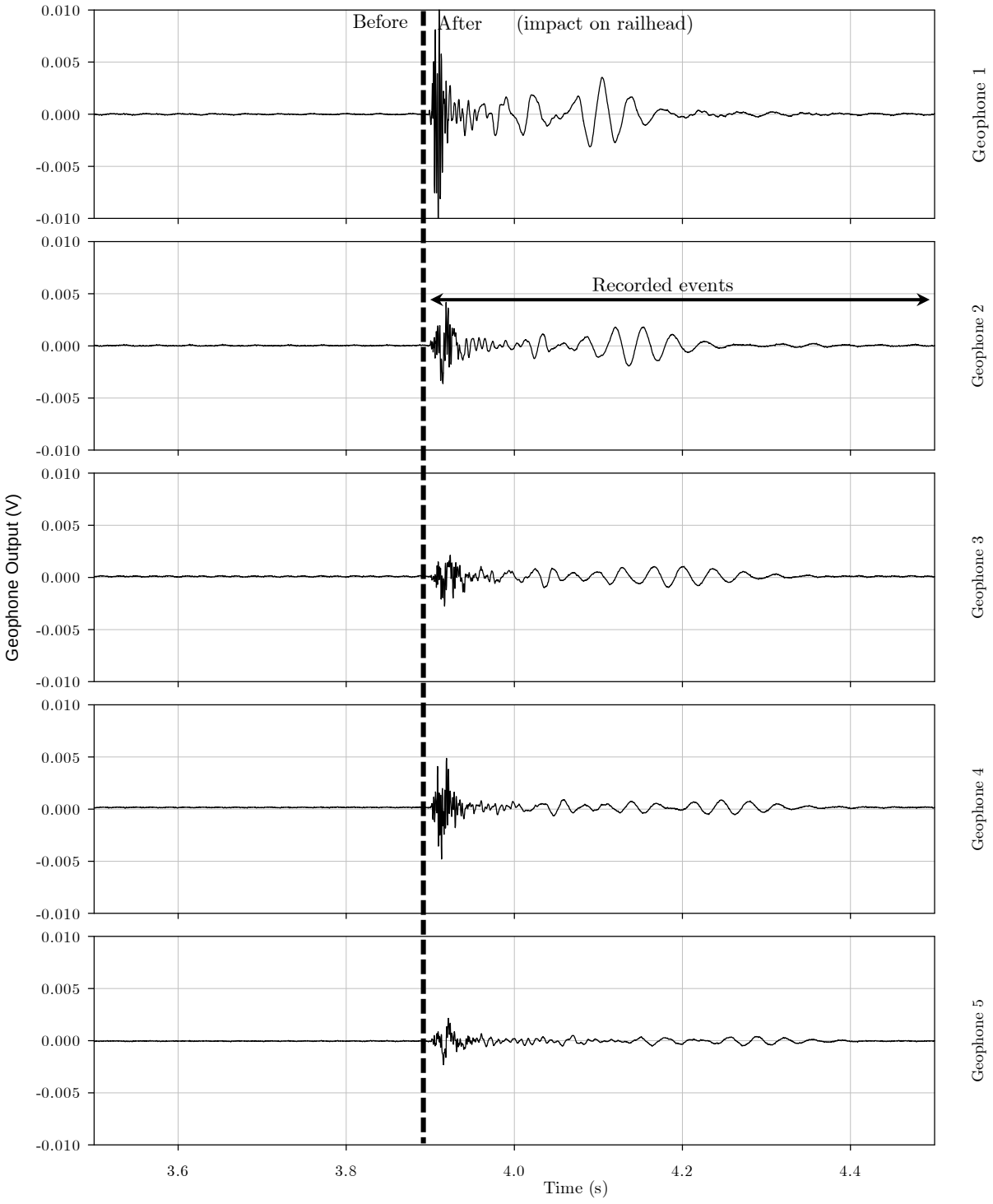

Figure 3-27: Typical partial data from a hammer impacting the railhead on the track

3.6.2 Track deflection measurements

Deflection (or displacement) time history was acquired from video analysis of targets placed on sleepers and steel rods driven into the subballast layer. Processing of the videos was conducted in a commercial video analysis software package (Tracker – Video Analysis and

Monitoring). Track response of loaded and unloaded trains was measured. Typical test data obtained from RVM measurements is shown in Figure 3-28 for deflections of sleeper in loaded and unloaded conditions.

Typical simultaneous deflection readings for sleeper and formation are shown in Figure 3-29 below.

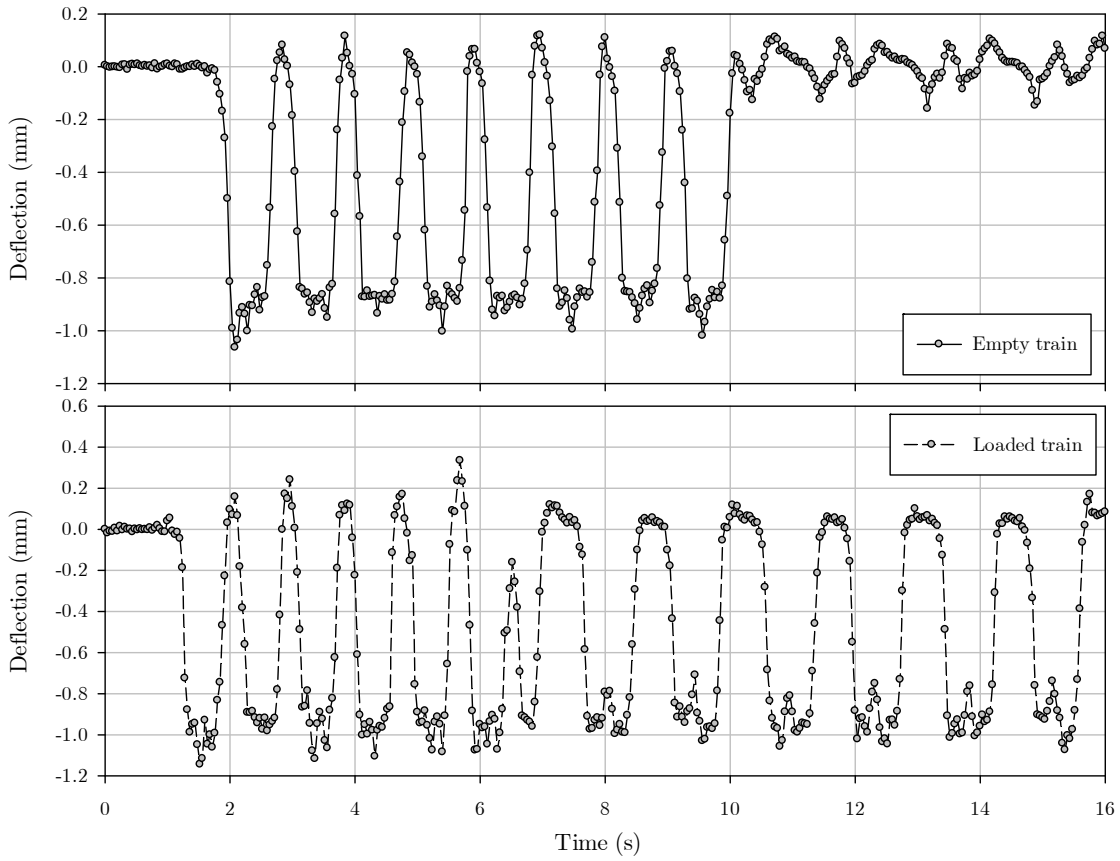

Figure 3-28: Sleeper deflection measurements at Amandelbult

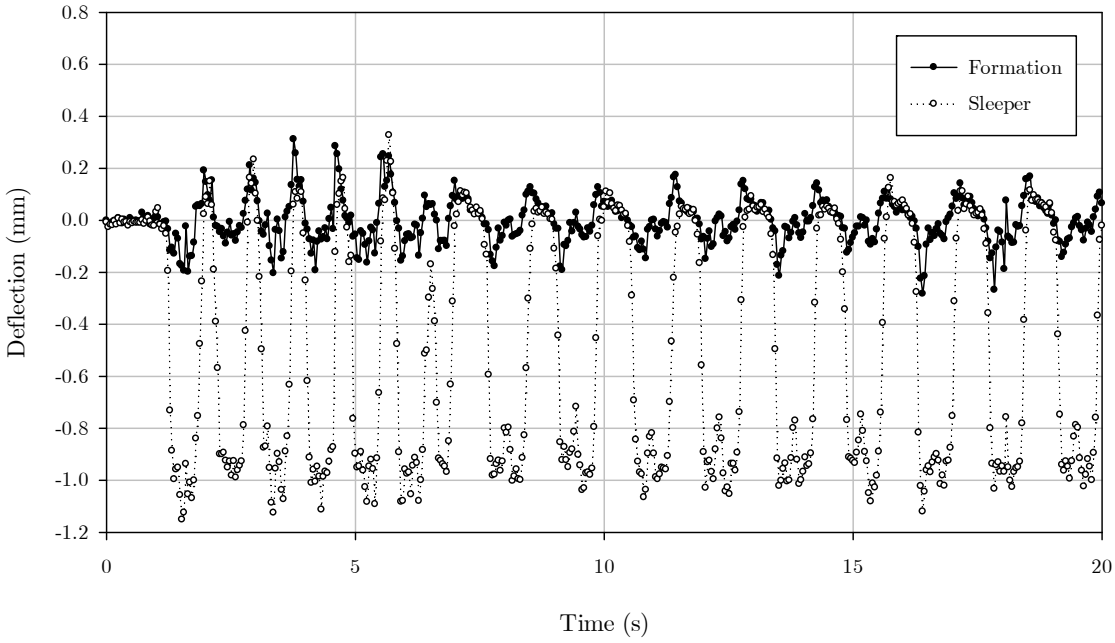

Figure 3-29: Sleeper and formation deflection measurements at Amandelbult (train 03)

3.6.3 Wheel load measurements

Left and right wheel load time history of the trains moving on the instrumented railway lines were measured using full bridge strain gauges as detailed above.

Bloubank and Izolof (before rehabilitation) tests were conducted simultaneously and strain gauges were only attached at the Bloubank test site. Remote Video Monitoring data for Izolof (before rehabilitation) was obtained at the end of the day of that particular test session. By the time these measurements were obtained, the measurements at Bloubank were finalized and no wheel load measurements were obtained at Izolof (before rehabilitation), although the type of locomotives were identified.

Typical measurement data of wheel loads is shown in Figure 3-30. Right wheel loads for two trains running at Bloubank are shown. The first train was empty (wagons are unloaded), whilst the second train had loaded wagons.

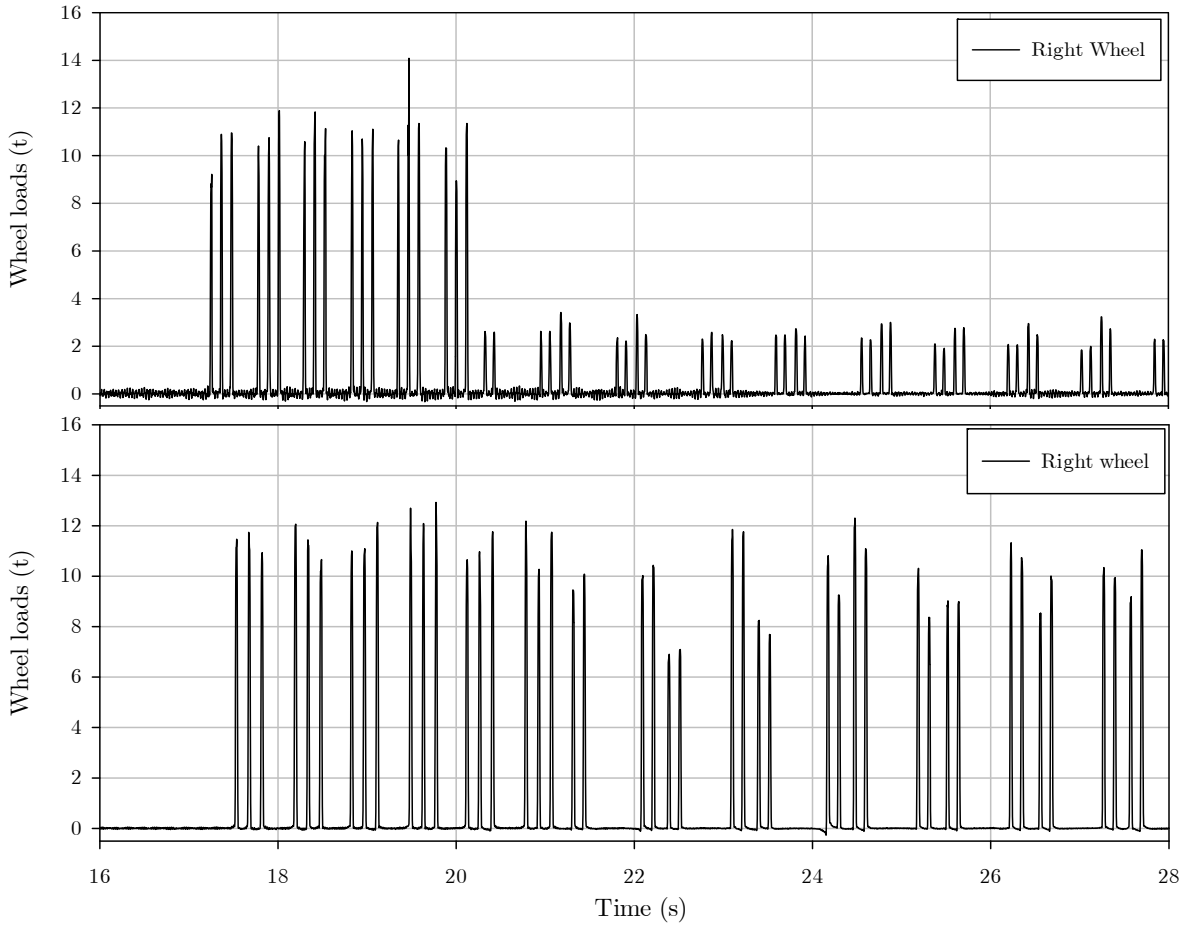

Figure 3-30: Right wheel load measurement for two trains at Bloubank

4. DATA ANALYSIS

This chapter presents the analyses conducted on the data collected during the course of the research. This includes analysis of loaded and unloaded train measurements as well as the analysis of impulsive testing.

The different testing configurations will be analysed and their results discussed and compared in terms of surface wave analysis. Before continuing with the geophysical analysis, track and formation characterization analysis using deflection data obtained from RVM testing will be conducted to benchmark the analysis and results from the surface wave analysis.

A description of the geophone calibration procedure and preliminary data analysis are included before the results of the dispersion calculation and analysis procedures are presented. The chapter concludes with a discussion of the results.

4.1 TRACK AND FORMATION CHARACTERISATION USING REMOTE VIDEO MONITORING DATA

4.1.1 Introduction

Axle load and deflection data were obtained from the wheel load and RVM measurements conducted at each site. RVM measurements were conducted by measuring the vertical sleeper and formation deflection during the passage of a train, also referred to as the resilient track deflection.

Separate analyses were conducted for sleeper and formation vertical deflections in the paragraphs below.

4.1.2 Analysis of sleeper vertical deflection and stiffness

A preliminary analysis of the deflection data was conducted for measurements obtained using the 7E type of locomotive (21 t/axle), which was common to all sites.

Izolof (after rehabilitation) had the lowest resilient track deflection value (0.6 mm) resulting from loading by 7E locomotive bogies (single and coupled bogies). This was expected, as this site underwent complete formation reconstruction due to its prior failure.

On the other hand, Izolof (before rehabilitation) had the highest resilient deflection value (3.1 mm) of all the sites investigated. This is typically a higher than normal value and is indicative of the poor condition in which the site was being operated.

Amandelbult (0.9 mm) had higher resilient track deflection than Bloubank (0.7 mm) at the time the measurements were conducted. In the visual assessment both sites were considered as having good track quality, although the underlying in situ soil material at Amandelbult formation was of poor quality. Results of this analysis are presented in Figure 4-1.

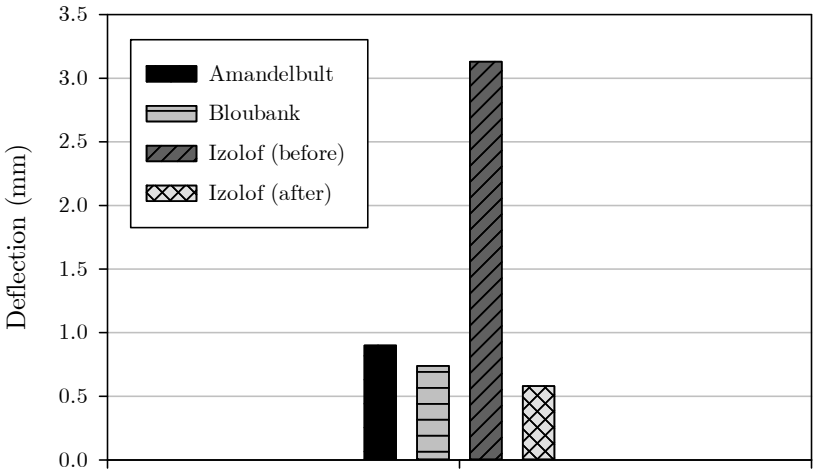

Figure 4-1: Resilient track deflection for a 7E locomotive at all sites (vertical sleeper deflection)

Empty and loaded trains were operating on the lines at the time of testing. Except for Izolof (before rehabilitation – hereafter referred as Izolof BR) where wheel load data was not collected during the RVM measurements, load related deflection data was obtained. From this data, load – deflection curves were prepared for each site[2] that could be used to determine the stiffness of the track.

[2] For Izolof (before rehabilitation) nominal axle loads for the locomotives and wagons (loaded and unloaded) were adopted to establish a trend with regard to the stiffness behaviour of this particular site.

Analysis of displacement time history for Izolof BR provided by RVM testing is conducted in a qualitative manner, due to the fact that no wheel load measurements were available.

Two measurements were made at the Izolof BR site: (i) a train with 7E locomotives running from Richards Bay to Vryheid (empty); and (ii) a train with 19E locomotives running from Vryheid to Richards Bay (loaded).

Nominal axle load for a 7E locomotive is 21,000 kg with a total weight of 123,500 kg and a 19E locomotive has a nominal axle load of 26,000 kg and a total weight of 104,000 kg. All types of wagons have a tare of approximately 20,500 kg, equalling approximately 5,000 kg per axle. It is therefore expected that an empty (or unloaded) train will have axle loads for the wagons around 5,000 kg and when loaded it is expected that the wagons will have an axle load varying between 20,000 kg and 26,000 kg, according to the type of locomotive that is providing the tractive effort. Generally, 19E locomotives are coupled to CCR-11 type of wagons with nominal axle load of 26,000 kg when fully loaded.

Figure 4-2 depicts the displacement time history of the two RVM measurements performed. The first measurement is from a train with 7E locomotives and empty wagons. Track response to the empty wagons produced deflections of 2 mm in magnitude, whilst the locomotives produced deflections of 3.5 mm on average. The second train produced deflections slightly higher than the deflections produced by the passage of the 7E locomotives. The magnitude of track lift is noticeable when the first locomotive axle is about to reach the targeted sleeper.

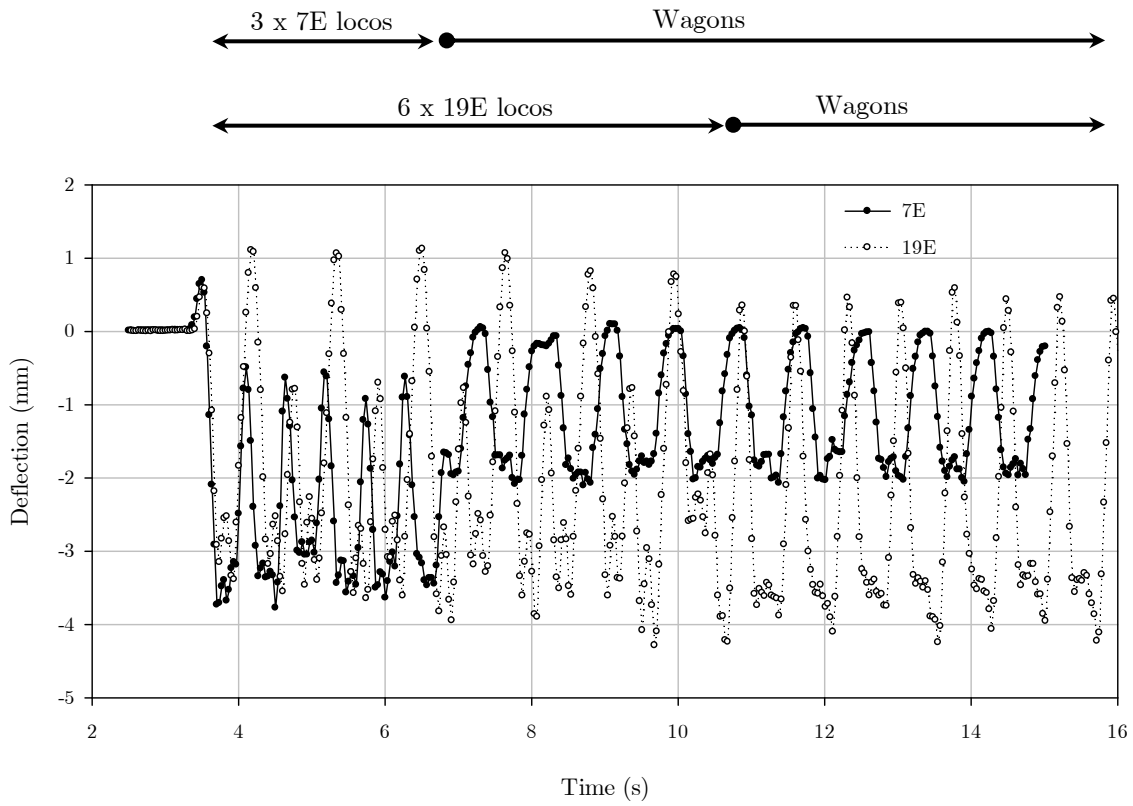

Figure 4-2: Resilient sleeper deflection data obtained at Izolof BR

Adopting these nominal values and the average deflections that they impose on the track, it is possible to estimate the track stiffness of this site and develop the corresponding load – deflection curve (see Figure 4-3).

Based on this curve, the track stiffness at 26 t axle load is 67.8 kN/mm. This value is largely inferior to the values calculated for any of the other three sites. At 20 t axle load the track stiffness has a value of 61.4 kN/mm.

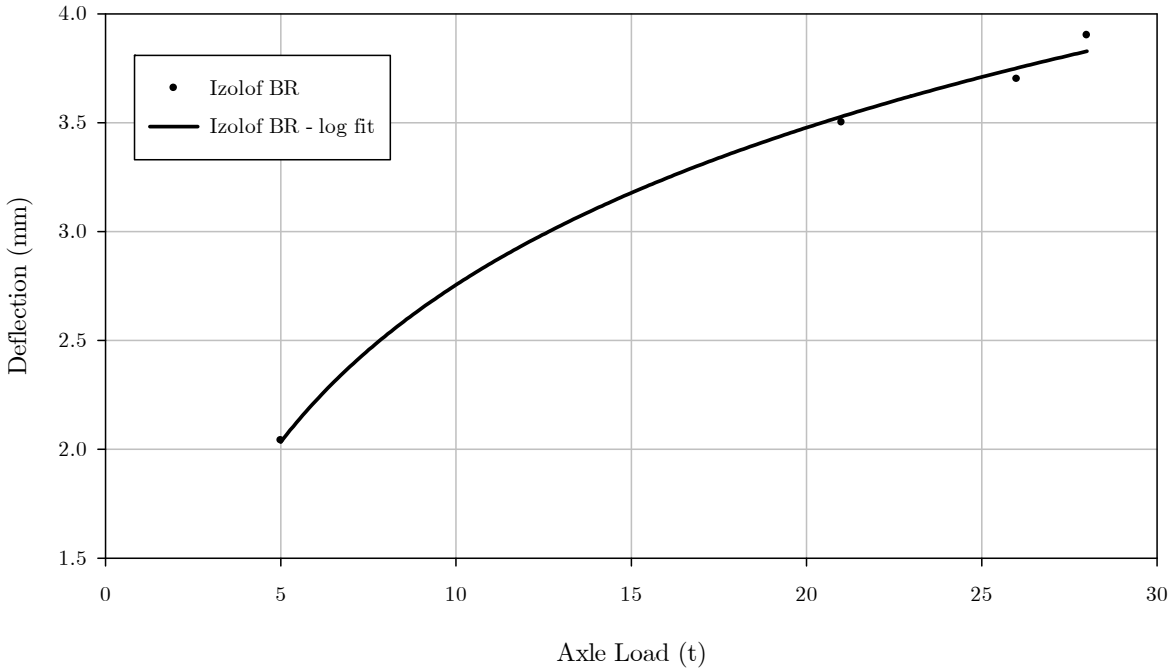

Figure 4-3: Load – deflection curve for Izolof BR (vertical sleeper deflection)

Figure 4-4 shows load deflection curves for Amandelbult, Bloubank, Izolof BR and Izolof AR.

The load – deflection curves enable the calculation of track stiffness at various load regimes (from unloaded to fully loaded trains). It is observed that for the average characteristic axle load of 20 t, Izolof BR had the lowest track stiffness of the 4 sites. At a characteristic axle load of 26 t, the newly reconstructed Izolof AR track had a higher stiffness than the Bloubank track site (Figure 4-4).

The curve for Izolof BR indicates clearly that the magnitude deflection of the sleeper at this site is considerably higher than all the other sites. This is indicative of a lack of ballast support at a sleeper or a number of sleepers in the vicinity of the test station, resulting in the sleeper of the test station having a blind slack.

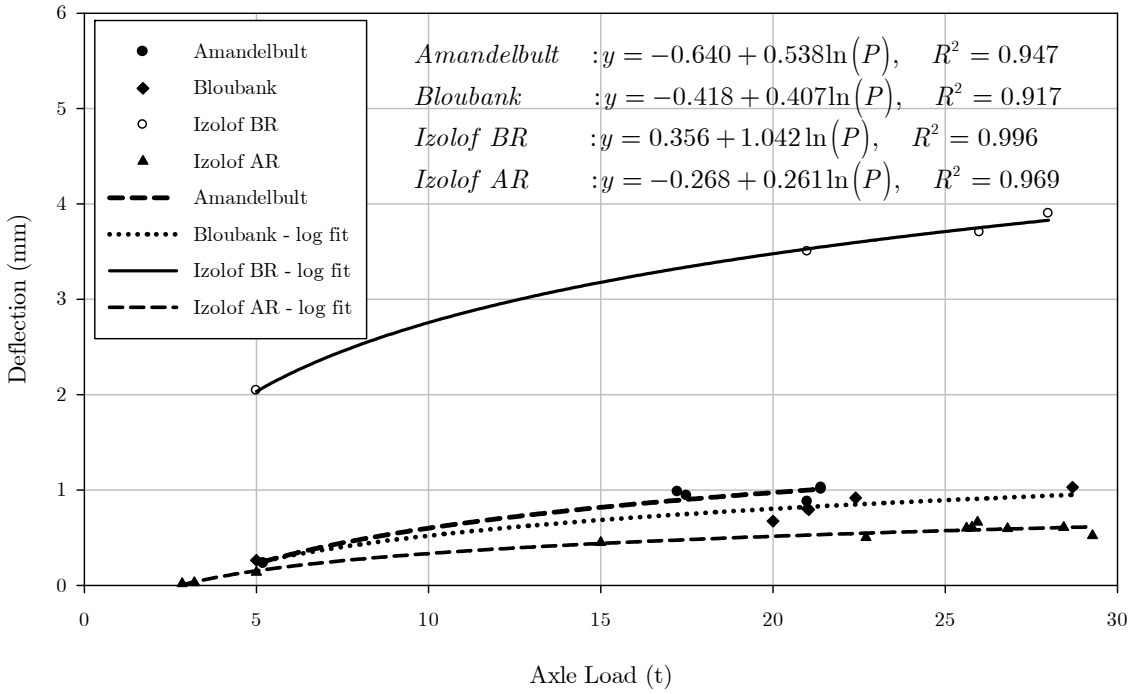

Figure 4-4: Load – deflection curves for all sites (vertical sleeper deflection)

Track stiffness values at two characteristic axle loads for Amandelbult, Bloubank and Izolof AR are presented in Figure 4-5. The characteristic values adopted are 20 t, (applicable to the Amandelbult line) and 26 t (applicable to the Coal line).

At 20 t axle load, Izolof AR had almost double the track stiffness than the corresponding value at Amandelbult. The Bloubank track stiffness was also higher than that of Amandelbult. The track stiffness for Izolof AR and Bloubank at 20 t axle load was calculated to enable a direct comparison with Amandelbult.

For the 26 t axle load which is only applicable to the sites on the Coal line (therefore Amandelbult is not included), the results show an increased stiffness as compared to the values obtained for the 20 t axle load. This behaviour is indicative of the non-linear relationship of the load – deflection curve and the fact that at higher loads the deflection gain or increase will reduce (also referred to as strain hardening).

For the 26 t axle load, Izolof AR had a greater stiffness value than the corresponding value at Bloubank, although the difference between the two values remained similar (approximately 150 kN/mm).

The track stiffness values for Izolof BR were 60 kN/mm and 68 kN/mm for the 20 t and 26 t axle loads respectively. These values are proportional to the high deflection readings obtained from sleeper measurements.

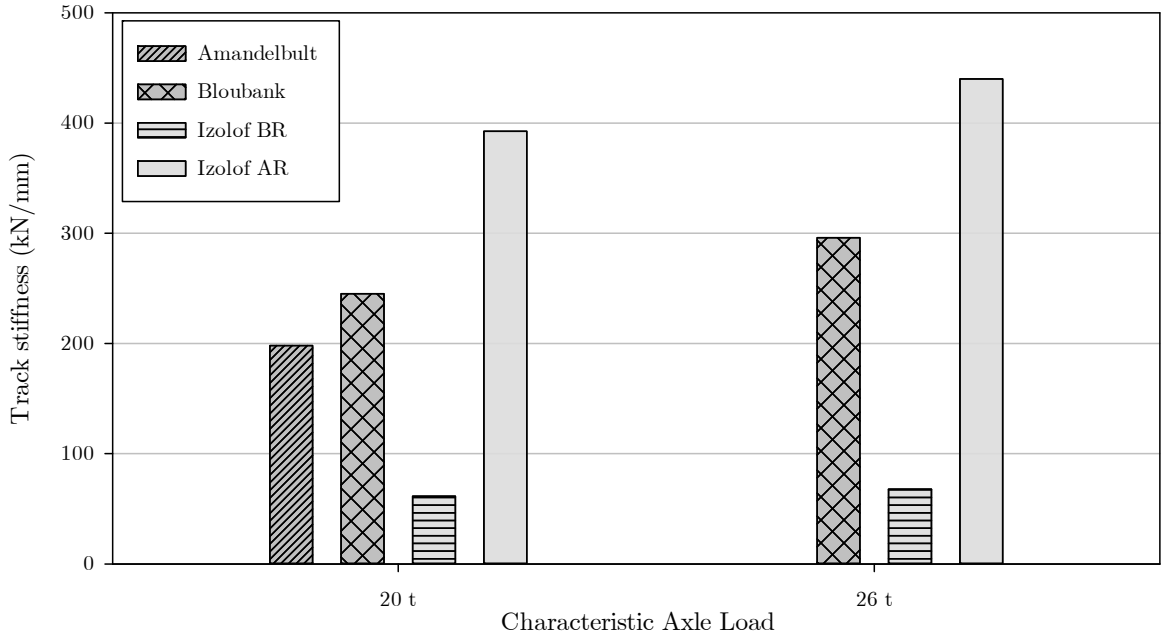

Figure 4-5: Track stiffness at 20 t and 26 t axle load

4.1.3 Analysis of formation deflection and stiffness

The analysis conducted for sleeper deflection measurements outlined above was also conducted for the formation deflection measurements.

Analysis of deflections from 7E train movements was conducted to obtain an initial assessment of the condition of the formation of the railway tracks tested. From the results shown in Figure 4-6 below, the following comments can be made:

- Amandelbult had the highest formation deflection value (0.487 mm);
- The deflection magnitude at Izolof AR (0.310 mm) and Bloubank (0.270 mm) were quite similar;
- Measurements at Izolof BR indicate that load transfer from the superstructure (rails, sleepers, ballast, etc.) to the formation was poor and a relatively small deflection value

of the formation (0.156 mm) was measured. Typical vertical deflection of the sleeper (superstructure) was in excess of 3 mm for the measurements of the same loading. The probable blind slack and the "mud pumping" phenomenon that were observed during the testing session indicate that the wheel loads were only distributed by sleepers and ballast adjacent to the unsupported sleeper (or sleepers). Grabe (2004) discusses in detail the implications of poor ballast support and the effects of applied loading/stress at the top of the formation layer.

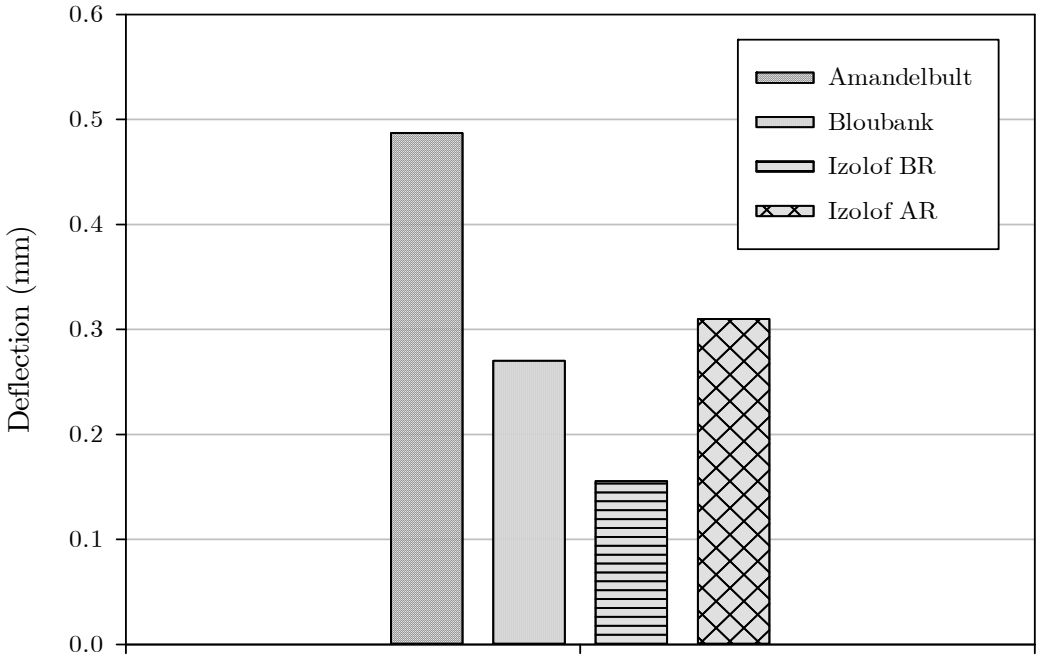

Figure 4-6: Maximum deflection measurements of formation under loading from 7E locomotives

Based on several measurements conducted at all 4 sites under consideration in this research, load – deflection curves were produced for each site in order to determine the formation stiffness.

Figure 4-7 below displays the deflections measured for the various train loading scenarios at all four sites. Curves were fitted to each set of data to predict deflection values at specific or characteristic loading values. From this graph it can be seen that the formation at Amandelbult generally yields higher deflection values when subjected to loaded trains. Deflections of around 0.4 mm can be observed for axle loads of around 20 t. Deflections of the formation at Izolof AR site are generally higher than the ones at Bloubank. Measurements at Izolof BR indicate very little formation deflection even with increased loading. As discussed previously, the poor

load transfer was responsible for the fact that the upper formation of this site was not being loaded properly.

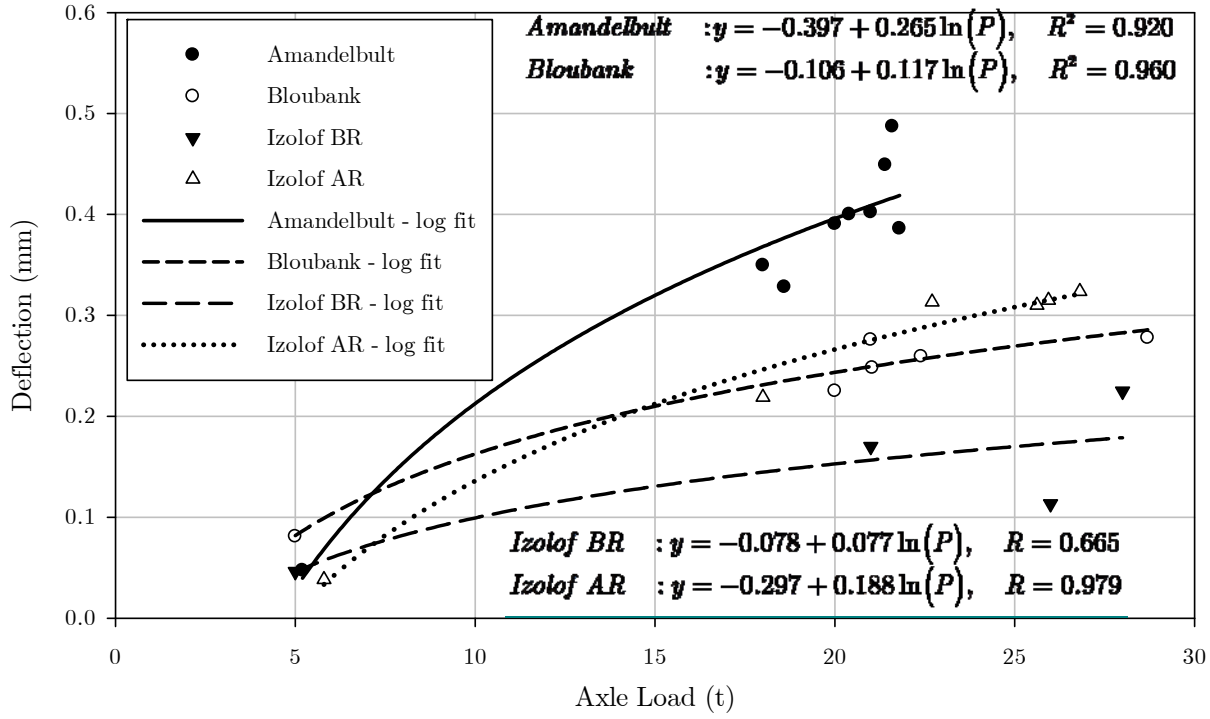

Figure 4-7: Load – deflection curves of formation measurements for all sites

Formation stiffness at two characteristic axle load values were also calculated for all sites (20 and 26 t). The following trends were observed for the stiffness values at both axle loads (Figure 4-8 below):

- Amandelbult had the lowest stiffness values (stiffness at 26 t was not calculated);
- Izolof AR had a lower stiffness value compared to Bloubank;
- There is a slight increase in stiffness values from the lower to the higher loading scenarios;

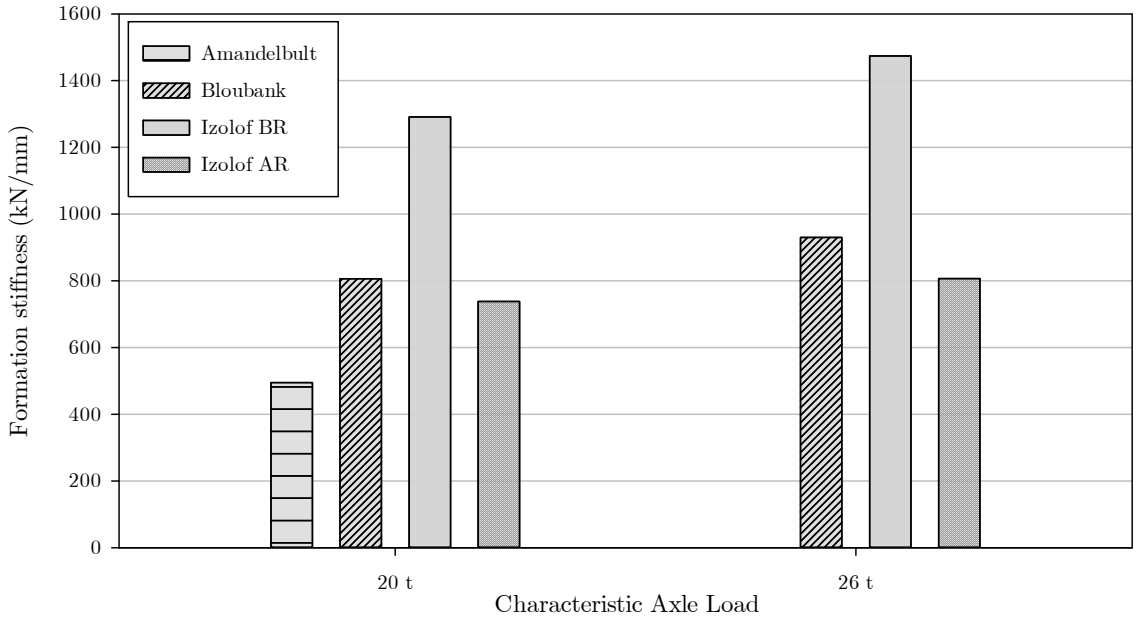

Figure 4-8: Formation stiffness at 20 t and 26 t axle load for all sites

4.2 PRELIMINARY ANALYSES OF THE SEISMIC MEASUREMENTS

Seismic site measurements comprised the recording of ground vibrations induced by trains operating on the lines identified above. From the numerous measurements conducted at each site and at a specific setup (array spacing and length), the following tabulated list indicates the selected tests that were adopted for further analysis.

The usable tests were selected based on the following criteria:

- Number of receivers on the linear array to be 5;
- A long enough measurement (at least 5 seconds) before the train reaches the first receiver on the line;
- Measurements for trains running on the main line instrumented;
- Hammer tests produced with the heaviest hammer available on site (same hammer used for Amandelbult and Bloubank).

Table 4-1: List of tests used for surface wave analysis of formation condition

Test Site	Test Code	Sampling Frequency (Hz)	Comments
Amandelbult	A1-1	4807.7	Locomotive type 7E; Travel speed 62 km/h. Loaded.
	A1-2	4807.7	Locomotive type 7E; Travel speed 40 km/h. Loaded.
	A1-3	4807.7	Locomotive type 7E; Travel speed 35 km/h
	H-AM	4807.7	Hammer impacting the railhead; 3 measurements from impacting from a distance 15 sleepers (9800mm) away from Geophone 1; and 1 measurement from impacting 10 sleepers away from Geophone 5. Test Setup used was A1.
Bloubank	B1-1	4807.7	Locomotive type 19E; Travel speed 47 km/h
	B1-2	4807.7	Locomotive type 7E; Travel speed 67 km/h
	B1-3	4807.7	Locomotive type 7E; Travel speed 31 km/h
	H-BL	4807.7	Hammer impacting the railhead, 15 sleepers (9800mm) away from Geophone 1. Measurement done using Test Setup B2.
Izolof	IB-1	4807.7	Locomotive type 19E; Travel speed 56 km/h. Loaded. March 2015 (before formation rehabilitation).
	IB-2	4807.7	Locomotive type 19E; Travel speed 46 km/h. Loaded. March 2015 (before formation rehabilitation).
	IG-1	2400	Locomotive type 19E; Travel speed 49 km/h. Loaded. August 2015 (after formation rehabilitation).
	IG-2	2400	Locomotive type 7E; Travel speed 45 km/h. Loaded. August 2015 (after formation rehabilitation).
	IG-3	2400	Locomotive type 7E; Travel speed 54 km/h. Loaded. August 2015 (after formation rehabilitation).

Due to mentioned selection criteria, only 2 measurements were selected for Izolof BR (during March 2015). Hammer tests performed at Izolof BR and Izolof AR (during March and August 2015) were done in different test setups, using different hammers. As such, no hammer tests were selected for the analysis at these 2 test sessions.

4.2.1 Calibration of geophones

The geophones used during the testing for this research project were calibrated using a shaker table to infer the accuracy of the measurements gathered and the validity of using such measurements for analysis. An LVDT was used to measure the motion of the shaker. Readings from the LVDT were used to calculate the sensitivity of the geophones used in the testing over the set frequency range.

The shaker used for the calibration was a SD-50-440 model from Spectral Dynamics, which has a frequency capability ranging from 5 Hz to 2.7 kHz.

Figure 4-9 illustrates the overall setup used, including the positioning of the geophones. A frame made of steel profiles was built to carry the LVDTs and to guarantee that its measurements would not be affected by the motion of the shaker table.

The geophones were fitted to the shaker table by means of screws welded together so that they could be attached to the table and to the geophone (replacing the spike of the geophone).

Figure 4-9: Setup adopted for geophone calibration

The geophones and LVDT were connected to a QuantumX amplifier. Measurements obtained with the sensors were recorded on a laptop using commercially available HBM software (Catman AP). Typical outputs of the geophones and LVDT are presented in Figure 4-10.

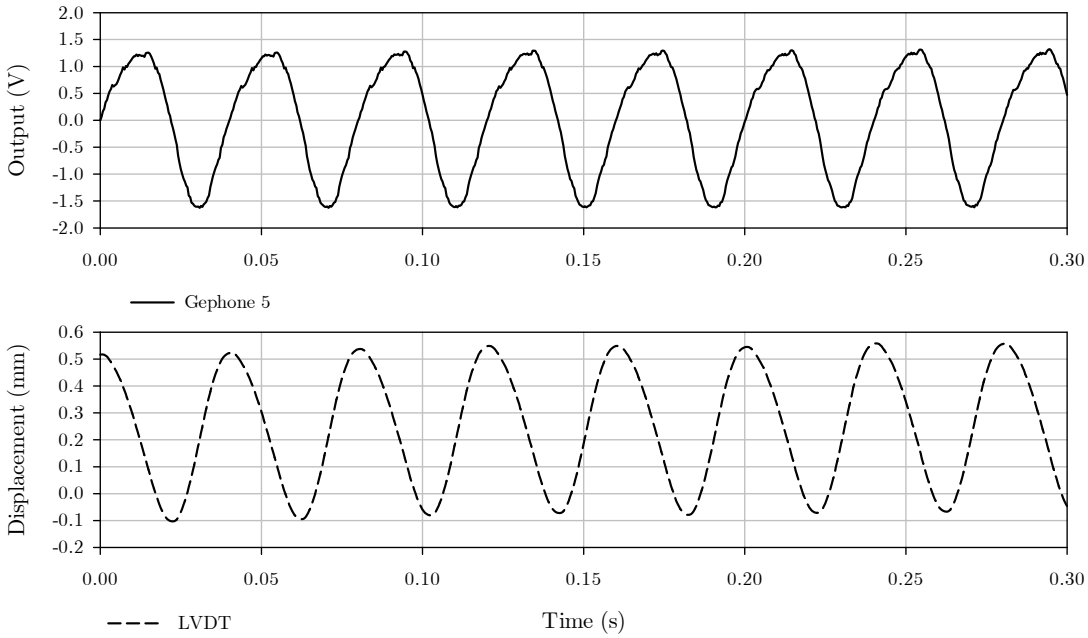

Figure 4-10: Typical data collected during calibration of the geophones

The calibration procedure was set out to be done between the natural frequency of the geophones, i.e. 4.5 Hz, up to 300 Hz, which is close to the high end scale of operation of the geophones. The calibration was done in monotonic frequencies, starting from 5 Hz at an

increment of 5 Hz to a frequency of 40 Hz. After that, an increment of 10 Hz was applied up to a frequency of 100 Hz. From the frequency of 100 Hz up to 300 Hz, the frequency was increased in 20 Hz steps.

For the dispersion data calculation, the most important element to be used is the phase angle. The amplitude of the power spectrum and therefore the sensitivity of the geophones for the attenuation analysis were not considered.

Extraction of the phase angle for each geophone was performed converting the time series to the frequency domain using the Fast Fourier Technique. For each geophone and at each discrete test, the dominant frequency in the power spectrum was obtained and the phase corresponding to that frequency.

Figure 4-11 shows the difference between the geophone phase angle and the average for each frequency. Main observations that can be made regarding the results are:

- The results indicate that the geophones have similar phase angles at the dominant frequency for each of the tests.

- At low frequency, close to the natural frequency of the geophones, differences in the phase angles can be up to 10 degrees (0.18 Radians).

- For frequencies above 20 Hz, the phase angle of the geophones are much closer, with differences being less than 1 degree (less than 0.017 radians);

- A slight difference in phase was observed for Geophone 5 at 120 Hz. However, the difference to the average value was observed to be less than 0.6 degrees. The same was also observed for Geophone 3, with a difference of 0.5 degrees.

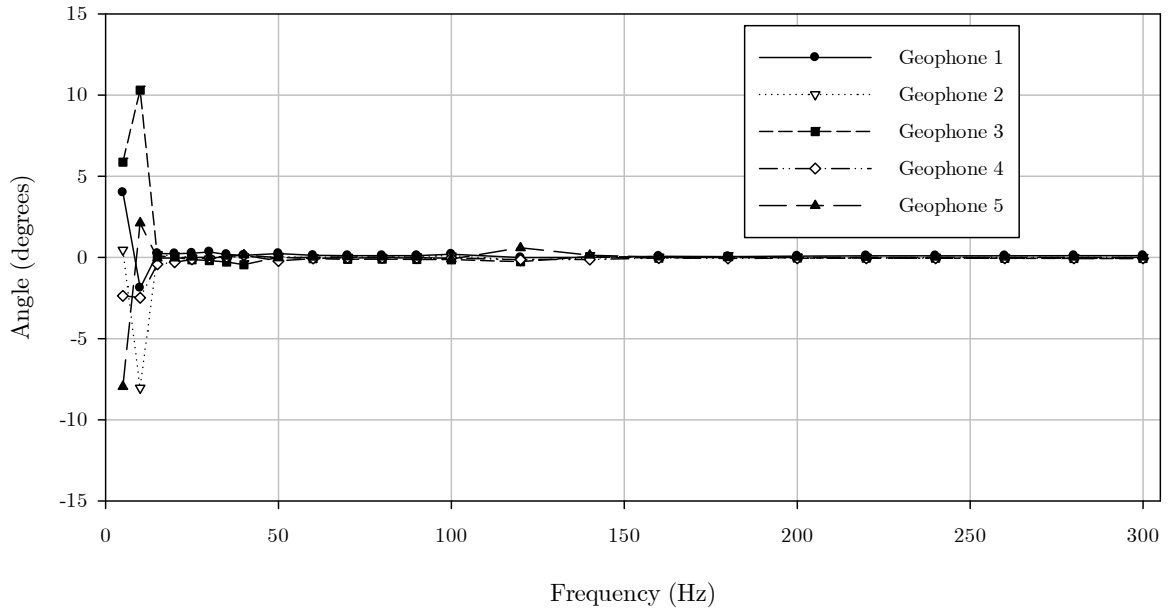

Figure 4-11: Difference in phase angle of geophones at different frequencies of calibration

The results confirmed that the geophones were in phase for the frequency range from 20 Hz to 300 Hz and the spurious frequency[3] for each geophone is not within this range. Detailed discussion about the importance of determining the spurious frequency can be found in Faber and Maxwell (1997).

4.2.2 Initial considerations for time domain series

The signal measurements in the time domain, mentioned in Chapter 3 (typical examples), were converted from the time domain to the frequency domain using Fast Fourier Transform (FFT) methods. This procedure allows for spectral parameters such as the amplitude spectra, phase angle and real and imaginary parts of the signal to be calculated and used to process the signal acquired by the geophones. In order to do that, the sampling of the surface wave propagating in front of the train has to be done before the first axle of the train's leading locomotive reaches the receivers. At the same time it is imperative to ensure that noise is minimized in the acquisition process.

[3] All discontinuities in the transfer function of the geophone above the natural frequency are termed spurious resonance.

Several time windows from 0.2 seconds to 16 seconds were investigated in order to establish suitable windows that carried signal with good quality in the desired frequency range. The calculation of the FFTs had a bearing on the size of the time windows, as well as the number of points in the analysis which ultimately influences the frequency resolution obtained. Finally, 3 time windows (or window lengths) were considered for the analyses of the train measurements: 0.5 s, 2 s and 4 s. A buffer zone, to avoid near-field effects, was considered, by offsetting the time window by 0.5 seconds[4]. Taking as an example the test IG-1, the following graphical presentation is illustrative of the process that is referred to (see Figure 4-12).

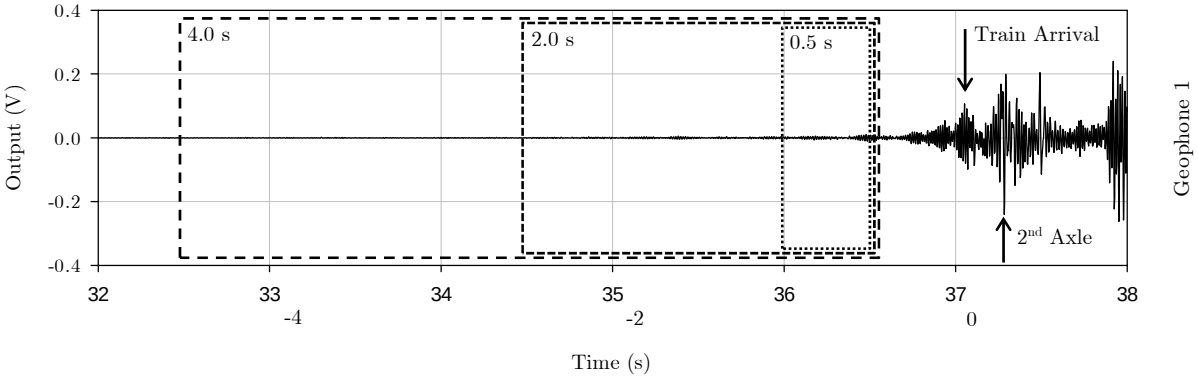

Figure 4-12: Illustration of several time windows analysed (0.5 s, 2 s and 4 s) for a train measurement

4.2.3 Effect of time window on the spectral parameters of the signal

4.2.3.1 Train measurements

The choice of the time window to be used in further analyses has an influence on the signal quality acquired by the geophones. To analyse the impact on the signal quality, two parameters were adopted for the preliminary assessment, in order to establish whether a trend was observable in terms of their impact. The two parameters were the auto power spectrum and the coherence function. Power spectrum relates to the quality of the signal for each geophone, whilst the coherence function relates to the quality of signal between two geophones.

A 4 s time interval during the 16.5 s before the train arrives at the first receiver (i.e -16.5 to -12.5 s and -12.5 to -8.5 s for example), was chosen for each site to establish the ideal window

[4] The end of the analysis period finishes 0.5 seconds before the first axle of the train arrives at the first geophone of the receiver array.

or windows for analyses. Analyses of shorter time intervals (0.5 s and 2.0 s) were also analysed and details are provided later.

Figure 4-13 below shows the variation in the amplitude of the power spectrum of the signal recorded by Geophone 1 for Test B1-3. The time windows closest to the arrival of the first train wheel at the first receiver have higher power spectrum values compared to those when the train is further away from the geophones array. From these time windows, the last one (-4.5 to -0.5 s) has the highest spectrum amplitude across the frequency range.

Regarding the frequency distribution of the spectrum, relatively higher amplitudes are observed between 20 Hz and 70 Hz. Some signal quality is also observed between 110 Hz and 170 Hz in the frequency domain.

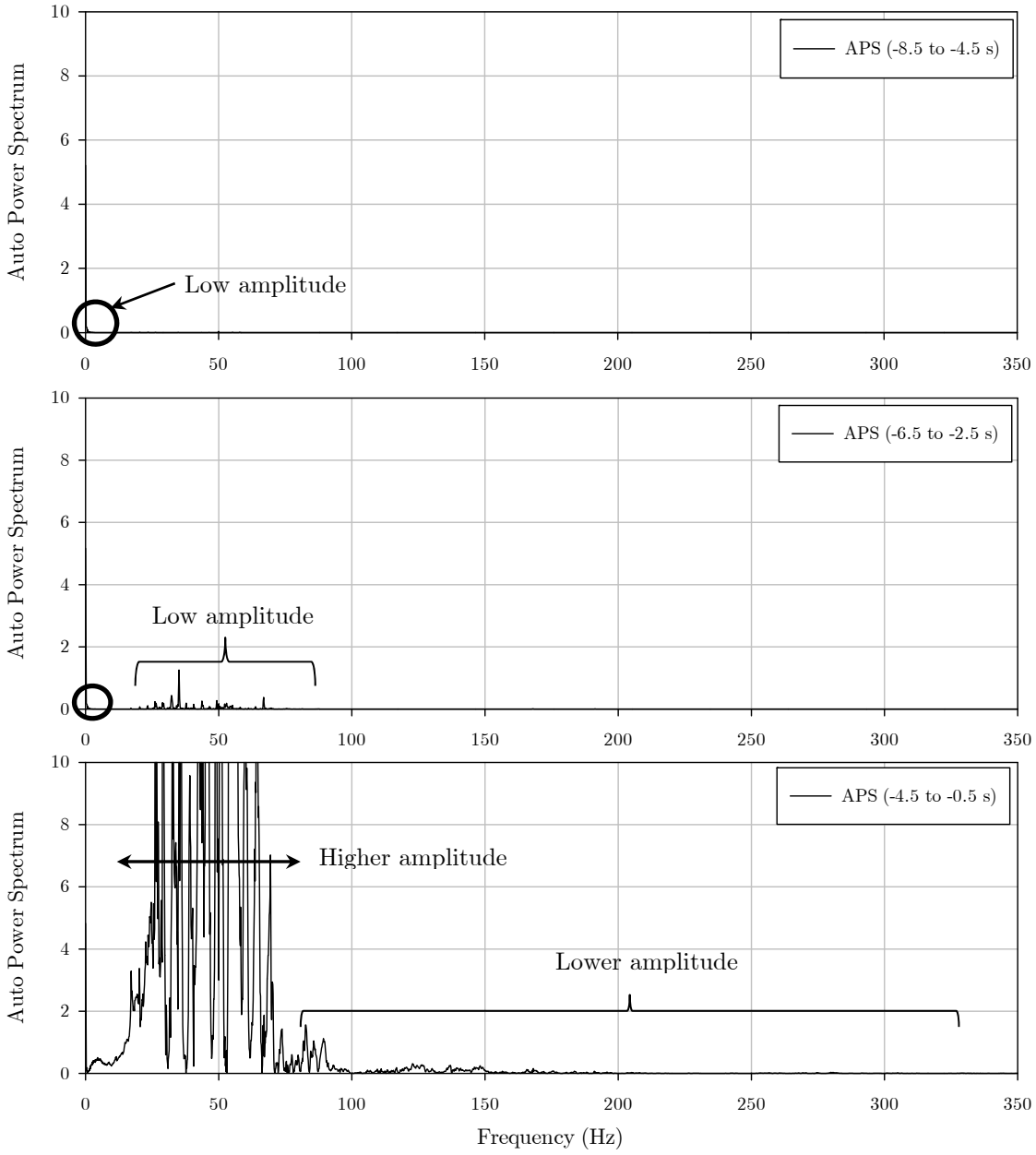

Figure 4-13: Variation of Auto Power Spectrum for 4 s intervals

Another procedure to analyse signal quality is by correlating the signal acquired between two geophones. The coherence function was calculated between two consecutive geophones of the array, namely Geophone 1 and Geophone 2 for this train measurement to establish a trend regarding signal quality. Based on the power spectrum results, 3 windows were investigated: (a) 8.5 – 4.5; (b) 6.5 – 2.5 and (c) 4.5 – 0.5 (in seconds for the first wheel to reach the first receiver). Results of the analyses are shown in Figure 4-14.

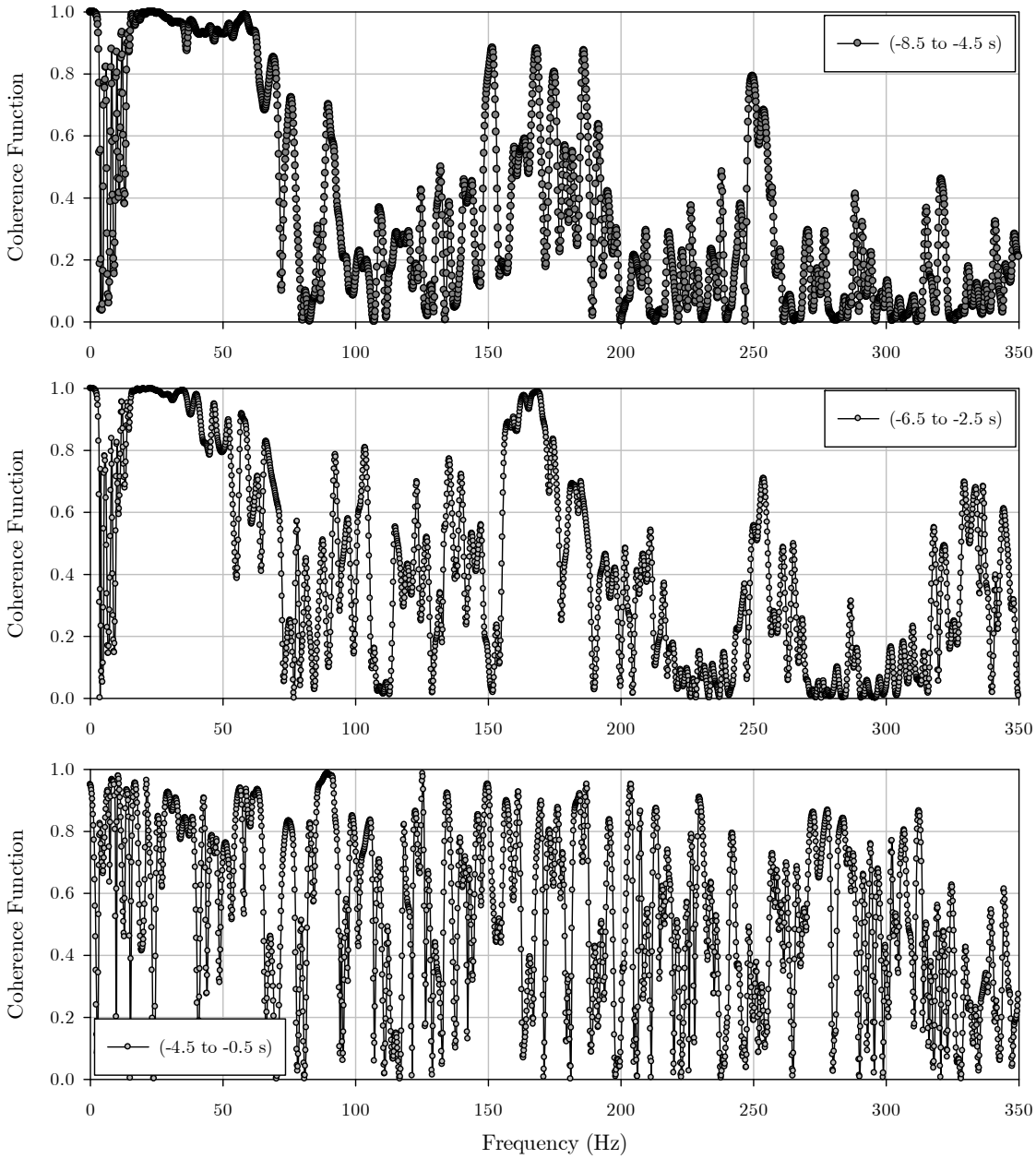

Figure 4-14: Coherence function for a train measurement at Bloubank for several time windows

Results of the coherence analysis presented in Figure 4-14 above provide the following trends:

- Windows of time further away before the train reaches the geophones array, show a broad region of coherence greater than 0.9 (frequency ranging from 15 Hz to 65 Hz).

- For the same windows (more than 4 seconds before the train arrives at the first sensor), the higher end of the frequency band exhibits poor coherence, indicating that the energy within that region of frequency is attenuated considerably.

- Coherence for the window closest to train arrival shows discrete or narrow bands with values above 0.9. However, these discrete areas of good quality are distributed over a wider frequency band. The discrete bands with good signal quality are likely due to an increase in noise (coherent or incoherent) caused by other events that are not significantly attenuated.

- Coherence for frequencies in excess of 200 Hz is generally poor.

- The low frequency band seems to be affected more by the train – track interaction. That is, the axle loading, bogie (or axle couplings) loading and sleeper spacing.

Comparison between different window lengths was also performed. The lengths analysed were 0.5 s, 2 s and 4 ss (graph for the 4 s window displayed in Figure 4-13). The fixed point adopted for the analysis is again the instant that the first wheel reaches the first receiver of the array and the 0.5 s for buffer.

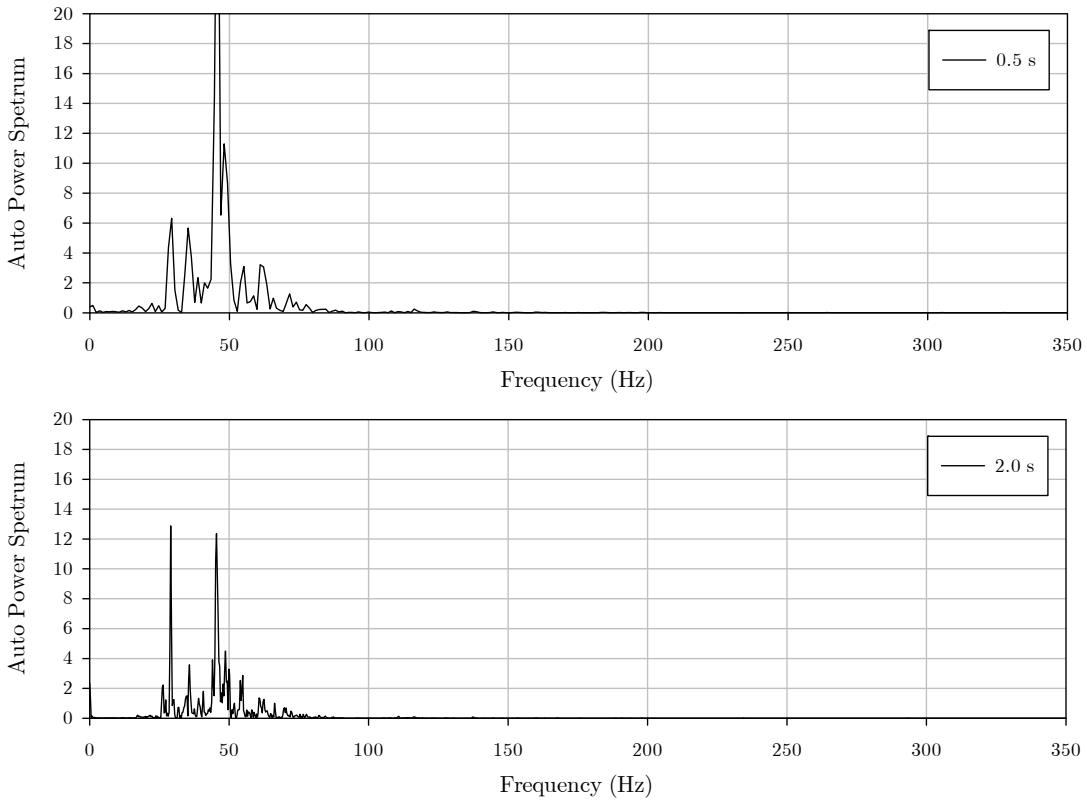

Figure 4-15: Auto power spectrum for 0.5 s and 2 s time window

The power spectrum for the adopted time window shows dominant frequencies carrying energy from the source. These frequencies are predominantly less than 100 Hz, concentrated in regions lower to 50 Hz. The amplitude of the dominant frequencies in the shorter time window (0.5 s) is greater than the amplitude of the dominant frequencies in the 2 s time window. The power spectrum for the 4 s window is broader in the frequency spectrum and the amplitude is higher than the other two shorter windows analysed.

Coherence functions were also calculated to establish the trend of signal correlation between two sensors. The time windows used for power spectrum analysis are also used for this analysis. The results of the analysis are shown in Figure 4-16 below.

Trends from the results show that for shorter time windows, signal quality between two sensors is poor over the majority of the frequency band. Signal quality increases with increased time window. Except for a frequency band between 155 Hz and 172 Hz were the coherence function is close to unity, the 2 s time window has poor quality between the 2 sensors for frequencies greater than 35 Hz.

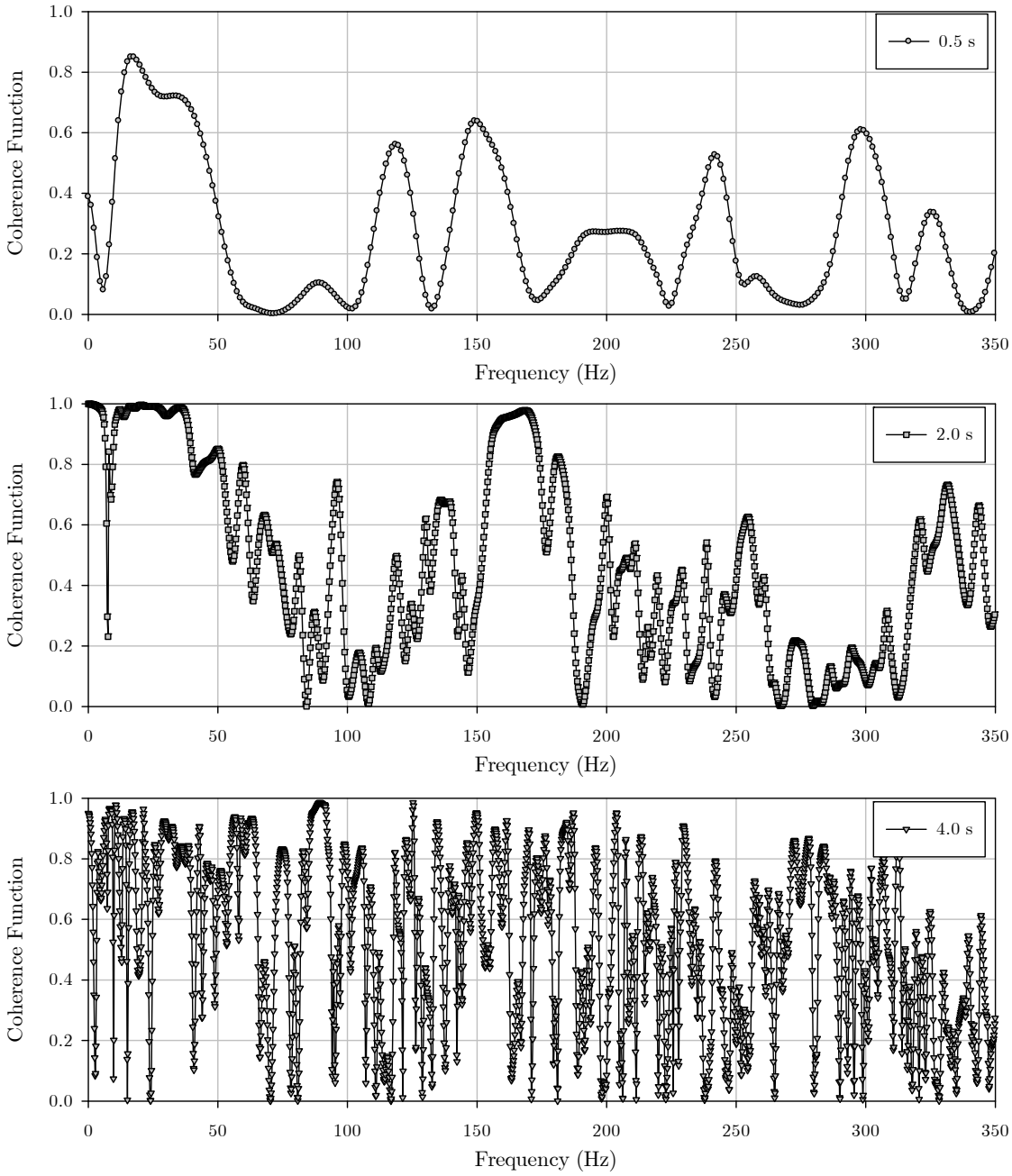

Figure 4-16: Coherence for different window length for a train measurement

4.2.3.2 Hammer impact measurements

Analysis of different time windows were also performed for the hammer tests to determine the impact that the time window would have on the signal quality before proceeding with detailed analysis.

Power spectrums for the hammer tests in time windows of 0.2 s, 0.5 s and 1.0 s were calculated. The results are shown in Figure 4-17 below. Energy is propagating in similar frequency bands

for all time windows analysed. The amplitude of the spectrum is stronger for shorter time windows.

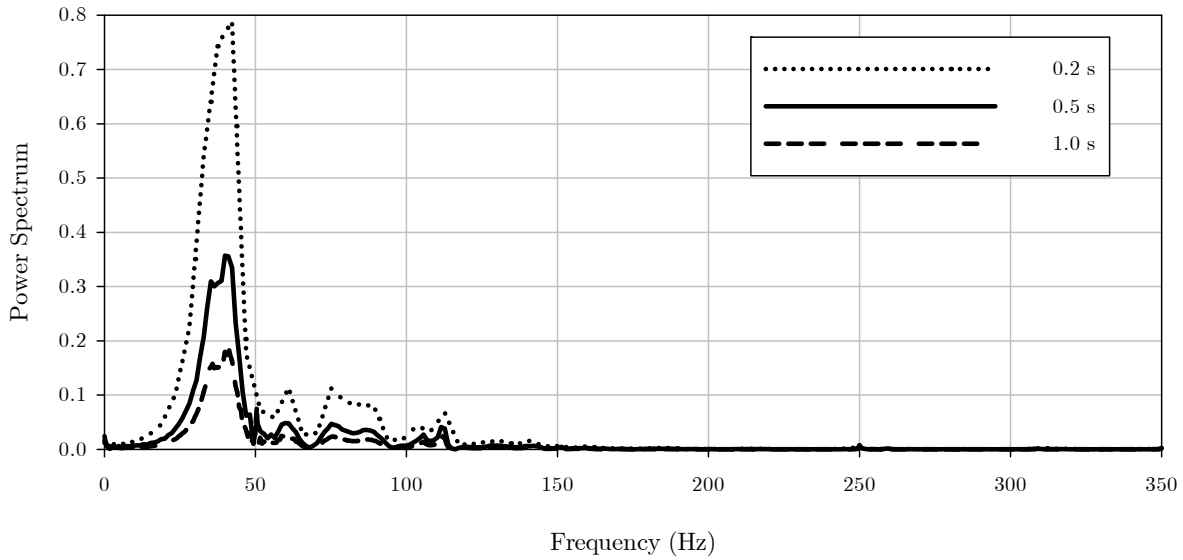

Figure 4-17: Auto Power Spectrum from a Hammer Test at Bloubank for different window lengths

The coherence function for the three time windows analysed in the hammer testing was calculated and the results are shown in Figure 4-18. Although the amplitude of the spectrum is stronger for shorter time windows, signal quality between two geophones decreases with decreasing time window length. All time windows have coherence values above 0.9 in the frequency range from 20 Hz to 45 Hz. The 1 s time window has high values of coherence in higher frequency bands, although the values are not equal to unity.

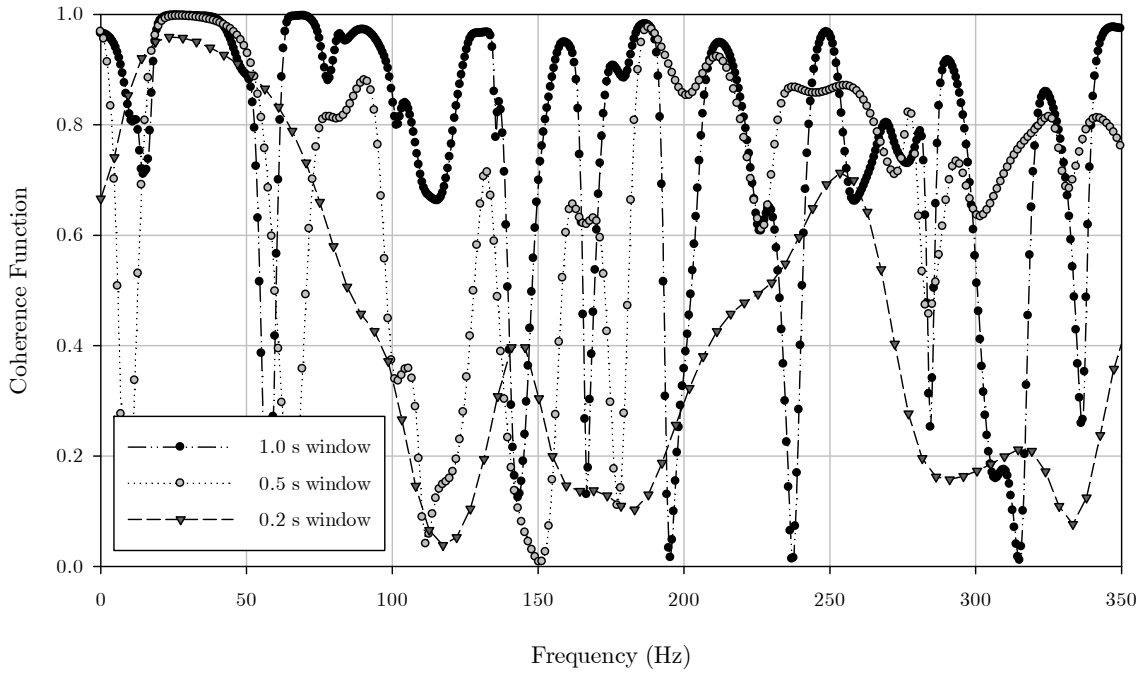

Figure 4-18: Coherence function between Geophones 1 and 2 from a Hammer Test at Bloubank for different window lengths

From the results of the analysis conducted above, considering several time windows (same or different lengths), it can be seen that the energy content will vary considerably as a function of the frequency.

Energy in the low frequency range is largely obtainable in time windows when the train is further away from the geophones array (i.e., 4.5 to 8.5 s). This is typically representative of passive testing and is aimed at characterizing the site at greater depth.

Energy in the high frequency range is largely obtainable in time windows when the train is closer to the geophone array (i.e., 0.5 to 4.5 s). However, the values with good signal quality are found in narrow or discrete bands. This is most likely due to increased noise in the signal.

Analysis of a railway track formation requires a shallow analysis and therefore high frequency data must be obtained. Typically results in the frequency range in excess of 100 Hz must be obtained in order to sample at shallow depths. The 4 s interval immediately before the train reaches the receivers, therefore seems to be the best window for train measurement to depict energy propagating in the high frequency range. Other intervals can be used to complement the results obtained in the analysis of the primary window.

4.3 SPECTRAL ANALYSIS OF THE MEASUREMENTS

Normalized power spectrums for all sites were calculated to investigate the frequency range footprint originating from the trains. These frequency transforms were done for a 4.0 s time window when the train is 4.5 s away from the first receiver in the receivers array as illustrated in Figure 4-12.

4.3.1 Frequency spectrum for the sites

Spectra for the Amandelbult train measurements are shown in Figure 4-19. The calculations indicate that the train induced ground vibrations had energy in frequencies predominantly concentrated under 100 Hz, mainly from 0 Hz to 80 Hz. Train measurement A1-1 had a broad frequency ranging from 0 Hz to 110 Hz with a considerably high spectrum amplitude, with a smaller range between 250 and 270 Hz of the wave energy with a smaller spectrum amplitude.

Energy in frequencies in excess of 100 Hz (discrete values) is observed for train measurements A1-2 at 320 Hz and A1-3 at 285 Hz, respectively. Clearly these high frequency events are associated with each particular train – track interaction, although from the measurements (or recorded data) it is not possible to determine exactly what that phenomenon is.

The spectrum for train measurements A1-2 and A1-3 for frequencies smaller than 100 Hz have lower amplitude values compared to the A1-1 train measurements. However, the trend in terms of energy in the $<$ 100 Hz frequency range is similar for all 3 measurements.

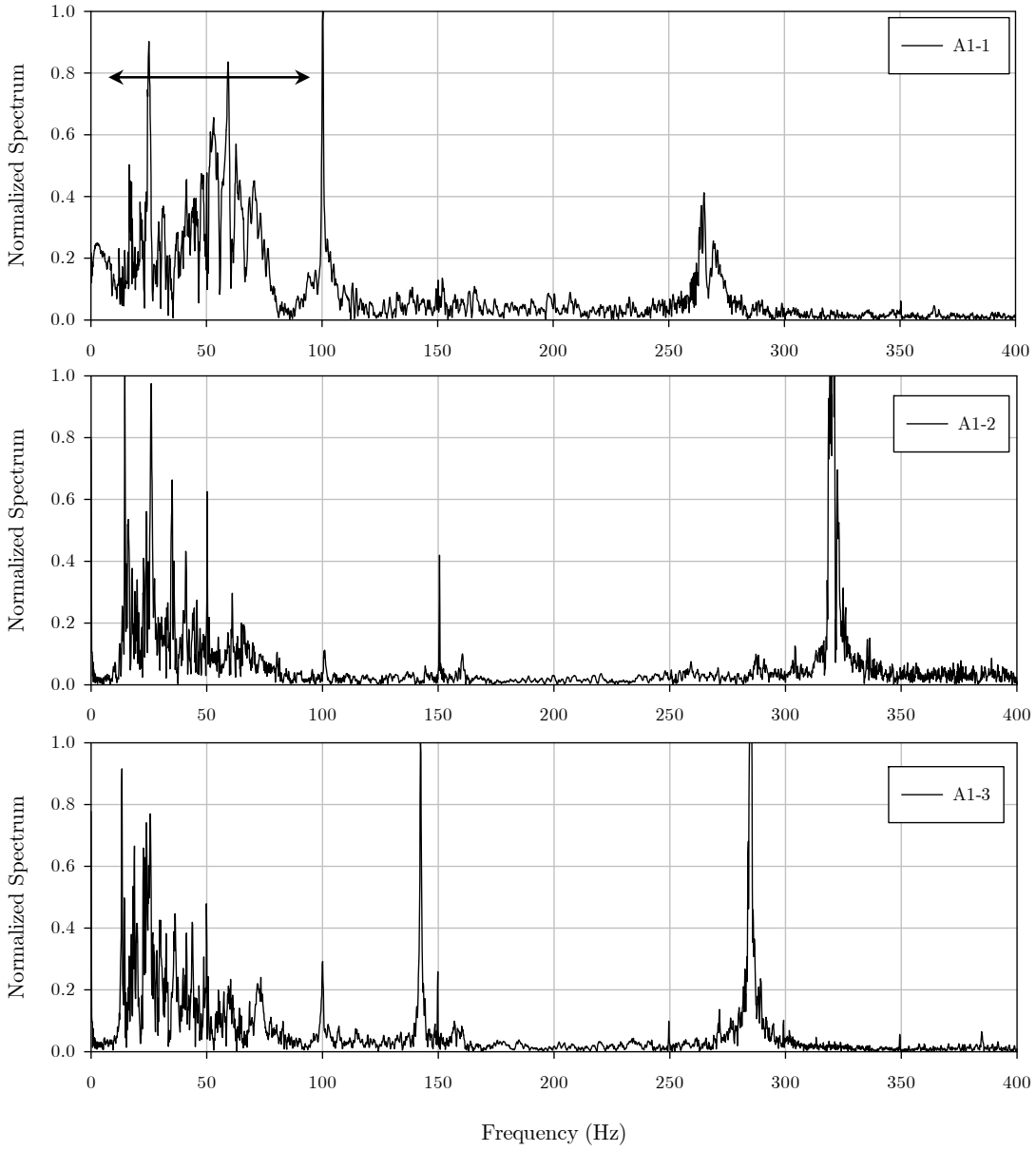

Figure 4-19: Normalized spectra for Amandelbult

All the spectrums for Bloubank show considerable energy stored between 0 Hz and 100 Hz. The presence of energy propagating in frequencies in excess of 100 Hz, especially for tests B1-2 and B1-3 was detected by the geophones. However, the magnitude of the spectrum on this high frequency region is comparatively smaller and occur in narrow bands. These narrow bands do not occur at the same frequency region (Figure 4-20).

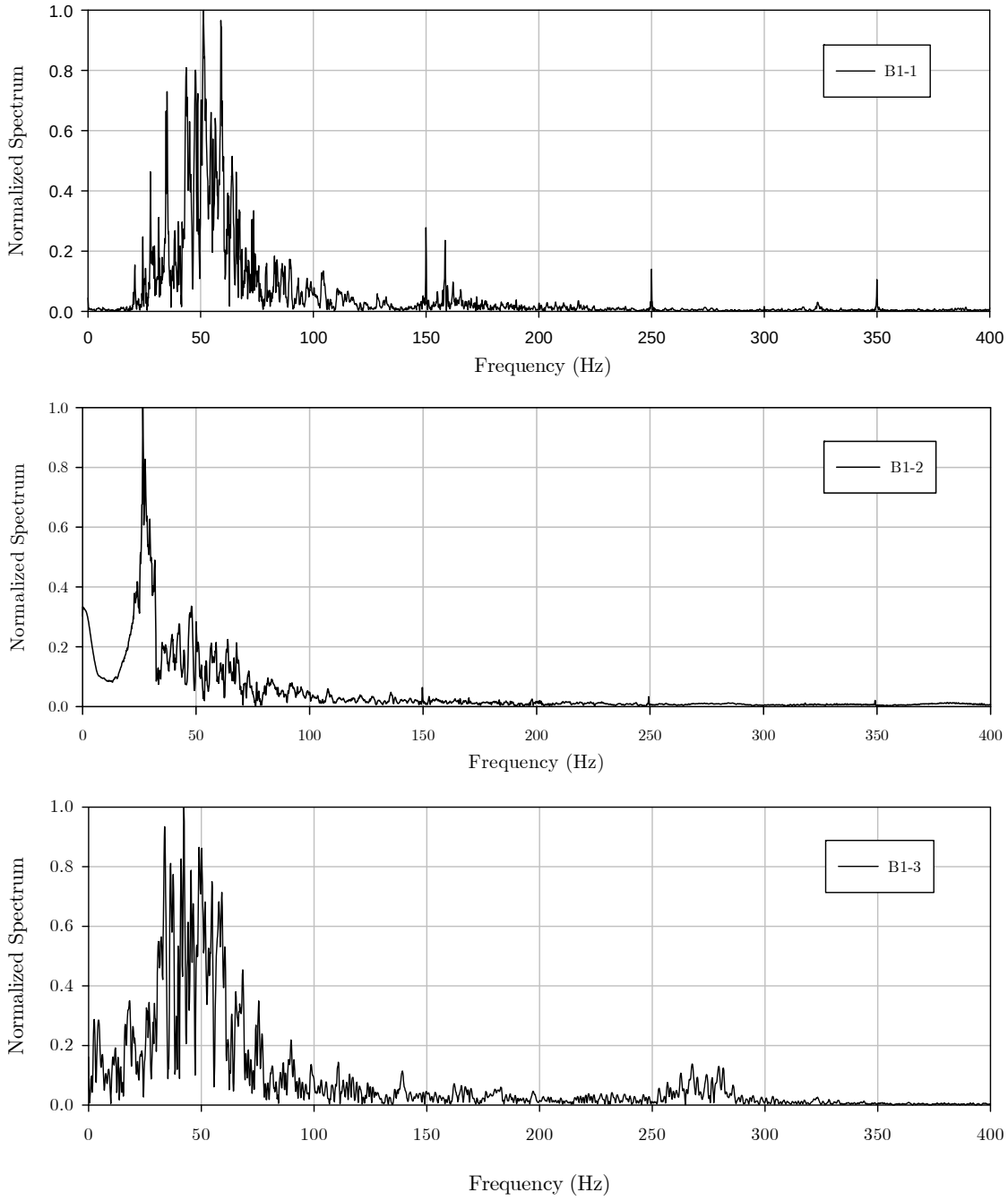

Figure 4-20: Normalized spectra for Bloubank

The spectrum analysis for Izolof BR also indicates energy propagating through the formation in the frequency region of 0 Hz to 100 Hz, with some dominant frequencies at discrete values (25, 45, 50 and 58 Hz for IB-1 and 30, 42, 54 and 65 Hz for IB-2) as shown in Figure 4-21. A spike is visible in the spectrum for Test IB-1 at 150 Hz, 250 Hz and 350 Hz (spike at this frequency is also observed for Test IB-2).

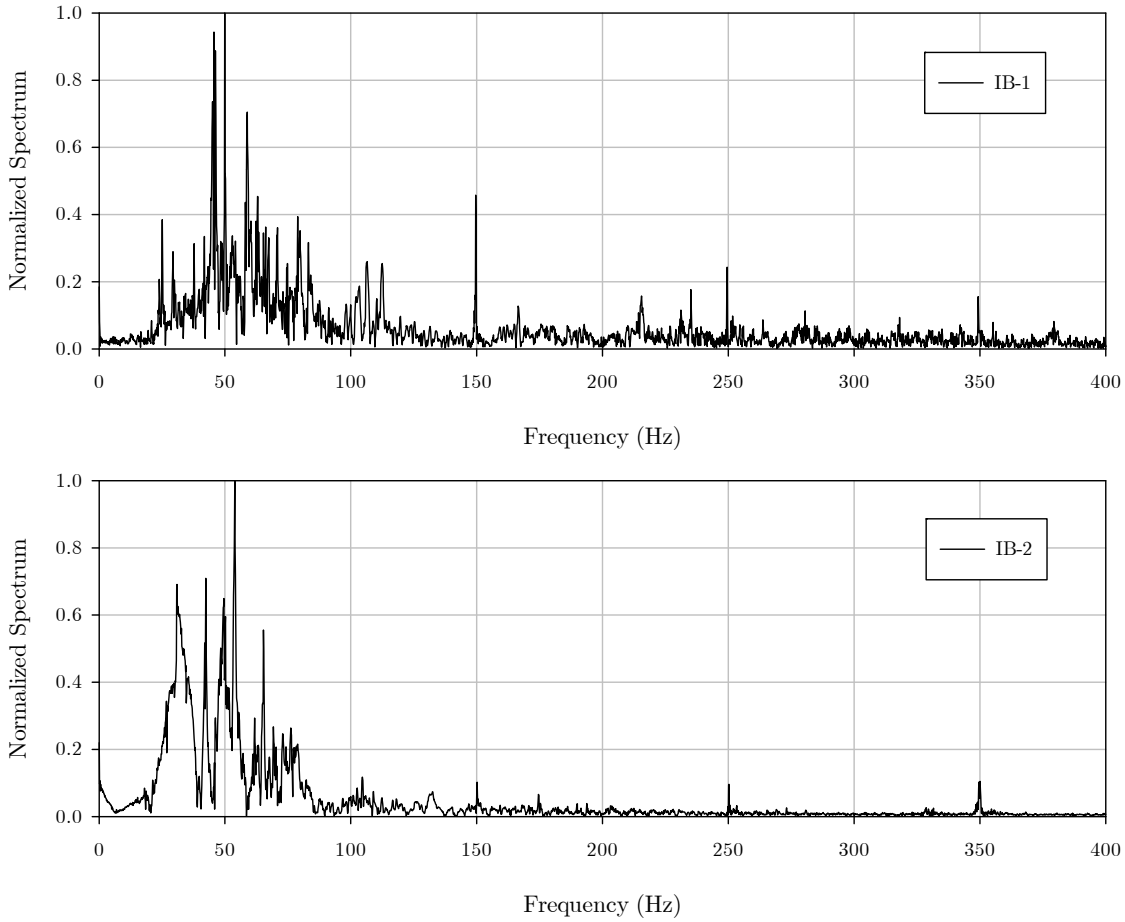

Figure 4-21: Normalized spectra for Izolof (before rehabilitation)

All spectrums for the Izolof measurements made in August 2015 show considerable energy stored between 0 Hz and 100 Hz. Energy in frequencies in excess of 100 Hz is visible, most notably for Test IG-2 (300 Hz to 315 Hz) but the spectrum amplitude is small. Results of the normalized spectra are shown in Figure 4-22.

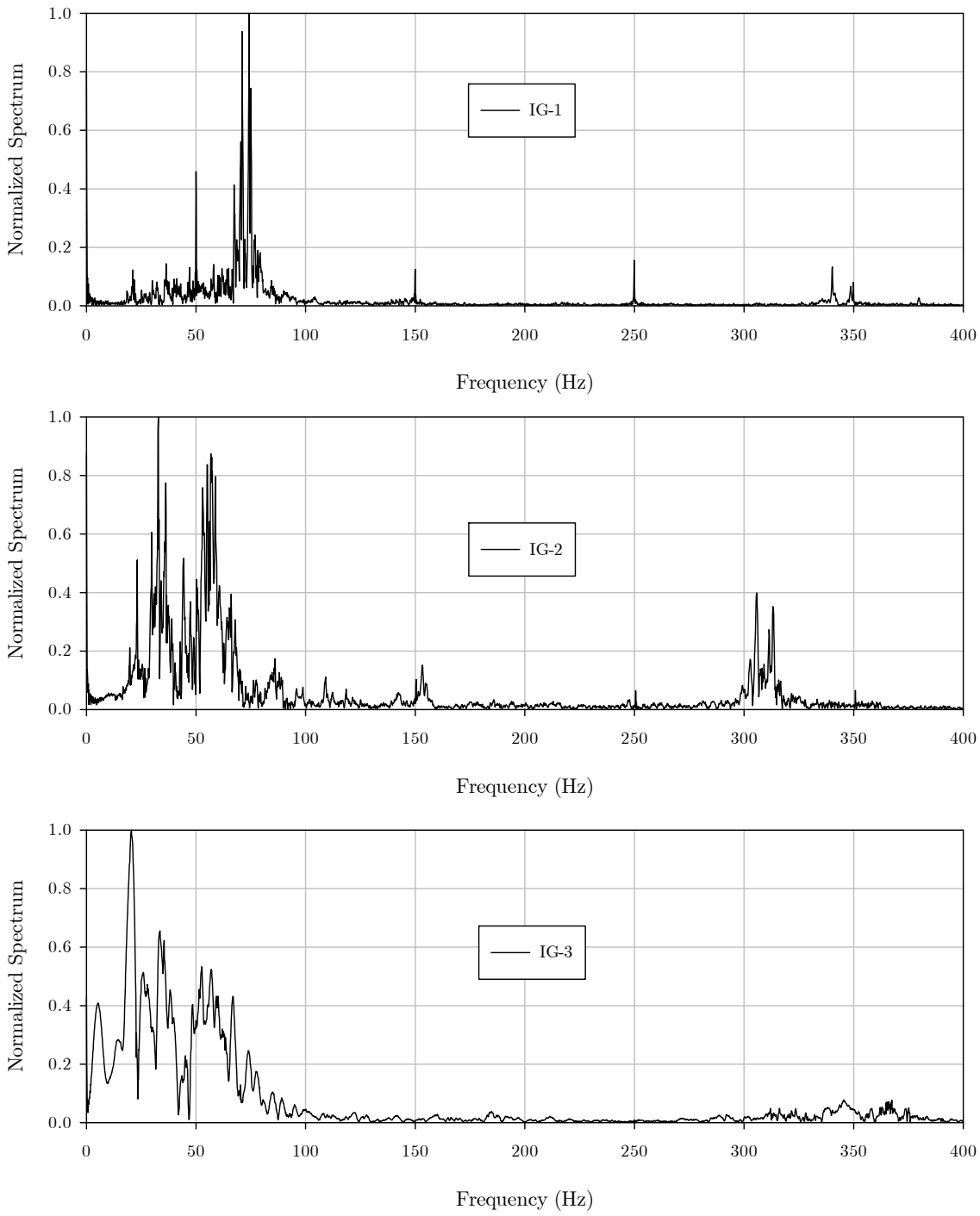

Figure 4-22: Normalized spectra for Izolof (after rehabilitation)

4.3.2 Frequencies associated with the train – track interaction

As a result of the movement of the rolling stock, frequencies associated with the train and train – track interaction were determined. The results of shown on Table 4-2 below.

The results can be summarized as follows:

- Car bogie generally has a dominant frequency of around 1 to 2 Hz;
- Train Axle has a dominant frequency between 4 and 8 Hz;
- Sleepers on the railway track have a dominant frequency between 15 to 29 Hz.

Table 4-2: Frequencies associated with train and track interaction

Test Code	**Locomotive**	**Speed (km/h)**	**Car bogie (Hz)**	**Axle (Hz)**	**Sleepers (Hz)**
A1 - 1	7E	36.0	1	5	15
A1 - 2	7E	36.0	1	5	15
A1 - 3	7E	36.0	1	5	15
B1 - 1	19E	47.0	1	4	20
B1 - 2	7E	67.0	2	8	29
B1 - 3	7E	31.0	1	4	13
IB - 1	19E	55.5	1	5	24
IB - 2	19E	-	-	-	-
IG - 1	19E	48.5	1	4	21
IG - 2	7E	44.7	1	6	19
IG - 3	7E	54.0	2	7	23

These values compare reasonably well with figures described by Priest et al. (2010).

4.3.3 Conclusions of the spectral analyses

From the spectrum analysis of all sites, the following remarks can be made regarding the train – track induced energy propagating in the formation:

- Trains generate energy throughout a broad frequency range, particularly from 0 Hz to 100 Hz;

- In some cases it is possible to see the influence of axle loading and bogie loading which is smaller than 10 Hz in the low end of the spectrum frequency. Sleepers induce energy in the frequency spectrum of 20 Hz;

- Energy in frequencies in excess of 100 Hz can be observed. However, the energy is generally limited to narrow frequency bands;

- It can be assessed that the train is able to produce energy associated with wave propagation in a broad (or wide) region, particularly from 0 Hz to 80 Hz. Energy for frequencies in excess of 80 Hz is generally produced in discrete or narrow bands.

4.4 DISPERSION ANALYSIS OF TRAIN MEASUREMENT DATA

Dispersion data (frequency dependent phase velocity) was calculated for all the measurements included in Table 4-1. The objective of the calculations was to establish whether a trend was observable to differentiate railway track formation response, and the repeatability of the test procedure.

Shot gathers[5] for the analysis process were created according to the findings of the window length analysis detailed above.

Dispersion data was calculated using the MOPA method. Phase information was calculated and unwrapped for each frequency. Two parameters were adopted as acceptance criteria:

- R^2 of 0.95 minimum for the linear regression;

- Frequency bands with energy, as shown by the spectrum graphs.

Coherence is a good indicator of signal quality between any 2 receivers. This indicator is even more relevant for the SASW analysis method. However, for multiple receivers (more than 2),

[5] A collection of seismic traces using multiple receivers

the linearity of the phase difference for the array configuration chosen is the accepted measure for accepting results of a particular frequency.

4.4.1 Initial considerations

4.4.1.1 Hammer tests

Dispersion analysis of the data obtained from the hammer tests was conducted to enable correlation to the dispersion analysis of data obtained from the train measurement. Considering the findings from the spectral analysis and the time window, a 1 s window was adopted for all hammer test analysis.

Typical results of a dispersion analysis are shown in Figure 4-23. Frequency dependent phase velocity and wavelength are calculated. From the results displayed on this graph it can be seen that for low frequency regions, values for phase velocity and wavelength are considerably higher. From the literature it is known that low frequencies usually are adopted for deeper geotechnical site characterization. A sudden increase in the wavelength and phase velocity at a frequency of 83 Hz is noted. This increase corresponds to a shift from a fundamental mode of propagation to a higher mode of propagation of the surface waves.

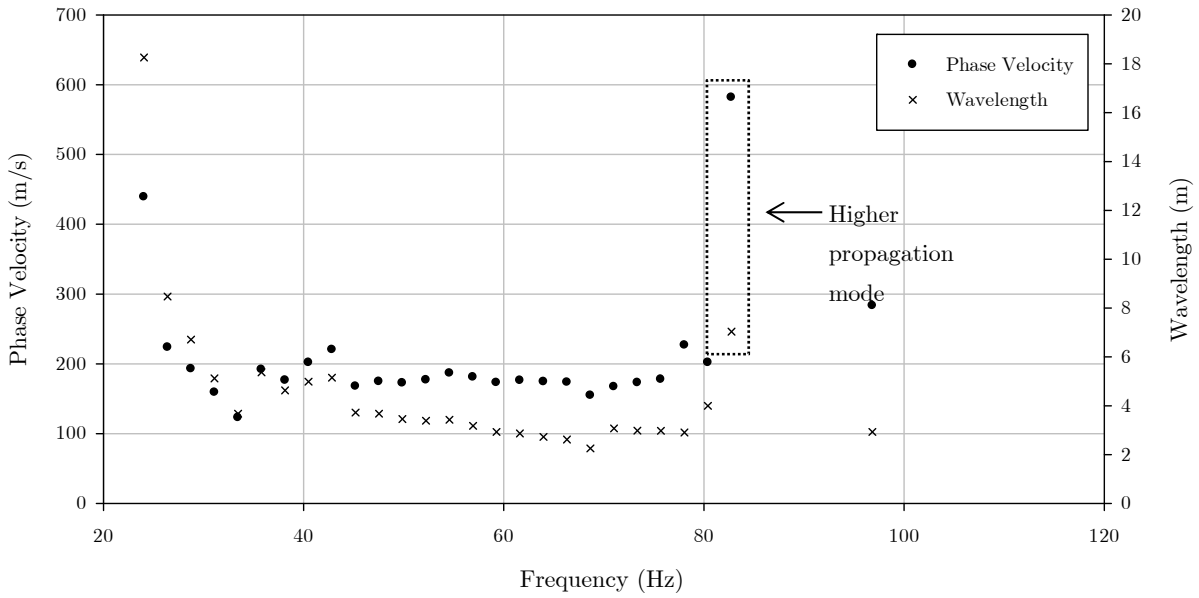

Figure 4-23: Frequency dependent phase velocity and wavelength for Hammer test H-AM

Figure 4-24 shows a profile of the wavelength versus phase velocity for the Amandelbult site. This profile can be used for the first step of the inversion process, establishing a relationship between phase velocity and shear wave velocity. It can be observed that most of the phase velocity values are smaller than 200 m/s for wavelengths varying between 2 m and 7 m.

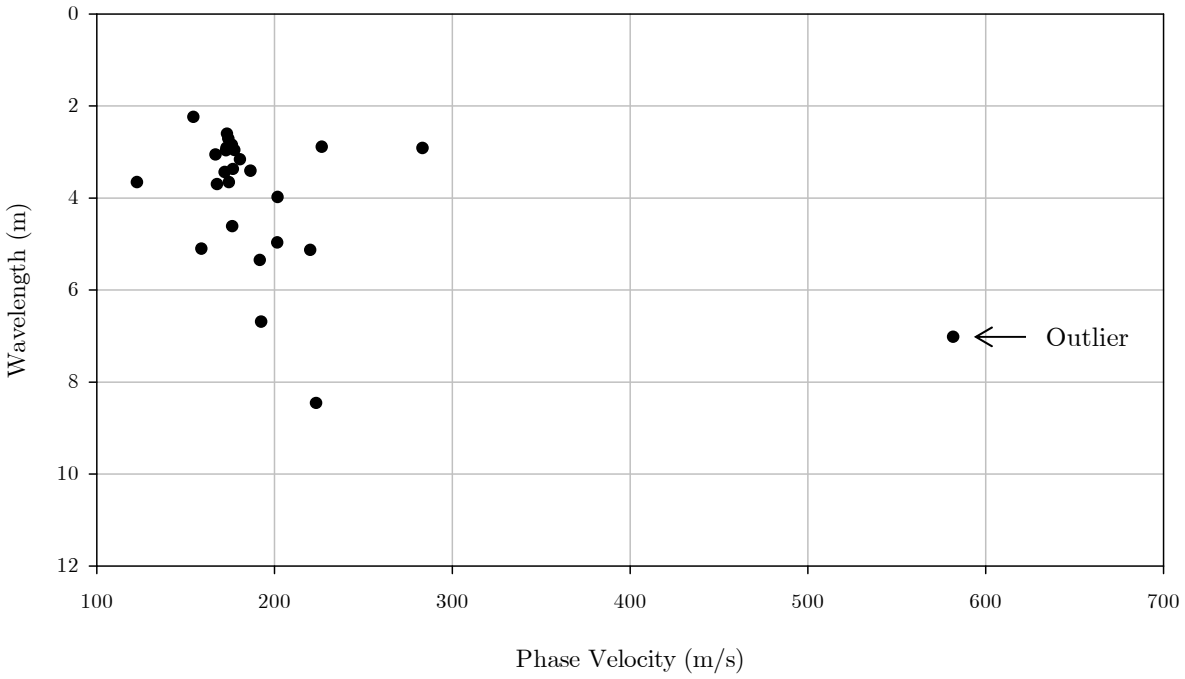

Figure 4-24: Wavelength profile for Amandelbult (window 4 to 5 seconds)

In order to have reliable results from the analysis process, several measurements must be included in the analysis process. A typical example of that procedure is shown in Figure 4-25 where the results of 4 hammer tests at Amandelbult are displayed. Three tests were conducted at the same location (15 sleepers from Geophone 1 – closer to MP6) and the fourth test was performed 10 sleepers away from Geophone 5 (thus closer to MP5).

The influence of higher modes of propagation results in increased scatter and makes the analysis process challenging, unless an inversion process is performed. Results from frequencies higher than 60 Hz include values of higher modes for some of the tests.

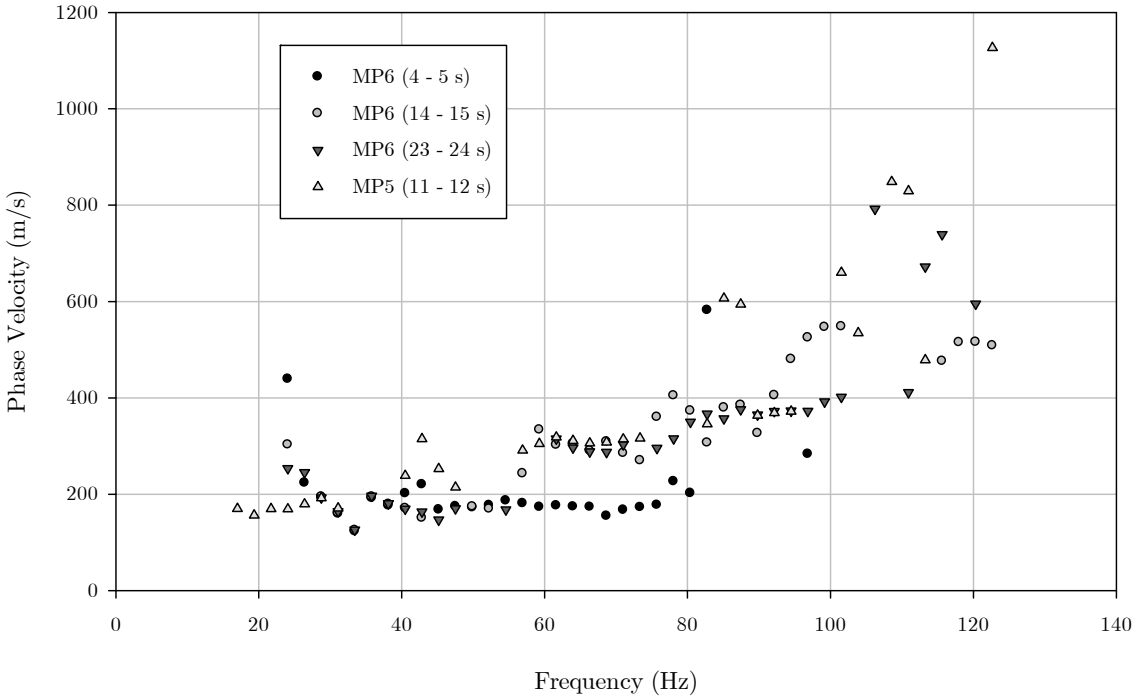

Figure 4-25: Hammer test dispersion data for 2 different impact locations at Amandelbult

A statistical analysis of the results is shown in Figure 4-26. Average and standard deviation were calculated. Standard deviation values increase in the high frequency range.

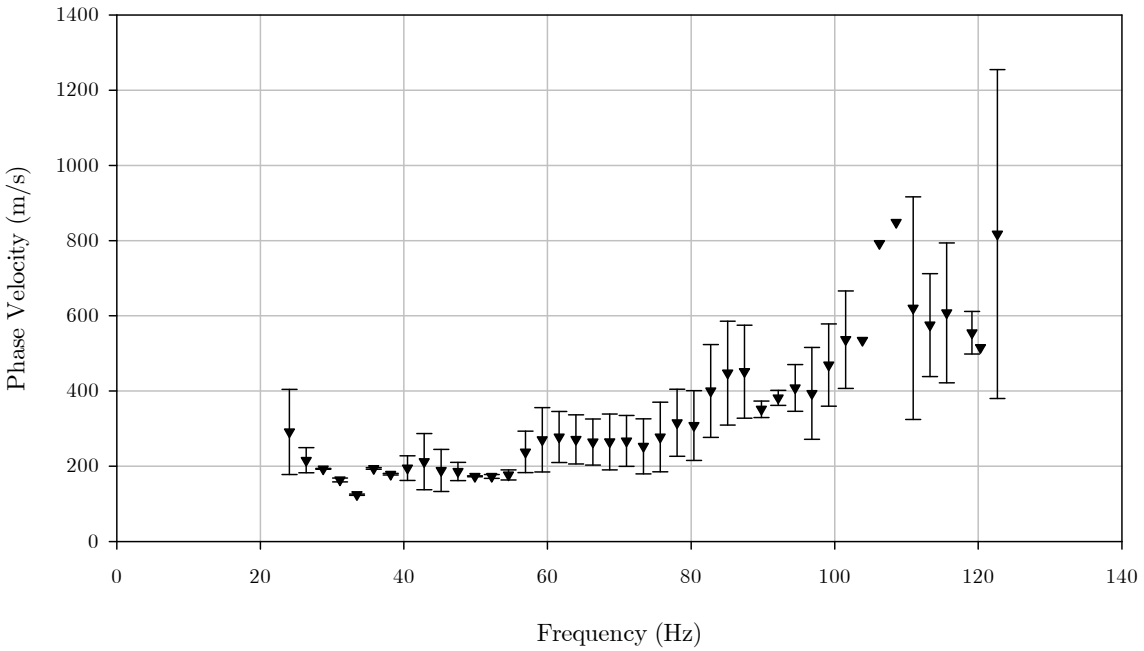

Figure 4-26: Average phase velocity for a hammer test at Amandelbult

4.4.1.2 Train measurements

Calculation of dispersion data for train measurements was also performed using the multi-offset phase angle method. Travel speed of the trains varied between 35 km/h and 60 km/h and several types of locomotives were included.

Typical results of a dispersion analysis for a train measurement are shown in Figure 4-27. Higher modes of propagation are evident both in the low and high frequency ranges. Data points follow the same trend as obtained using the impact hammer test, namely higher phase velocity values in the low frequency range and phase velocity between 150 m/s and 200 m/s in the high frequency range.

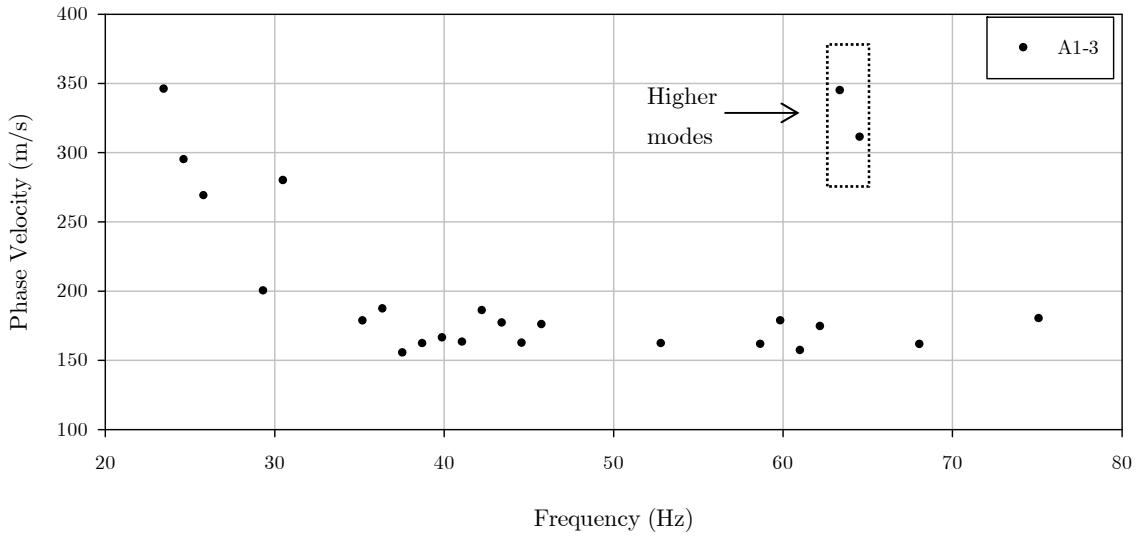

Figure 4-27: Dispersion data for train measurements at Amandelbult

The corresponding wavelength versus phase velocity profile is shown in Figure 4-28. Data points from higher modes of propagation changes the pattern of the wavelength profile.

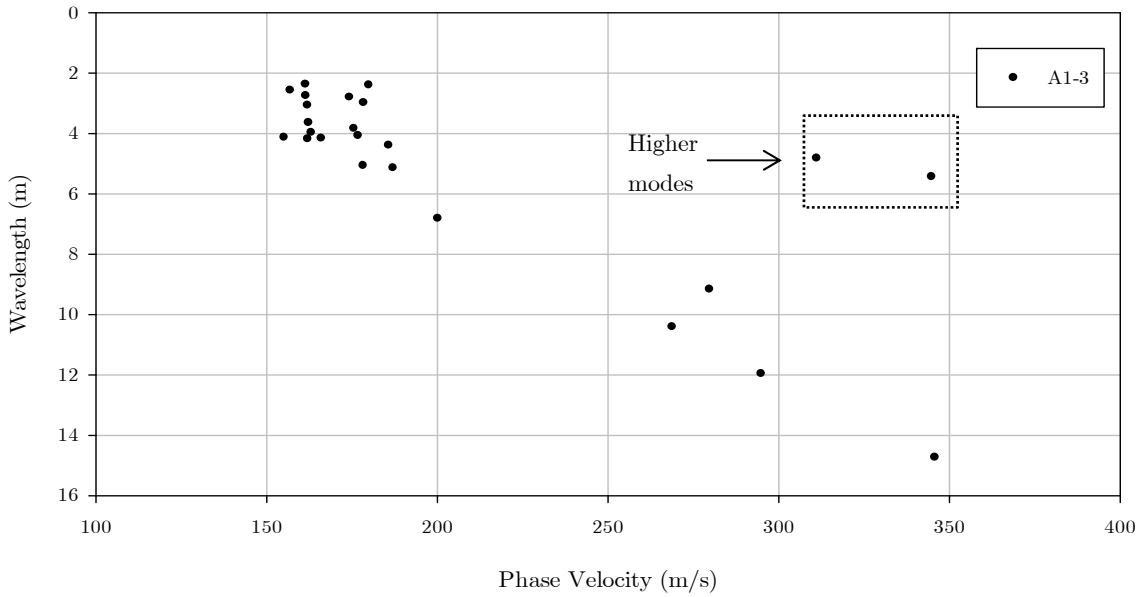

Figure 4-28: Wavelength for a train measurement at Amandelbult

4.4.2 Dispersion results

4.4.2.1 Site dispersion results

The results of the dispersion data calculations shown in Paragraph 4.4.1 indicate that several modes of propagation are observable. These higher modes of propagation are valuable information for the inversion process and increase the resolution of the shear velocity profile.

Inversion analysis will not be performed for this research project. To compare and analyse the data obtained, results of phase velocity for higher modes will therefore not be considered. This will have an effect of reducing the scatter of the results, but will also considerably reduce the frequency range where the fundamental mode is the predominant mode.

The dispersion data of all 4 sites were fitted with a polynomial, inverse third order curve in the form of $y = y_0 + \frac{a}{x} + \frac{b}{x^2} + \frac{c}{x^3}$ where a,b,c are coefficients; x is the frequency and y_i is the phase velocity.

Additionally, profiles of wavelength versus phase velocity were also created for each specific site. These profiles fitted with trend lines complement the information obtained in the dispersion analysis (from which the dispersion curves are calculated).

Figure 4-29 below shows the curve fitted to the dispersion data after removing the higher modes. Phase velocity for the frequency range from 30 Hz and higher seems to be uniform, varying between 150 m/s and 200 m/s. These values are comparatively low, typical of silty and clayey material.

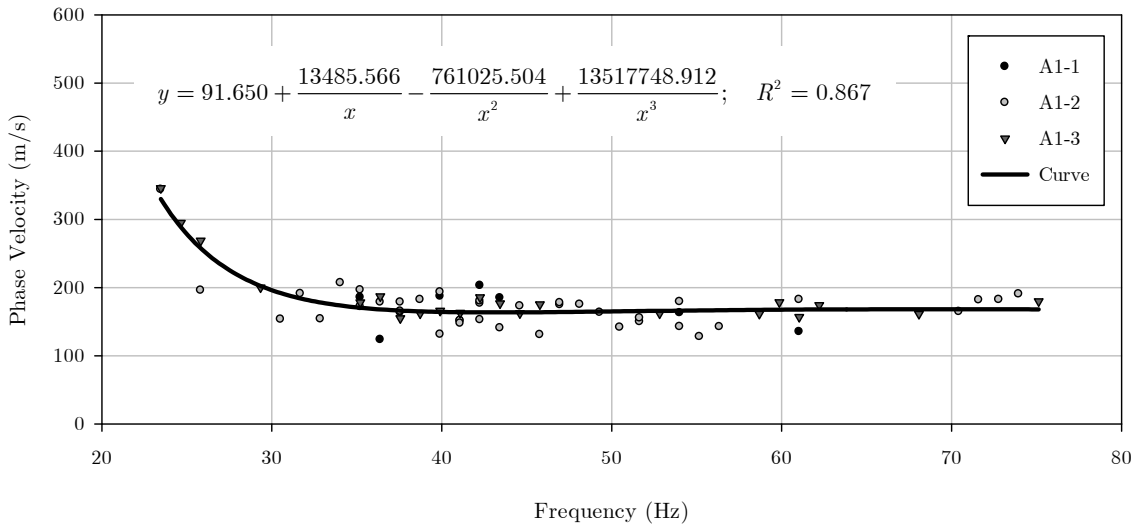

Figure 4-29: Dispersion curve for Amandelbult

Variation of the phase velocity versus the wavelength for Amandelbult is shown in Figure 4-30 below. From these results it can be seen that there is a general trend of constant phase velocity for wavelengths between 2 and 5 m. Phase velocity in this range has an average of 175 m/s. Phase velocity of lower magnitude (less than 150 m/s), for wavelengths of around 2 m are visible. Lower values of wavelength were not obtained as a result of the frequency range produced by the source that was limited to 75 Hz.

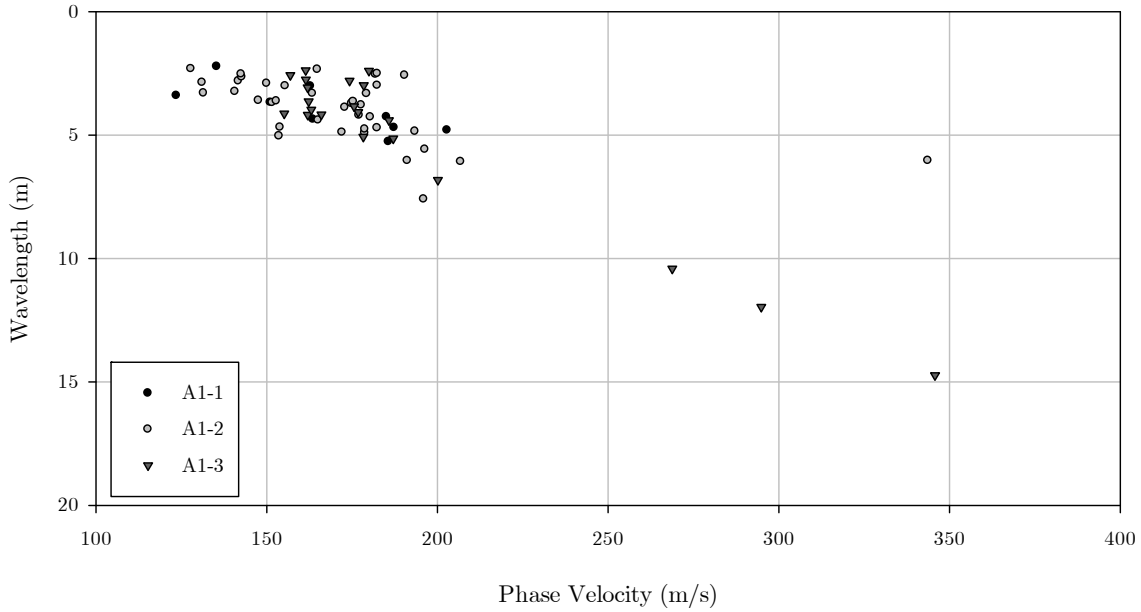

Figure 4-30: Wavelength profile – Amandelbult

The dispersion curve for the Bloubank measurements is shown in Figure 4-31 below. The phase velocity for frequencies from 20 to 30 Hz is in excess of 1000 m/s. Phase velocities in the 200 m/s region are calculated for frequencies around 40 to 60 Hz before they start to increase gradually with the increase in frequency. The fitted curve parameters are displayed in the graph.

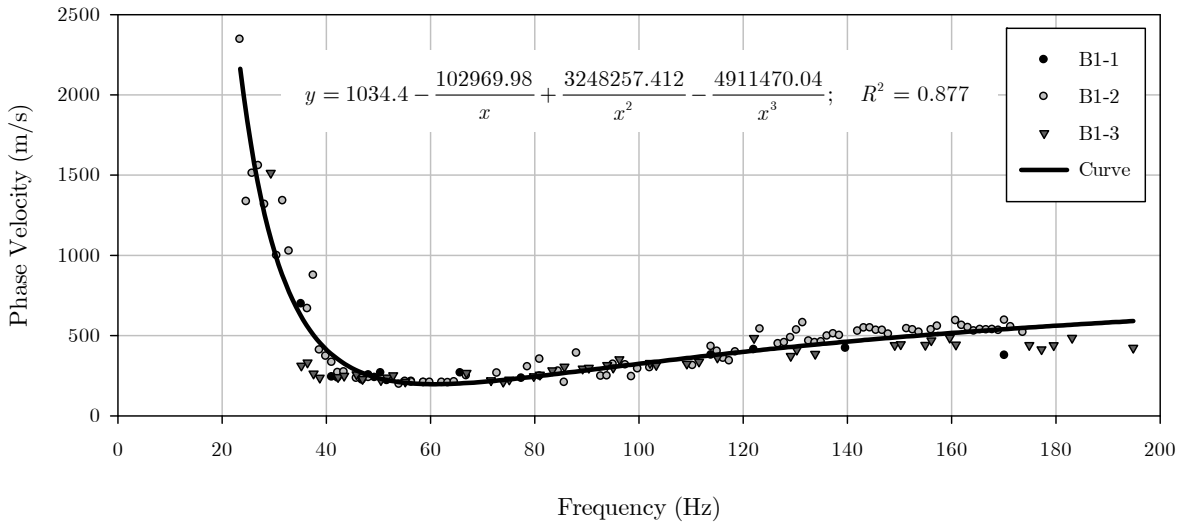

Figure 4-31: Dispersion curve for Bloubank

The wavelength versus phase velocity profile is plotted in Figure 4-32 below. Wavelengths of 2 m to 3 m have phase velocities in the region of 300 m/s to 400 m/s. Phase velocity reduces for wavelengths of 4 m to 6 m to velocities between 200 m/s and 300 m/s before they increase with increasing wavelength values.

The larger wavelengths were sampled at frequencies in the 20 Hz region, and have values in excess of 40 m, with phase velocities in excess of 1200 m/s.

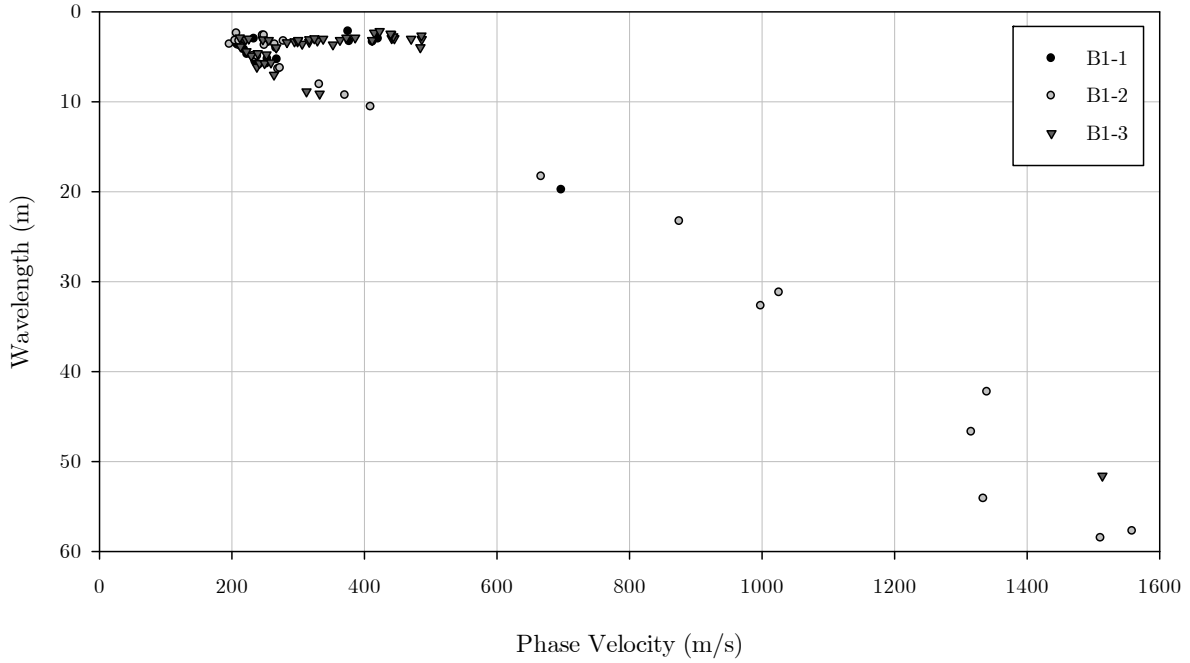

Figure 4-32: Wavelength versus phase velocity profile – Bloubank

The dispersion data of the Izolof site (before rehabilitation was undertaken) was obtained using two train measurements. Only a few points were obtained that satisfied the set criteria in the dispersion analysis for the frequency region between 20 Hz and 100 Hz.

Between 20 Hz and 30 Hz, phase velocity is in excess of 400 m/s, but limited to a maximum of 800 m/s. The lowest value occurs at 50 Hz with a phase velocity of 100 m/s. Phase velocities between 200 m/s and 350 m/s were calculated for frequencies between 80 Hz and 130 Hz (Figure 4-33).

Measurements for Test IB-2 yielded phase velocities comparatively slower than results obtained for Test IB-1 for similar frequencies (mainly between 60 Hz and 90 Hz). However, the phase

velocity – wavelength graph shows that the wavelengths generated in these two tests had similar phase velocities. Due to the mud pumping phenomenon that was prevailing at the time that those tests were conducted, and the time lapse between the first and the second test (5 hours), it was observed that the second test was conducted under increased moisture of the formation layers.

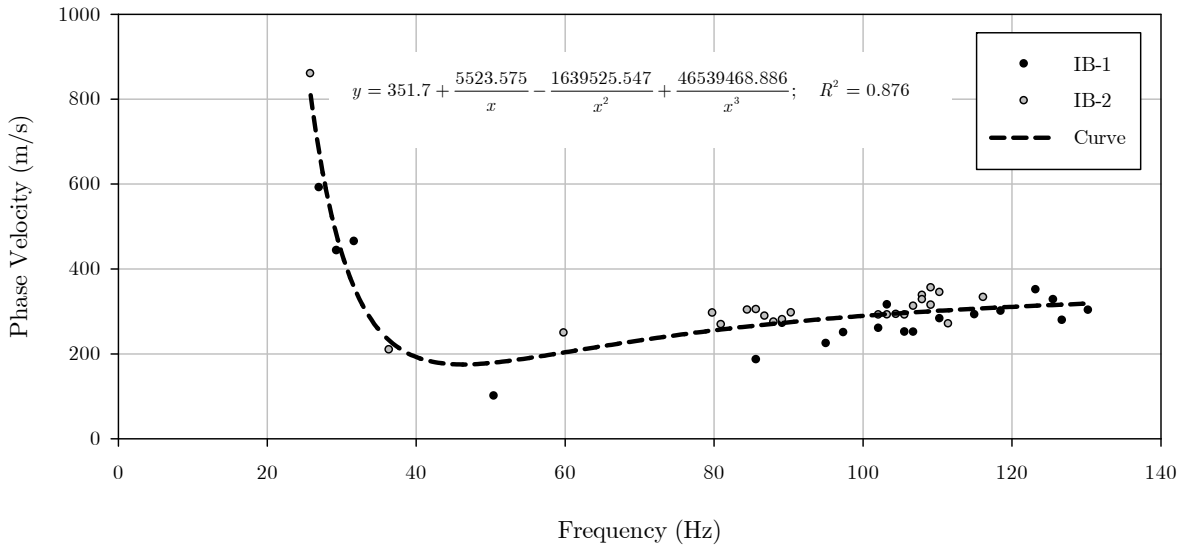

Figure 4-33: Dispersion curve for Izolof BR

The profile of the wavelength versus the phase velocity for the Izolof site before rehabilitation shows that phase velocity increases continually with an increase in the wavelength, starting with a value of 100 m/s for a wavelength of 2.0 m. For wavelengths less than 4.0 m, the phase velocity is consistently in the 250 m/s to 380 m/s region (Figure 4-34).

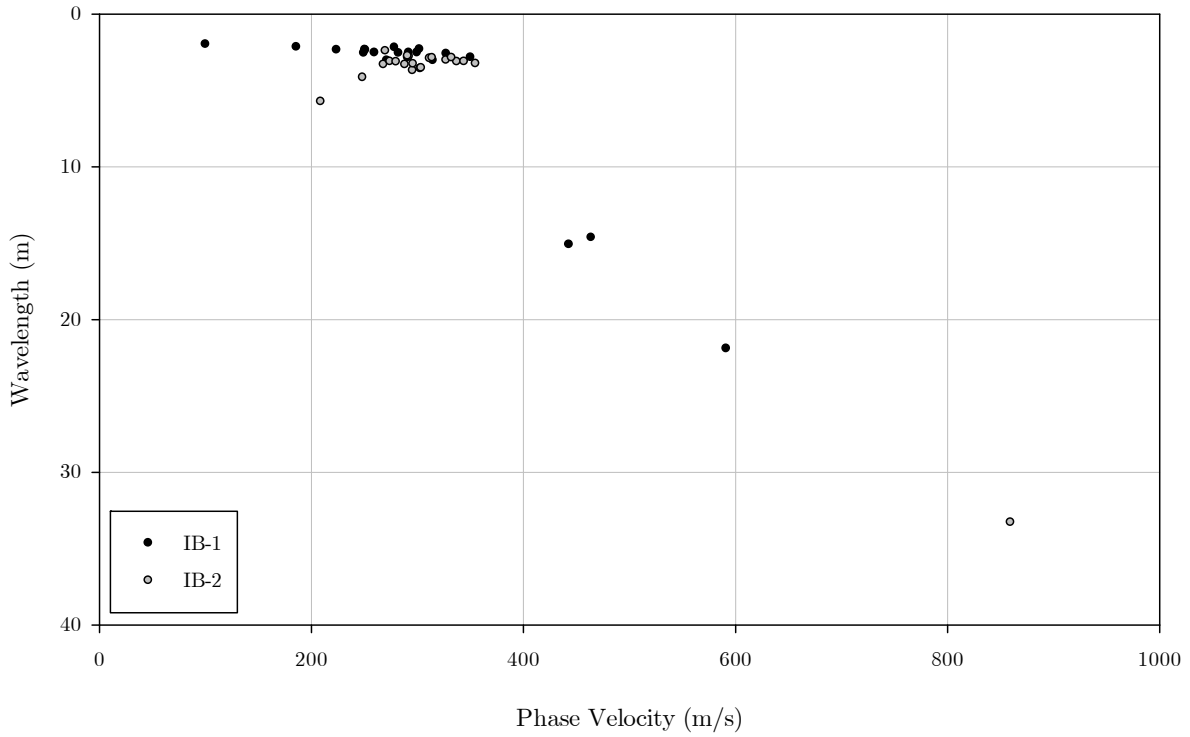

Figure 4-34: Wavelength versus phase velocity profile for Izolof BR

Dispersion data for the Izolof site (after rehabilitation) was calculated for measurements acquired at a lower sampling frequency of 2400 Hz.

Phase velocities are consistently greater than 200 m/s throughout the frequency range of interest. Figure 4-35 shows the general trend of the data, with a curve fitted.

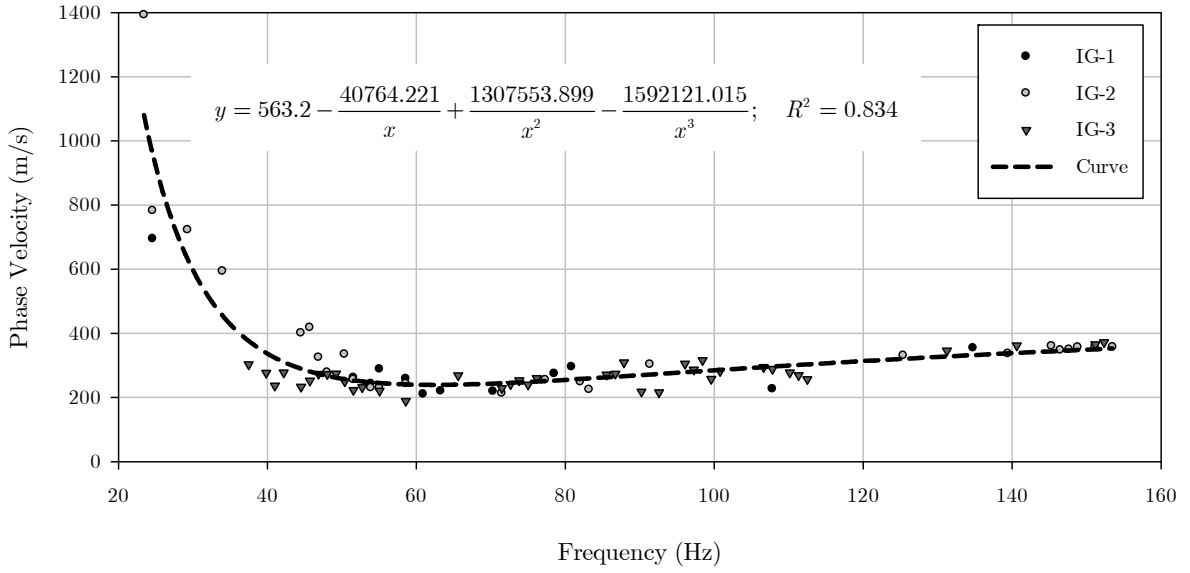

Figure 4-35: Dispersion curve for Izolof AR

Wavelengths of 2 m to 6 m are mostly propagating at velocities between 200 m/s and 300 m/s, although some higher velocities are achieved for wavelengths between 2 m and 3 m. As the wavelength increases, the phase velocity also increases, achieving speeds of 400 m/s for a wavelength of 9 m.

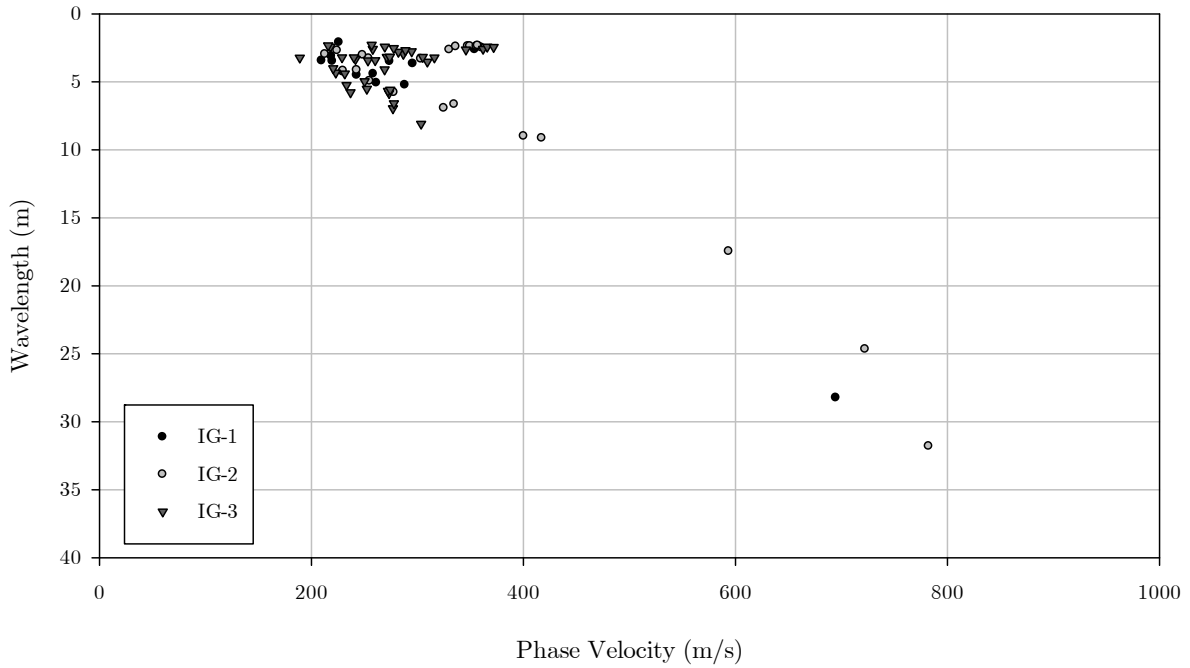

Figure 4-36: Wavelength versus phase velocity profile for Izolof AR

4.4.2.2 Comparison of dispersion curves

After calculating the dispersion curves for each specific site, they are plotted together in Figure 4-37 and Figure 4-38 below.

From the results displayed on the graphs below, the following comments can be made regarding the dispersion curves of possible mode superposition of the four sites investigated:

- Amandelbult has the lowest phase velocities in the frequency range 20 to 80 Hz.
- Similar phase velocities are observed for the dispersion curve of the Izolof site (before rehabilitation) and the Amandelbult site in the frequency region between 40 Hz and 60 Hz.

- The frequency range for the Amandelbult site is shorter (from 22 Hz to 75 Hz), compared to the other 3 sites. The following short frequency range is Izolof (before rehabilitation).

- For frequencies lower than 40 Hz, Bloubank has the highest phase velocities. The same is also true for frequencies higher than 100 Hz.

- Dispersion curves for both Izolof sites are similar for most of the frequency range, except for the region from 25 Hz to 60 Hz where phase velocities for Izolof (after rehabilitation) are greater than the phase velocities for Izolof (before rehabilitation).

For the train measurements, the fundamental mode of the propagation dispersion data was obtained in the frequency band between 20 Hz and 190 Hz.

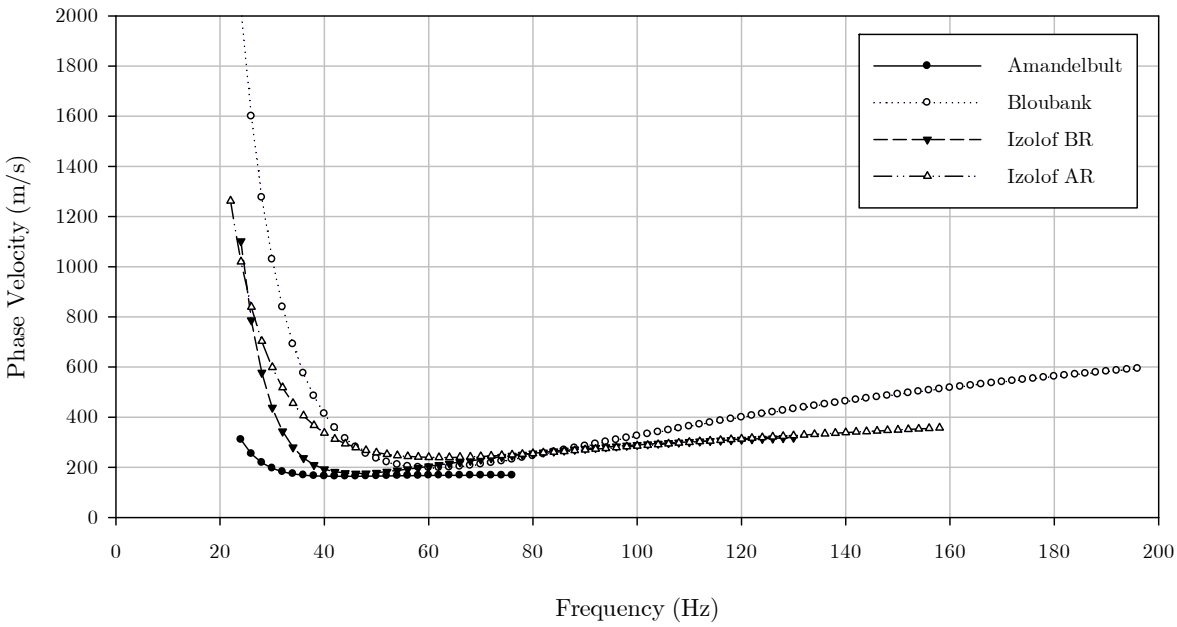

Figure 4-37: Comparison of dispersion curves for all sites

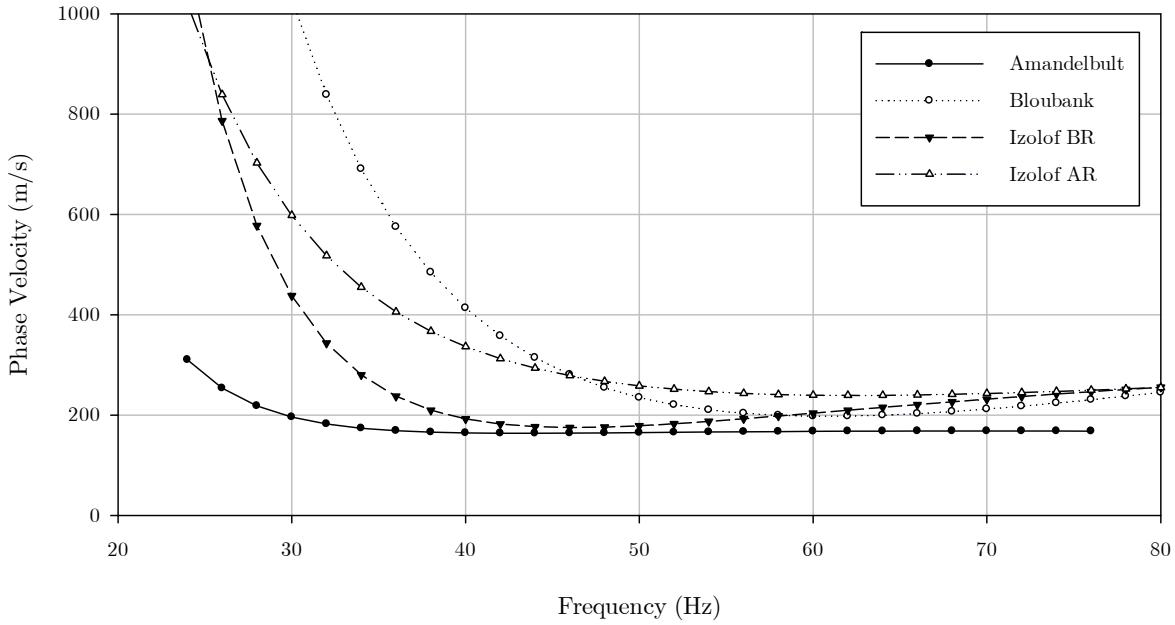

Figure 4-38: Detailed comparison of dispersion curves on a narrow frequency range (20 to 80 Hz)

4.4.2.3 Comparison of wavelength versus phase velocity profiles

Comparison of wavelength profiles is aimed at identifying the phase velocity trends at all four sites analysed.

From the individual data profiles it is visible that most data points are concentrated in the region of less than 5 m long wavelengths. The minimum wavelength obtained was 1.9 m and the maximum 58 m. Formations for heavy haul railway lines typically are in the order of 800 mm in thickness for the imported layers, with a thickness of 200 mm each. The propagation of these shorter wavelengths will then be influenced by the overall formation structure.

Taking into account the distribution of the wavelength between the minimum and maximum value and the formation thickness, analysis of the profiles was divided into the following bands: (a) wavelengths less than 3 m; (b) wavelengths between 3 m and 5 m; (c) wavelengths between 5 m and 10 m; and (d) wavelengths greater than 10 m.

Of importance for this study is the first interval (wavelength less than 3 m), as it is related to propagation characteristics within the formation layer. Average values and standard deviations for each of the analysis bands were obtained for each site and are presented in Figure 4-39.

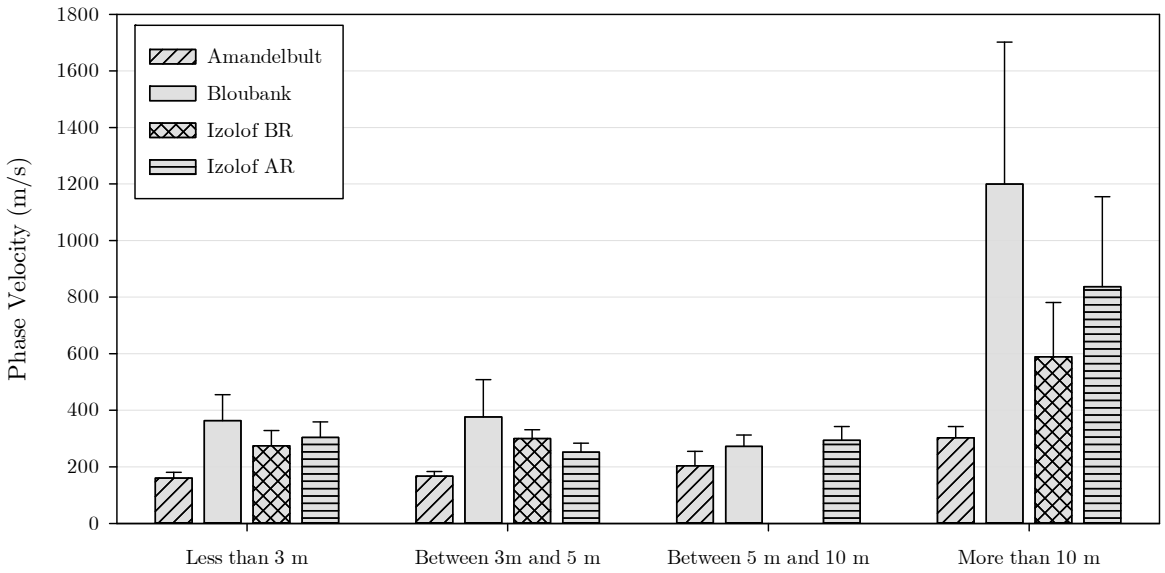

Figure 4-39: Analysis of wavelength profile

From the results shown in Figure 4-39, the following conclusions can be drawn:

- Amandelbult has the lowest phase velocity in all bands analysed. Its phase velocity is fairly constant for surface waves propagating with wavelengths up to 5 m (between 160 m/s and 167 m/s). An increase in phase velocity is attained for longer wavelengths (between 200 m/s and 300 m/s).

- Bloubank has the highest phase velocity in the band for wavelengths shorter than 3 m. The phase velocity for the Izolof site is greater for the measurements conducted after rehabilitation of the formation in May 2015 (304 m/s), compared to the measurements conducted before rehabilitation of the line (274 m/s).

- The phase velocity for Izolof before rehabilitation (300 m/s) is higher than the phase velocity for Izolof after rehabilitation (252 m/s) for the band of wavelengths between 3 m and 5 m. Just a single dispersion data point was obtained for Izolof (before rehabilitation) for the band of wavelength between 5 m and 10 m (with a phase velocity of 208 m/s) and was not included in the statistical analysis.

- Higher standard deviations were calculated for the band containing wavelengths greater than 10 m. This is due to the fact that for all sites (except Amandelbult), longer

wavelengths have greater phase velocities, thus increasing the deviations from the average value.

4.5 DISCUSSION OF RESULTS

The geophysical analysis of the surface waves propagating at the surface of the formation when a train moves over the railway line were discussed in the preceding paragraphs. The analysis is now complemented using a more conventional approach, using the deflection data collected during the geophysical testing and a visual assessment conducted before the testing commenced.

4.5.1 Conventional analysis of track condition

From visual assessment, the evaluation of the condition of the 4 sites indicated the following:

- The section under consideration at Amandelbult was in good condition, although the track was established on poor formation geomaterials. This was considered to be a bad site, for the purposes of this work.

- Bloubank was considered to be a good site, on a sound geological formation.

- Izolof shares the same geological formation as Bloubank. It is located in a cut section. However, due to lack of subsurface drainage and deteriorating geometrical condition, the site was in extremely poor condition when the first test session was conducted (March 2015) with "mud pumping" clearly visible. During the May 2015 Coal Line shutdown (10 day maintenance operation), this section was completely reconstructed. The site was therefore considered to be in a good condition in August 2015, during the second test session.

Summarizing the results for the deflection analysis, using a characteristic 20 t axle load (typical axle load for a 7E locomotive) which is applicable to all sites under investigation, the following can be stated for track analysis:

- The site with the highest track stiffness value was Izolof AR.

- Bloubank had the second largest track stiffness value, whilst Amandelbult had the third highest stiffness value.

- Deflection values at Izolof BR were considerably higher and resulted in a track stiffness value much smaller compared to the other sites due to unsupported sleepers at the vicinity of the test station.

Results of the sleeper deflection analysis are summarized in Figure 4-40.

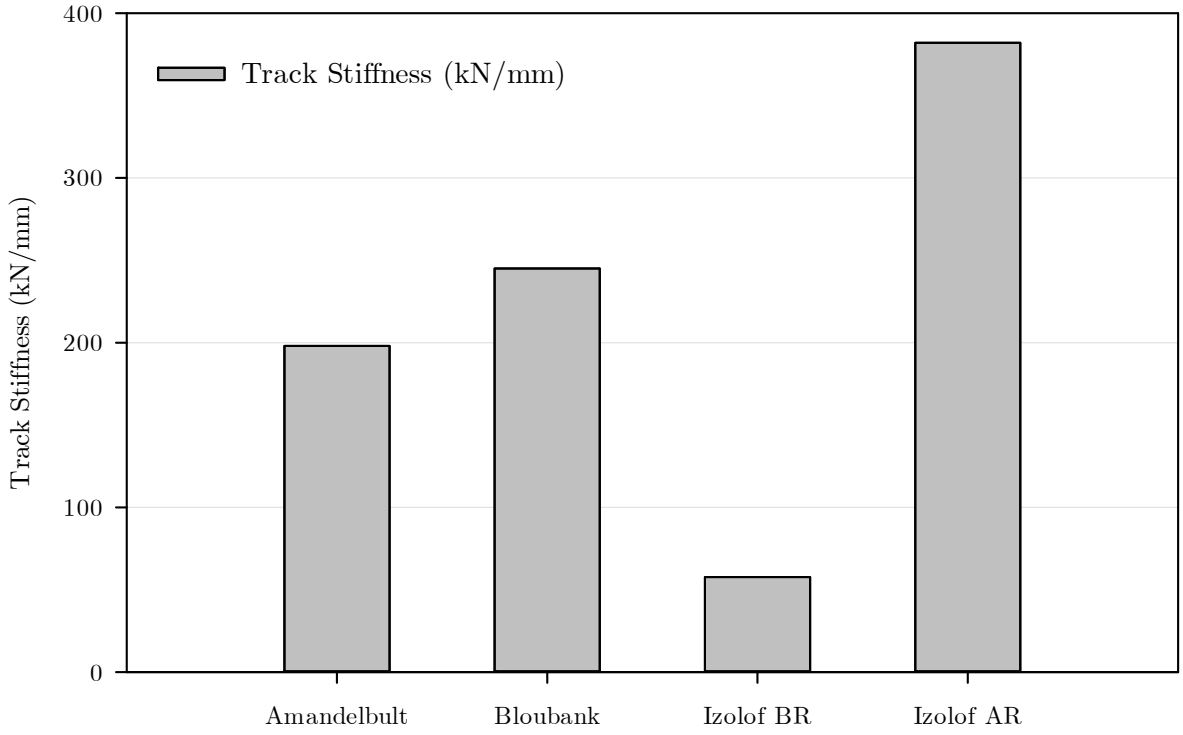

Figure 4-40: Track stiffness of the 4 sites for a 20 t axle load train

The results of the deflection analysis confirmed the observations of the visual analysis. The sites which were identified as having a poor formation exhibited the lowest track stiffness, for the entire load range on the railway lines investigated, although Amandelbult did not differ significantly compared to Bloubank.

Analysis of deflection of the formation for all sites resulted in the following observations:

- Poor load transfer resulted in significantly reduced deflection values for Izolof BR, thus yielding higher than expected formation stiffness values for this site.

- Of the other 3 sites, Amandelbult had the lowest formation stiffness and Bloubank the highest.

Results of formation deflection analysis are summarized in Figure 4-41 below.

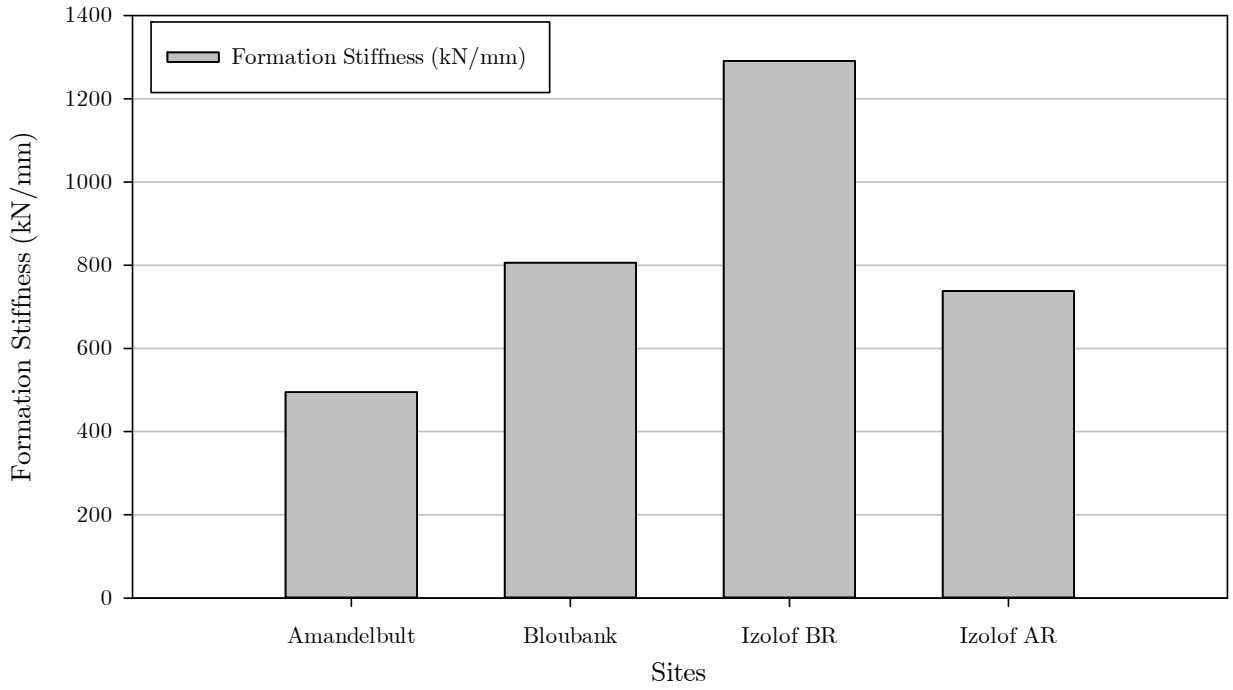

Figure 4-41: Formation stiffness of the 4 sites for a 20 t axle load train

4.5.2 Testing setup and equipment

The geophones were tested to check the reliability of the readings it produced during testing. It was found that the geophones were operating properly in the frequency range of 20 Hz to 300 Hz. The higher end of the frequency range used for the geophone calibration was adopted to minimize the risk of spurious frequencies in the collected data. Because only dispersion analysis was conducted, only phase angle information was taken into account during geophone calibration. The main conclusions were:

- The results indicate that the geophones have similar phase angles at the dominant frequency for each of the tests.

- At low frequency, close to the natural frequency of the geophones, differences in the phase angles can be up to 10 degrees (0.18 Radians).

- For frequencies above 20 Hz, the phase angle of the geophones are much closer, with differences being less than 1 degree (less than 0.017 radians).

- Spurious frequencies were not observed for any of the geophones used for testing, in the frequency range analysed.

These results confirm that the readings from the geophones are reliable and can be used for further processing.

4.5.3 Spectral analysis

The signal measurements in time series were converted from the time domain to the frequency domain using Fast Fourier Transform (FFT) methods. Phase angle and real and imaginary parts of the signal were calculated and used to process the signal acquired by the geophones. Several windows of time series in the time domain were investigated to understand which carried significant information for the purposes of the surface wave analysis related to this research.

In order to minimize the complexity of the signal being acquired, only time series that were recorded before the train reached the first receiver of the array, were taken into consideration for further analysis. Additionally, the strain regime of the dispersion analyses methods also contributed for this approach.

To analyse the impact on the quality of signal being measured by the geophones in different time series, auto power spectrum and coherence function calculations were adopted for the preliminary assessment.

For the auto power spectrum the following observations were made (Figure 4-13):

- The shapes of the transforms of all time windows were similar throughout the frequency range.

- For the transforms of the earlier time windows (i.e. when the train was further away from the receiver array) the highest amplitude of the frequency range were on the lower side (closer to 0 Hz);

- For the transforms of the later time windows (i.e., when the train was closer to the receiver array) the highest amplitudes occurred in the 0 Hz to 100 Hz range. Some energy was visible for higher frequencies (although of lower amplitude);

- The distribution of energy within the frequency range with considerably higher power spectrum amplitude was discrete and not continuous as it might have been when obtained from a controlled vibration generator (i.e., mechanical shaker).

Taking into consideration that the power spectrum indicates the signal quality of each geophone and the trends established above, it is apparent that the energy associated with the propagation of the surface waves is dependent on the time from which the propagation is being sampled.

It is also apparent that for signals recorded when the train was further away from the receiver array, energy would be stored at the lower end of the frequency range. If the signal is recorded when the train is closer, the energy associated with the ground vibration is spread over a higher frequency range.

Analysis using the coherence function showed good signal quality (coherence function greater than 0.95), over the following frequency ranges:

- *Between 10 Hz and 60 Hz* for time windows of measurements where the train was further away from the receivers. Good coherence values at frequencies higher than 100 Hz were also found, although in narrow bands. Signal quality was found to be low for frequencies in excess of 200 Hz.

- *Between 10 Hz and 200 Hz* for time windows of measurements where the train was closer to the receivers. Good coherence values were found at discrete frequencies with good quality signals throughout the frequency range.

For frequencies greater than 200 Hz (and all time window scenarios analysed), poor signal quality was observed. Good quality signals were mainly found for frequencies smaller than 200 Hz (Figure 4-14). This was also observed for the auto power spectrum analysis.

Trends from the results show that for shorter time windows, signal quality between two sensors is poor over the majority of the frequency band. Signal quality increases with increased time window (Figure 4-16).

Because of the fact that the main factors influencing these measurements (or signals) and the spectral results of signals acquired are (i) the train and (ii) the train-track interaction, it can be stated that the quality of the seismic signals are greatly influenced by these 2 variables.

From the spectrum analysis of all sites (see Figure 4-42 below), the following remarks can be made regarding the train and train – track induced energy propagating in the formation of the railway:

- Trains generate energy throughout a broad frequency range, particularly from 0 Hz to 100 Hz.

- In some cases it is possible to see the influence of axle loading and bogie loading which are smaller than 10 Hz in the low end of the spectrum frequency. Sleepers induce energy in the frequency spectrum of 20 Hz. Further analysis of these signal contributors was not carried out due to the relatively low frequencies.

- Energy in frequencies in excess of 100 Hz can be observed. However, the energy is generally limited to narrow frequency bands.

- It can be assessed that the train is able to produce energy associated with wave propagation in a broad (or wide) region, particularly from 0 Hz to 80 Hz. Energy for frequencies in excess of 80 Hz is generally produced in discrete or narrow bands.

- The condition of the formation does not seem to have a significant effect on the results of the spectral analysis.

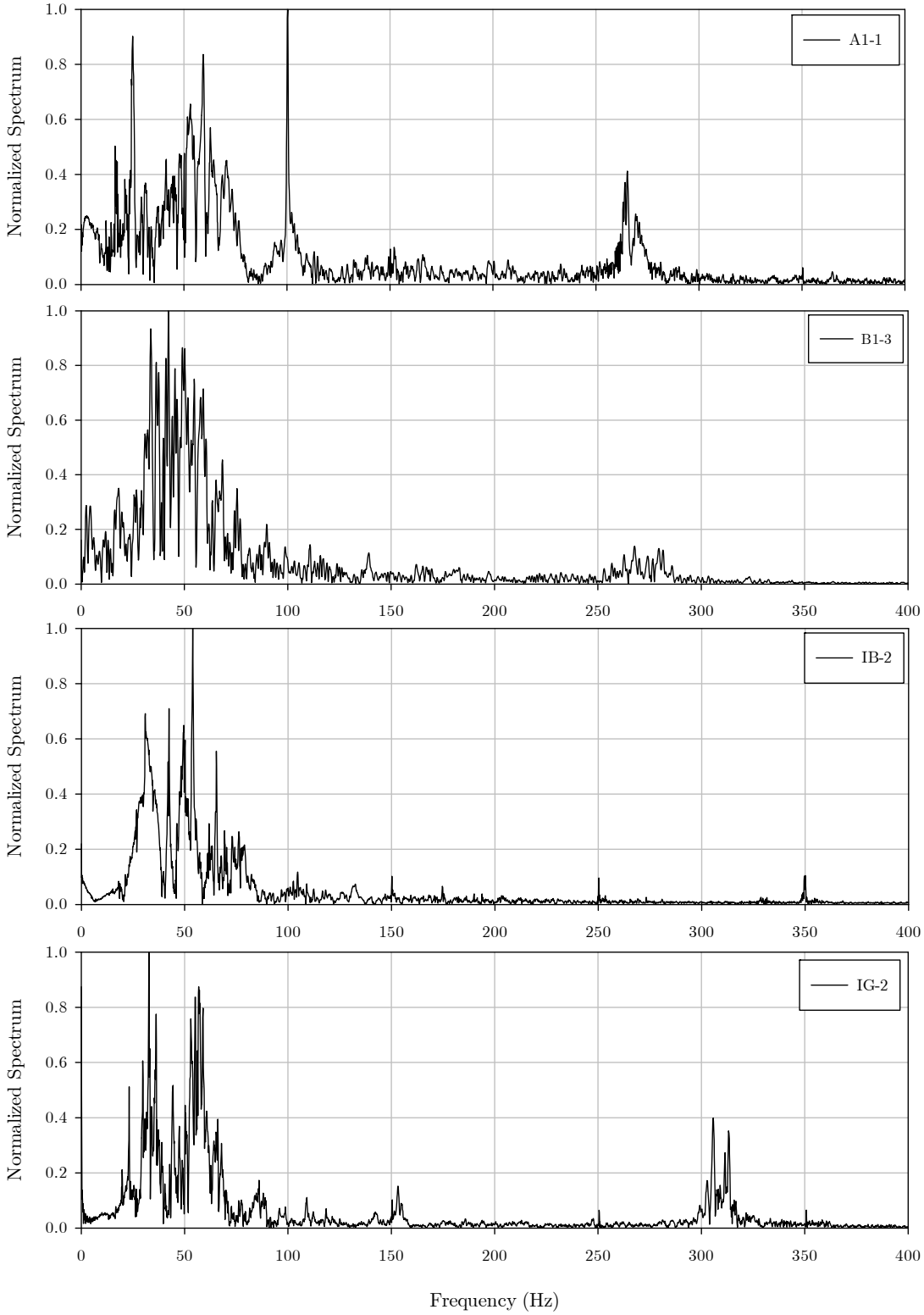

Figure 4-42: Comparison of spectral results for all sites

4.5.4 Comparison of dispersion analysis and conventional stiffness method

Dispersion analysis provided dispersion curves (phase velocity versus frequency) from which wavelengths were also calculated. Although dispersion analysis is used for the inversion process in which shear velocity profile can then be established, for this research its results were used to determine whether a trend in the formation condition could be established.

Two hammer test time histories were analysed to observe the events that were recorded as a result of the impact on the railhead (for Amandelbult and Bloubank). The velocity of propagation of such events were different between the two sites, with Bloubank exhibiting the higher value, but the limited number of tests available makes the analysis of these tests harder to draw a meaningful conclusion on the relevance of such findings.

Average phase velocity values were derived for groups with varying wavelength, from which values calculated for wavelengths of 3 m or shorter were used to make comparisons between all 4 sites.

It was established that Amandelbult had the slowest phase velocity and Bloubank had the highest. This means that in terms of assessment, Bloubank was the site with the best formation characteristics and Amandelbult the worst (see Figure 4-39). Izolof AR was established as performing better than Izolof BR, although the difference in phase velocity was not considerable.

A comparison between the results provided by the track & formation deflection analysis and the dispersion analysis are provided in Figure 4-43 and Figure 4-44 below. The following observations can be made:

- Both methods indicate that Bloubank and Izolof AR performed better than Amandelbult and Izolof BR.
- Track deflection results indicated that Izolof AR had the greatest track stiffness at 20 t axle load, whilst Izolof BR had the lowest. For the formation analysis, Bloubank had the highest stiffness value and Amandelbult the lowest.

- Within the deflection method (for sleeper and formation measurements) there is no agreement regarding performance or condition of formation at Izolof BR.

- A poor correlation was found between the analysis results of the three methods for Izolof BR.

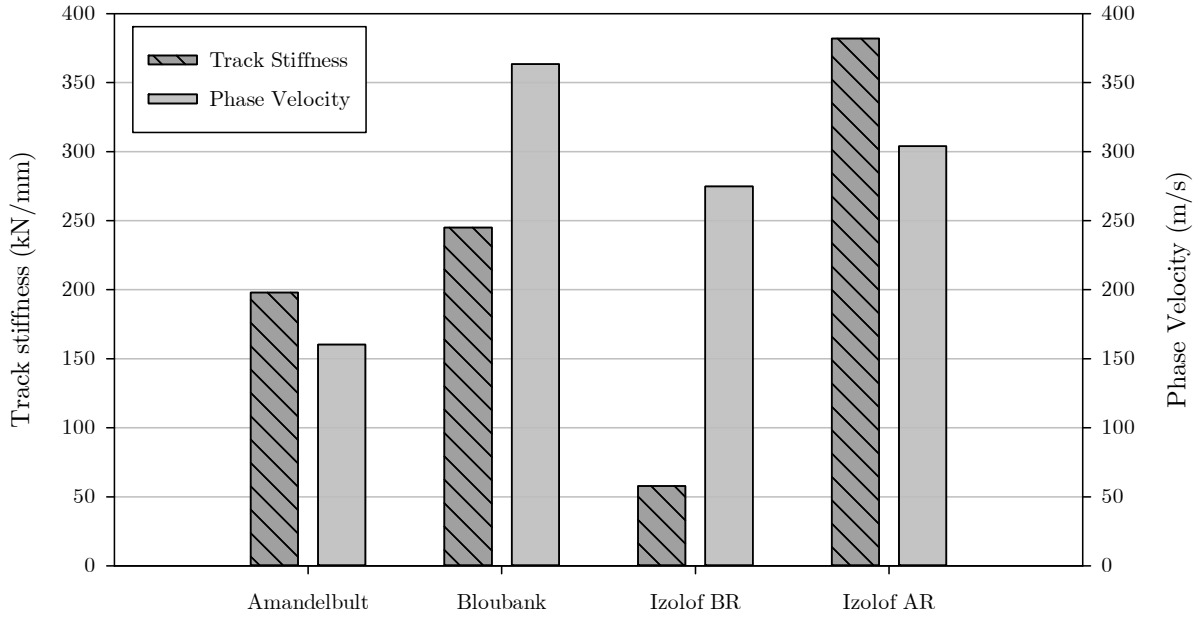

Figure 4-43: Comparison of track stiffness and phase velocity for all 4 sites

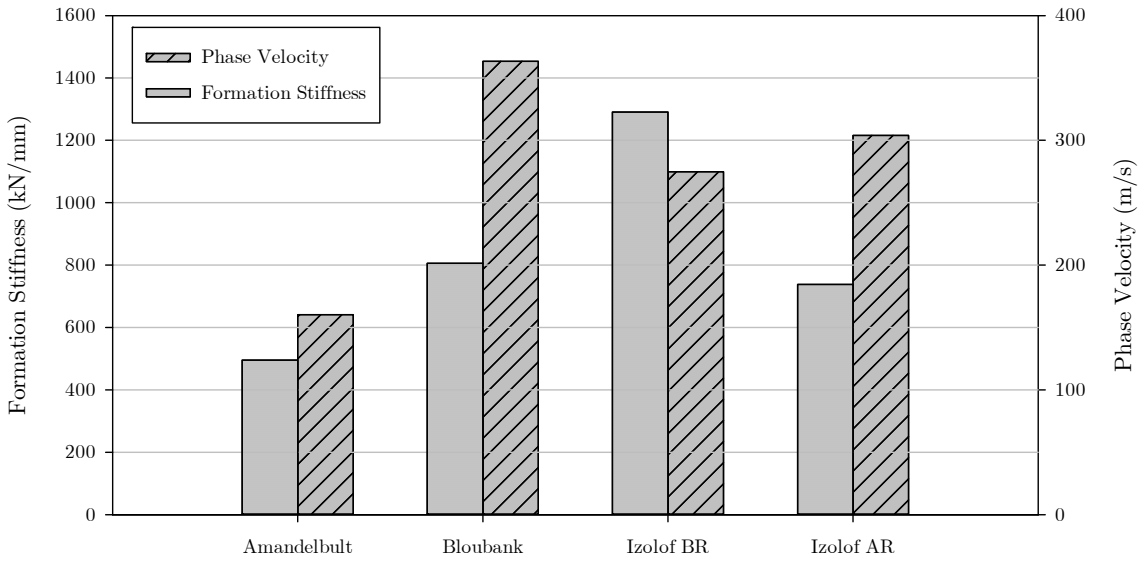

Figure 4-44: Comparison of formation stiffness and phase velocity for all sites

The apparent disagreement of the results for Izolof BR is likely due to the fact that the train (and train-track interaction) did not produce short enough wavelengths that would propagate through the formation at shallow depth. This is a limitation of the test setup that could have been improved by generating surface wave energy in higher frequency range that ultimately results in very short wavelengths. However, the train-track interaction alone does not produce this type of very low wavelength and a mechanical shaker might be required to be incorporated in the test setup.

Figure 4-45 below plots the track stiffness results versus the phase velocity results. By fitting a linear trend line through the data, it is possible to observe that a good correlation is not obtained. A contributing factor for this is the fact that Bloubank, having the highest phase velocity, has a lower track stiffness compared to Izolof AR. This indicates that a good correlation between track stiffness (or track deflection) and phase velocity is not likely to be obtained. Izolof BR was not included in the assessment of the correlation, due to limitations found on the testing data (number of tests run and unsupported sleepers resulting in excessive deflection at the test station).

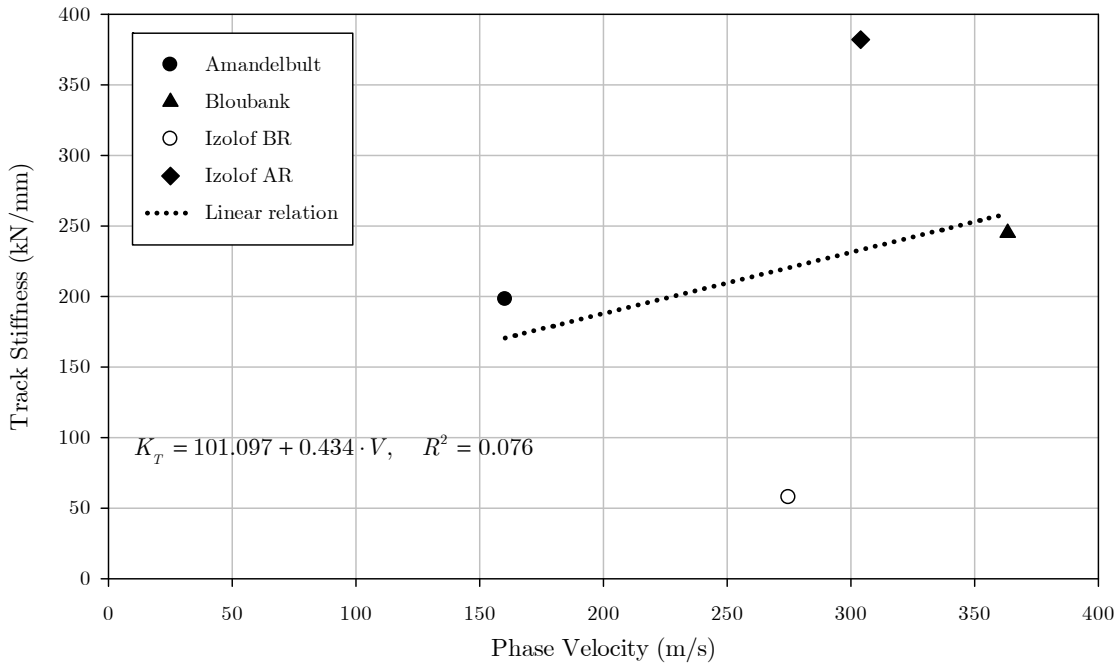

Figure 4-45: Trend line for comparison of track stiffness versus phase velocity

Figure 4-46 below plots the formation stiffness results versus the phase velocity results. By fitting a linear trend line through the data, a good correlation is obtained. From this result it is possible to correlate phase velocity with formation stiffness (or deflection).

Due to the poor load transfer noted at Izolof BR, this site was not included in the correlation analysis. However, with the phase velocity value that was calculated for this site, it is possible with the linear relationship developed for these two parameters (phase velocity and formation stiffness) to calculate the expected deflection value.

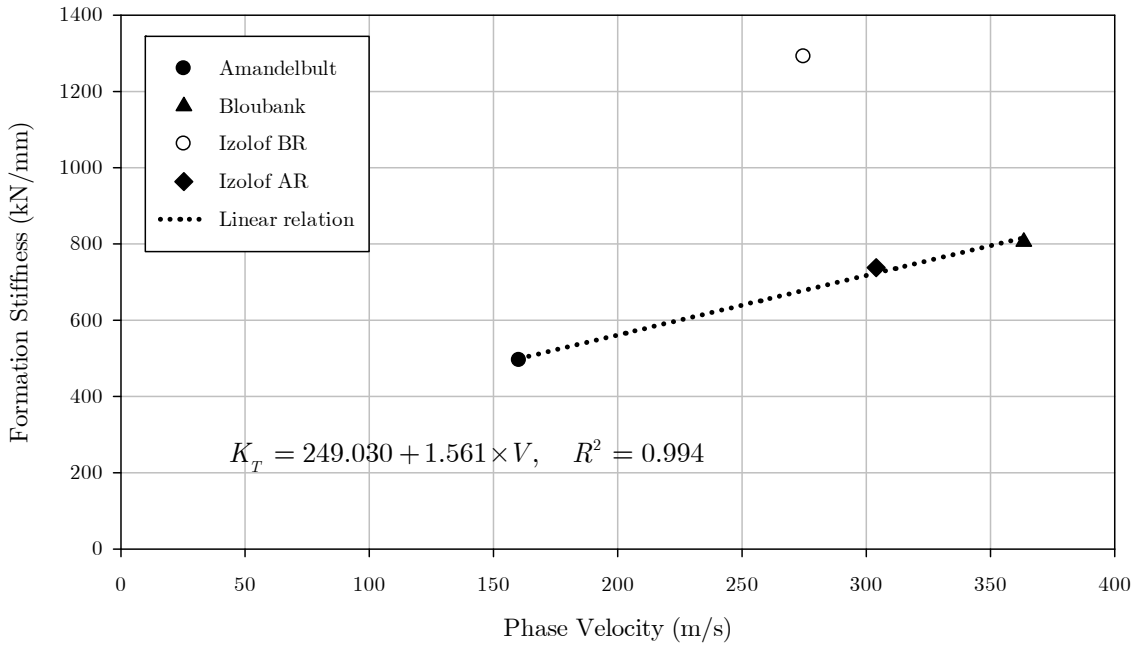

Figure 4-46: Trend line for comparison of formation stiffness and phase velocity

5. CONCLUSIONS AND RECOMMENDATIONS

5.1 CONCLUSIONS

The objective of this research work was to develop and validate a testing procedure to assess the condition of formation of a ballasted railway track using surface wave methods. Comparison of the results obtained using dispersion analysis and track deflection methods were conducted. The following conclusions can be made:

- The generated ground vibration during the passage of a train can be properly measured using an array of receivers (in this case geophones). A linear array is recommended, with equal spacing between the receivers.

- The receivers can be placed adjacent to the track within the limits of the subballast layer.

- Results of the dispersion analysis were found to be similar for the two sources used, namely an impact test with a hammer and a train approaching the instrumented site.

- Multiple modes of surface waves were observed in the dispersion analysis of the formation structures.

- The phase velocity calculated from the dispersion analysis of the fundamental mode can be adopted as a measure to indicate a trend in relation to the formation condition or stiffness.

- A linear relationship between phase velocity and formation stiffness was obtained for surface waves with a wavelength of 3 m and shorter.

- As expected, track stiffness does not correlate well with phase velocity.

- The train and the train-track interaction produced surface waves with energy in the frequency range from 0 Hz to 100 Hz. Some energy was visible at higher frequencies, but with lower amplitude and at discrete frequency values.

- The frequency range that was produced by the ground vibration measurements was relatively short for analysis of shallow (thin) structures and did not produce short enough wavelengths that can enable the determination of mechanical properties of individual layers.

- The generated wavelengths from the train movement can be used to perform "deep" characterisation of the site in which the railway track is operating.

- Signals recorded when the train was further away from the receiver array resulted in energy being stored at the lower end of the frequency range. When the signal was recorded with the train being closer to the receiver, the energy associated with the ground vibration was spread over a higher frequency range.

- The use of low frequency geophones limits the analysis to the region of 5 Hz - 300 Hz. For analysis of signals with higher frequency, it is required to incorporate accelerometers in the experimental test setup.

- The source (train) generates frequency too low to measure formation stiffness.

5.2 RECOMMENDATIONS

The following recommendations can be made:

- Accelerometers should be incorporated in the experimental setup in order to further investigate the nature of the signal generated by the ground vibration during the passage of a train in the high frequency range.

- Additionally, in terms of experimental setup, a campaign of testing that incorporates a mechanical shaker with sufficiently high frequency range (in monotonic or sweep modes) should also be considered together with the train and the hammer, to measure ground vibration and analyse the obtained data.

- Data obtained from this testing campaign can then be analysed using active and passive surface wave methods, to investigate which methods are better suited to analyse ground

movements resulting from train – track interaction. In this regard, it is also important to consider that the train position relative to the receivers array is of relevance.

- The spacing between the receivers should be further investigated by conducting tests with shorter spacing and more receivers (reduce spacing and maintain length of the array).

- The increased number of receivers should be used to accurately determine the multiple modes of propagation of the surface waves, in order to achieve a better dispersion analysis.

- Inversion of the results from the dispersion analysis should be carried out to investigate the resolution of the shear wave velocity profile.

- The linear relationship that was established between phase velocity and formation stiffness should be confirmed by conducting additional tests. A parametric study to develop factors or coefficients should also be undertaken.

6. REFERENCES

ATHANASOPOULOS, G., PELEKIS, P. & ANAGNOSTOPOULOS, G. 2000. Effect of soil stiffness in the attenuation of Rayleigh-wave motions from field measurements. *Soil Dynamics and Earthquake Engineering,* 19**,** 277-288.

BENDAT, J. S. & PIERSOL, A. G. 2011. *Random data: analysis and measurement procedures*, John Wiley & Sons.

BOWNESS, D., LOCK, A., POWRIE, W., PRIEST, J. & RICHARDS, D. 2007. Monitoring the dynamic displacements of railway track. *Proceedings of the Institution of Mechanical Engineers, Part F: Journal of Rail and Rapid Transit,* 221**,** 13-22.

CONNOLLY, D. P. & FORDE, M. C. Calculating Critical Velocity of Trains from Rayleigh Waves Using Conventional Site Investigation Parameters. Transportation Research Board 94th Annual Meeting, 2015.

ESVELD, C. 2001. *Modern railway track,* Zaltbommel - Netherlands, TU Delft.

FERRY, J. D. 1980. *Viscoelastic properties of polymers*, John Wiley & Sons.

FOTI, S. 2000. *Multistation methods for geotechnical characterization using surface waves.* PhD Dissertation, Politecnico di Torino.

FOTI, S., LAI, C. G., RIX, G. J. & STROBBIA, C. 2014. *Surface Wave Methods for Near-Surface Site Characterization*, Crc Press.

GRABE, P. J. 2004. New Insights Into Railway Vehicle, Track and Formation Interaction. *Proceedings of the IPET Conference.* Tshwane University of Technology, Pretoria.

GRAFF, K. F. 1975. Wave motion in elastic solids. Clarendon Press, Oxford.

HALL, L. 2003. Simulations and analyses of train-induced ground vibrations in finite element models. *Soil Dynamics and Earthquake Engineering,* 23**,** 403-413.

JAMIOLKOWSKI, M., LANCELLOTTA, R., MARCHETTI, S., NOVA, R. & PASQUALINI, E. Design parameters for soft clays. Proceedings of the 7th European Conference on Soil Mechanics and Foundation Engineering, Brighton, UK, 1979. 10-13.

JONGMANS, D. & DEMANET, D. 1993. The importance of surface waves in vibration study and the use of Rayleigh waves for estimating the dynamic characteristics of soils. *Engineering geology,* 34**,** 105-113.

KAEWUNRUEN, S. & REMENNIKOV, A. M. 2007. Field trials for dynamic characteristics of railway track and its components using impact excitation technique. *Ndt & E International,* 40**,** 510-519.

KINNAIRD, J. A. 2005. The Bushveld large igneous province. *Review Paper, The University of the Witwatersrand, Johannesburg, South Africa, 39pp.*

KJARTANSSON, E. 1979. Constant Q - wave propagation and attenuation. *Journal of Geophysical Research: Solid Earth (1978 – 2012),* 84**,** 4737-4748.

KRYLOV, V. V. 1995. Generation of ground vibrations by superfast trains. *Applied Acoustics,* 44**,** 149-164.

KRYLOV, V. V., DAWSON, A., HEELIS, M. & COLLOP, A. 2000. Rail movement and ground waves caused by high-speed trains approaching track-soil critical velocities. *Proceedings of the Institution of Mechanical Engineers, Part F: Journal of Rail and Rapid Transit,* 214**,** 107-116.

KRYLOV, V. V. & FERGUSON, C. C. 1993. Calculations of ground vibrations from heavy-freight trains.

LAI, C. G. & RIX, G. J. 1998. *Simultaneous inversion of Rayleigh phase velocity and attenuation for near-surface site characterization*, School of Civil and Environmental Engineering, Georgia Institute of Technology.

LIU, H.-P., ANDERSON, D. L. & KANAMORI, H. 1976. Velocity dispersion due to anelasticity; implications for seismology and mantle composition. *Geophysical Journal International,* 47**,** 41-58.

MENKE, W. 2012. *Geophysical data analysis: discrete inverse theory*, Academic press.

NELDER, L., ENGLAND, C., ARMITAGE, R., BROUGH, M., FLEMING, P. R. & FROST, M. W. 2008. A comparison of trackbed design methodologies: a case study from a heavy haul freight railway.

PAOLUCCI, R., MAFFEIS, A., SCANDELLA, L., STUPAZZINI, M. & VANINI, M. 2003. Numerical prediction of low-frequency ground vibrations induced by high-speed trains at Ledsgaard, Sweden. *Soil Dynamics and Earthquake Engineering,* 23**,** 425-433.

PRIEST, J., POWRIE, W., YANG, L., GRABE, P. & CLAYTON, C. 2010. Measurements of transient ground movements below a ballasted railway line. *Géotechnique,* 60**,** 667-677.

RICHART, F. E., HALL, J. R. & WOODS, R. D. 1970. Vibrations of soils and foundations.

SANTAMARINA, J. C. & FRATTA, D. 2005. *Discrete signals and inverse problems: an introduction for engineers and scientists*, John Wiley & Sons.

SELIG, E. T. & LI, D. 1982. Track modulus: Its meaning and factors influencing it. *Transportation Research Record,* 1470**,** pp 47-54.

STROBBIA, C. 2003. Surface wave methods: acquisition, processing and inversion. *Torino: Politecnico di Torino.*

STROBBIA, C. & FOTI, S. 2006. Multi-offset phase analysis of surface wave data (MOPA). *Journal of Applied Geophysics,* 59**,** 300-313.

STRUTT, J. W. & RAYLEIGH, L. 1885. On waves propagated along the plane surface of an elastic solid. *Proceedings of the London Mathematical Society,* 17**,** 4-1.

SUIKER, A. S., CHANG, C. S., DE BORST, R. & ESVELD, C. 1999. Surface waves in a stratified half space with enhanced continuum properties. Part 1: Formulation of the boundary value problem. *European Journal of Mechanics-A/Solids,* 18**,** 749-768.

TARANTOLA, A. 2005. *Inverse problem theory and methods for model parameter estimation*, siam.

VIKTOROV, I. A. 1970. *Rayleigh and Lamb waves: physical theory and applications*, Plenum press.

VORSTER, J. & GRABE, H. 2010. Axle load and track deflection on a heavy haul line. *Civil Engineering= Siviele Ingenieurswese,* 18**,** 44-49.

WHITHAM, G. B. 2011. *Linear and nonlinear waves*, John Wiley & Sons.

YANG, Y., HUNG, H. & CHANG, D. 2003. Train-induced wave propagation in layered soils using finite/infinite element simulation. *Soil Dynamics and Earthquake Engineering,* 23**,** 263-278.